ERRATA

Page 41, para4, line 22.

"Less than 1% of the π^0 decay as $\pi^0 \rightarrow e^+ + e^- + \gamma$ should read as "About 1% of the π^0 decay as $\pi^0 \rightarrow e^+ + e^- + \gamma$

Page 58, para 1, line 1.

Para 1 should read as :
The maximum angle of diffraction scattering calculated from the Optical Model in the Black Sphere Limit is $\sim 12^\circ$.

A Thesis

entitled

THE DESIGN AND USE OF SPARK CHAMBERS TO DISTINGUISH ENERGETIC ELECTRONS FROM PIONS

by

Abdul Raffey Faruqi, M.Sc.

Submitted for the

Degree of Doctor of Philosophy

of the University of London.

Department of Physics,

Imperial College,

London S.W.7.

January 1965

ABSTRACT

The 1st Chapter describes the early work (1960-61) on Spark Chambers done at the Imperial College. The main object was to gain experience with the detector before using it in any experiment.

An application of Spark Chambers is found in the experimental study of the two electron decay of the ω^o-meson. Chapter 2 describes the production of ω^o's and the kinematics of the two electron decay. Due to the small expected branching ratio of the $\omega^o \longrightarrow e^+ + e^-$ decay, and the high rate of $\pi^+ \pi^-$ background events, two important conditions are imposed on the Spark Chambers: (a) a high efficiency for electron detection, and (b) a low probability for pions to simulate electrons.

Preliminary considerations concerning the use of a Spark Chamber system for the study of ω^o-decays is presented in Chapter 3, mainly to try and maximise their usefulness in the experiment. Some results of the Shower Theory are used to propose several Spark Chamber Arrangements, expected to have a high efficiency for electron detection. An estimate is also made for the number of pions likely to simulate electrons.

The Spark chambers have to satisfy several requirements peculiar to this experiment. Tests, described in Chapter 4, are carried out to find out whether it is possible to fulfill these requirements.

Chapter 5 describes the experimental arrangements used to determine the efficiency of detection of 500 MeV/$_c$ electrons and the probability

of simulation of electrons by pions of the same momenta. The results of the experiment are described in Chapter 6. It is found that if the efficiency for electron detection is $\sim$ 90%, less than 0.5% π's simulate electrons. This means that less than 1 in 4.10^4 $\pi^+ \pi^-$ events would simulate a $\omega^o \rightarrow e^+ + e^-$ decay.

CONTENTS

		Page
ABSTRACT		2
CHAPTER 1. -	Spark Chambers: Historical Background and Early Work at Imperial College	
1.1	Introduction	7
1.2	Historical Account	7
1.3	Early Work at Imperial College	13
1.4	Conclusions	23
CHAPTER 2. -	Experimental Background of the Study of ω^0-Decays	
2.1	Introduction	25
2.2	Production of ω^0-mesons	27
2.3	Kinematics of the $\omega^0 \to e^+ e^-$ and $\omega^0 \to \pi^+ \pi^-$ Decays	30
2.4	Rate of ω^0-Production and Background Processes	35
2.5	General Requirements on the ω^0-Decay Particle Detection System	37
CHAPTER 3. -	Feasibility of Employing Spark Chambers in the ω^0-Decay Experiment	
	Part I	
3.1	Choice of a Detector for the ω^0-Decay Products	38
3.2	Discussion on a Spark Chamber Arrangement	40
	Part II	
3.3	Features of Electron Showers	43
3.4	Special Requirements on Spark Chambers	47

		Page
3.5	Construction of Spark Chambers	53
3.6	Spark Chamber Systems for Electron Detection	54
	Part III	
3.7	Features of π^--Interactions	57
CHAPTER 4. -	Preliminary Tests with Aluminium Foil Spark Chambers	
4.1	Introduction	61
4.2	Construction of the Spark Chamber and Trigger Circuit	61
4.3	Measurement of Efficiency for Cosmic Rays	65
4.4	Photography	68
4.5	Power tests	68
4.6	Measurements on Angular Tracks	71
CHAPTER 5. -	Description of the Experimental Set-Up at NIRNS	
5.1	Introduction	78
5.2	The Beam Composition	78
5.3	The Cerenkov Counter	79
5.4	The Spark Chamber Arrangements and Associated Electronics	84
CHAPTER 6. -	Experimental Results	
6.1	Introduction	91
6.2	Spark Chamber Performance	91
6.3	F.1 (π^--mesons in Arrangement I)	93
6.4	F.2 (electrons in Arrangement I)	98

		Page
6.5	Criterion No. 1	110
6.6	Criterion No. 2	111
6.7	Criterion No. 3	11
6.8	F.3 and F.4 (Arrangement II)	116
6.9	F.5 and F.6 (Arrangement III)	124
6.10	Conclusions regarding F.1 - F.6	124
6.11	F.7 and F.8 (Arrangement IV)	133
6.12	Application of Results to the ω^{o}-Decay Experiment	139
ACKNOWLEDGMENTS		141
REFERENCES		142

CHAPTER 1

Spark Chambers: Historical Background and Early Work at Imperial College

1.1 Introduction

Spark Chambers constitute an important part of nuclear particle detectors nowadays. They are constructed in a variety of geometries and configurations and have been recently applied very successfully in a number of high energy physics experiments. Most of this success has resulted from innovations introduced to the old spark counter detector by Fukui and Mujamoto[1]. It may be appropriate therefore, in presenting an historical account of Spark Chambers, to begin with Spark Counters.

1.2 Historical Account

(a) Spark Counters

The first attempts to construct and operate a Spark Counter were made by Keuffel[2] and independently by Pidd and Madansky[3]. The common objective was to have a detector capable of measuring short time intervals between ionizing events. The contemporary time resolution attainable was about 100 n.s. set by Geiger counters employing cylindrical geometry (giving a non-uniform field). Keuffel recognised the advantage of using plane parallel geometry which gives a unfirm field - thus reducing the delay between the production of an ion in the sensitive volume and the resultant discharge.

The constructional features of the spark counter were similar in (2) and (3). Two plane parallel conducting plates were held at a certain distance apart in a glass enclosure which could be evacuated and filled with the desired gas mixture. The mixture was usually $\frac{1}{2}$ an

atmosphere of Argon + a few mm Hg. of some organic vapour.

A steady field of 8-12 kV/cm was maintained across the plates. When an ionizing particle left behind a trail of ions, the electrons were accelerated by the electric field and under favourable conditions produced a streamer. Favourable conditions being those when at least one of the electrons was produced in the sensitive region of the gap.

Keuffel measured the efficiency of his counters by measuring cosmic ray coincidences between two counters spaced apart and comparing it with the expected rate. He arrived at a figure of about 90% for the efficiency which was much higher than the 10% obtained by Pidd and Madansky. It was pointed out later, however, that the lower efficiency could have resulted from the lower fields employed by Pidd and Madansky.

The problem of Quench Time was studied in some detail by Pidd and Madansky. If V is the threshold voltage of the counter and $(V + \Delta V)$ the operating voltage, ΔV is called the overvoltage. Quench Time is defined as the shortest time after a Spark Discharge when the overvoltage can be reapplied without causing a spurious breakdown (due to leftover ionisation from the previous discharge). One remarkable result found was that it was impossible to obtain Quenching Times of less than a few seconds with pure Argon. With the addition of 10% butane, however much shorter Quench Times could be obtained and some of the values are quoted below.

These large variations in the quenching time were explained on the basis of the Malter Effect[4] described below. If the cathode is covered

Table 1.1

Quench Times	Material of Cathode
$\geq$ 0.1 sec	Al, Au, Pt and Brass
0.01 sec	Cu, Bi
0.001 sec	Pb, Sn

with an insulating layer, (e.g. an oxide) it may become highly positively charged during a discharge, resulting in a strong field at the cathode and the emission of electrons. Smaller dead times in Pb and Sn are ascribed to the lower resistivities of their respective oxides; the charges leak off in a shorter time.

The associated problem of spurious breakdowns was explained by Keuffel on the basis of the Paetow effect which is as follows. Sub-microscopic particles of dust and/or oxide get charged up during the discharge and set up high fields. Electrons or photons are produced due to either breakdown of the insulating layer or field emission.

Spark Counters have been used by Robinson[5] to ascertain the "Time Structure" of Cosmic Rays. This involves measuring the time delay of one group of particles relative to another e.g. in Extensive Air Showers the delays of electrons relative to the muons. As the time resolution of his counters was $\lesssim$ 5 n.s. they were ideally suited for the experiment.

Another use of the Spark Counter was made by Allkover et al[6] to investigate the scattering of μ's in lead with the help of three counters. Later the momentum of sea-level μ's was measured, with the help of spark counters and a magnet, up to 60 GeV/c.

(b) The Hodoscope Chamber

The principle of the Hodoscope Chamber[7] is based on the fact that if a strong electric field is produced in a gaseous region soon enough after the passage of an ionizing particle, a luminous discharge occurs all over the region due to the acceleration of the liberated electrons.

The construction of the chamber, in simple terms, consisted of a parallel plate condenser filled with a large number of glass tubes which had a filling of Neon at $\frac{1}{2}$ an atmosphere. The passage of a particle through the chamber was detected by a Geiger Counter telescope which switched on a high field $\sim$ 10 kV/cm across the gap. This voltage was sufficient to produce a luminous discharge in those tubes through which the particle passed.

In a later report the same group[8] has given more detailed results on the operating conditions of the chamber and some of them are quoted below.

(i) The efficiency reached a maximum of $\sim$ 75% at a field $\sim$ 8kV/cm and stayed constant to $\sim$ 12kV/cm.

(ii) The efficiency decreased from $\sim$ 80% to $\sim$ 70% on slowing down the rise time of the high voltage pulse from 0.2 to 1 μs. Presumably the slower rising pulse acted as a clearing field to reduce the efficiency.

(iii) With a fixed high voltage pulse the effect of delaying it was observed on the efficiency. There was no serious change to 1μs but after 5μs it had dropped to about half its original value.

This can be explained on the basis of diffusion of electrons to the walls. The diffusion set the resolving limit on time to about 10 μs.

Apart from its simple construction, the Hodoscope chamber was stable during operation and could be triggered. The main drawback was the poor spatial resolution and low efficiency, $\eta_{max.} \sim 75\%$.

(c) The Triggered Spark Counter

Cranshaw and De Beer[9] incorporated the trigger system of Conversi et al[7] with the Spark Counter, introducing photography of sparks as a means of location of particles.

The counter consisted of two metal plates held parallel and separated by 1 mm in air. On receiving a coincidence signal from a G-M counter telescope, a high voltage pulse was applied across the plates which resulted in a breakdown along the ionization. A constant clearing field swept out ions from older tracks.

Some of the features of the triggered counter are given below.

(i) The efficiency was ~90% for a high voltage pulse putting on a field ~ 70kV/cm.

(ii) For a pulse widths varying from 0.1 to 100 μs, no change in efficiency was noted. However, as the pulse width was increased beyond 50 μs spurious discharges appeared.

(iii) It was shown that only negative oxygen ions were instrumental in starting the discharge. Electrons formed by the incident particle were immediately captured by oxygen to form negative ions. As

the binding energy of the electron to the oxygen molecule is only 0.34 Volt, it became detached at a value of $\frac{E}{P}$ ~ 90 V/cm-mm Hg and gained enough energy to initiate an electron-photon avalanche.

(iv) As the rise time of the high voltage pulse was made slower, the efficiency dropped due to the clearing action of the field.

(v) It was possible to keep the spurious discharges below 1%.

(d) The Discharge Chamber

The next major improvement in the technique was made by Fukui and Mujamoto[10] which transformed the spark counter into what is now known as a Spark Chamber. The special feature of this new detector was that it could give simultaneous tracks of several particles and had a better time resolution than either the air-filled counter or the Hodoscope Chamber.

In construction, the spark chamber was simply a combination of several spark counters enclosed in a box. The gas filling used was Argon or Neon at a pressure of just above one atmosphere.

A GM counter telescope registered the passage of a particle and triggered a 10kV/cm pulse across the gaps. Photographs of triggered sparks were taken which were reasonably in line indicating the correlation between the incident particle and the sparks.

The pulse width employed was about 100 n.s. but it was found that if it was increased to 1 μs. spurious discharges occurred in the chamber. The efficiency was ~ 100% for a 2 μs. delay in triggering but fell drastically at a delay of 10 μs. This, then set the resolving time of the chamber to 10 μs. For some inexplicable reason no clearing field was

used (as in the earlier Cranshaw and De Beer's counter) which would have improved the resolving time by an order of magnitude. The recovery time was quoted as 100 m.s. which was mainly due to the slow recovery of the power supplies.

1.3 Early Work at Imperial College

It was evident, after the investigations of Fukui and Mujamoto[10] that Spark Chambers could be profitably employed in numerous High Energy Physics experiments. Mainly to gain experience in the field, a Spark Chamber of the Fukui and Mujamoto type was constructed at the Imperial College. Some details of the construction of the chamber along with the accompanying trigger circuit are given in the following section. Finally some results obtained with the chamber are given in (b), (c) and (d).

(a) Description of the Spark Chamber and Trigger Circuit

Fig. 1.1 shows a photographic view of the Spark Chamber which had 14 gaps enclosed in a sealed box. This was achieved by mounting 15 plane Al plates, 9" x $6\frac{1}{2}$" and a $\frac{1}{4}$" thick, parallel to one another. Alternate plates were criss-crossed to prevent edge sparking and also belonged to a set. Plates of each set were mounted independently off the base, and a constant gap separation of $\frac{3}{4}$" was maintained between consecutive plates; this resulted in an effective gap separation of $\frac{1}{4}$" between consecutive plates of dissimilar sets. Plates belonging to a common set were connected together electrically but remained insulated from the other set. The two electrical connections were brought outside and

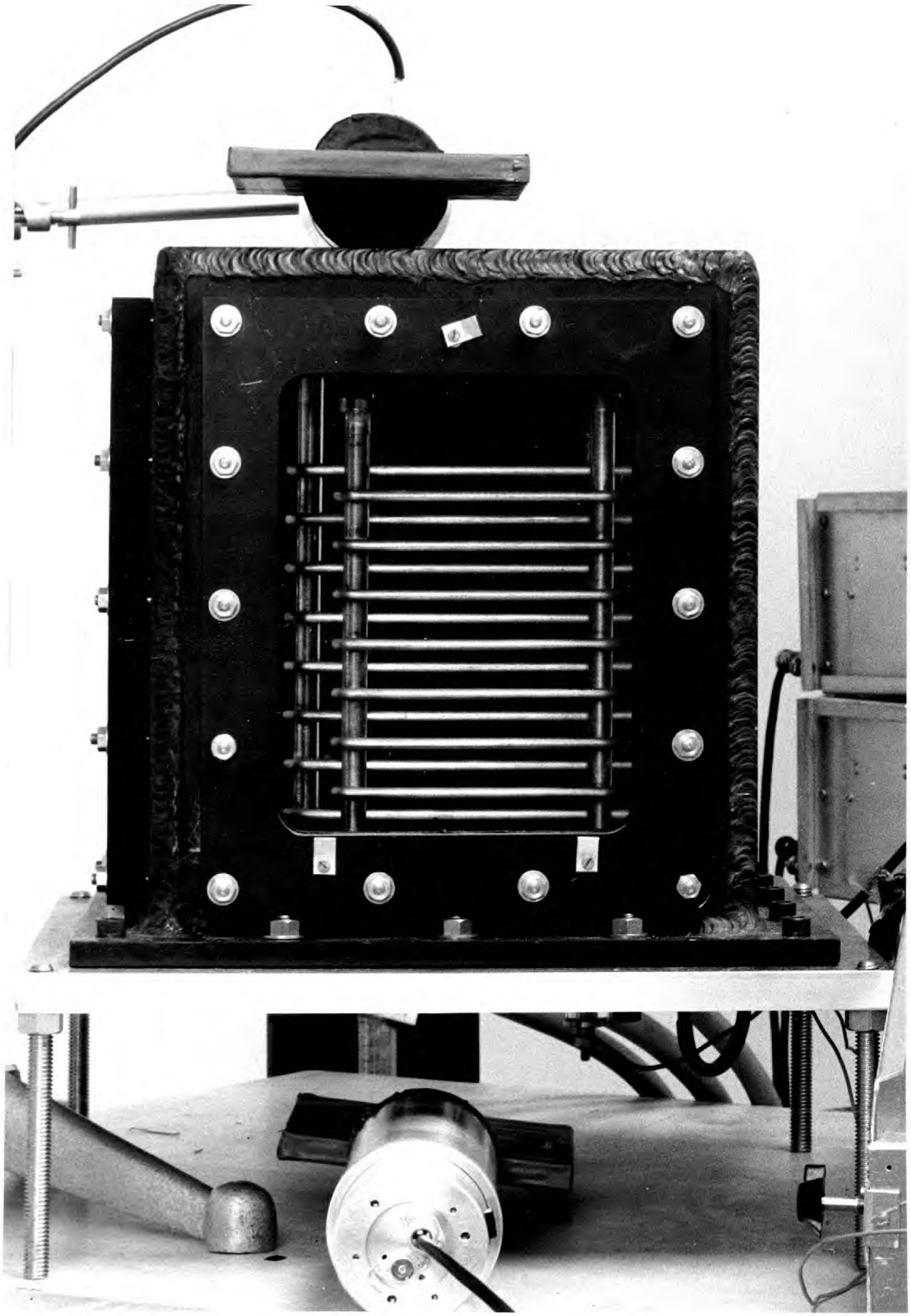


Fig 1·1

connected to the high-voltage pulser.

The whole plate structure was enclosed in a metal box made of welded HP10 alloy which had glass windows on two sides. The box was screwed to the base plate and provided a leak-free volume which was evacuated and filled with the required gas.

A block diagram of the electronics is shown in Fig. 1.2 but a more detailed circuit is given in Fig. 1.3. The function of the electronics was:

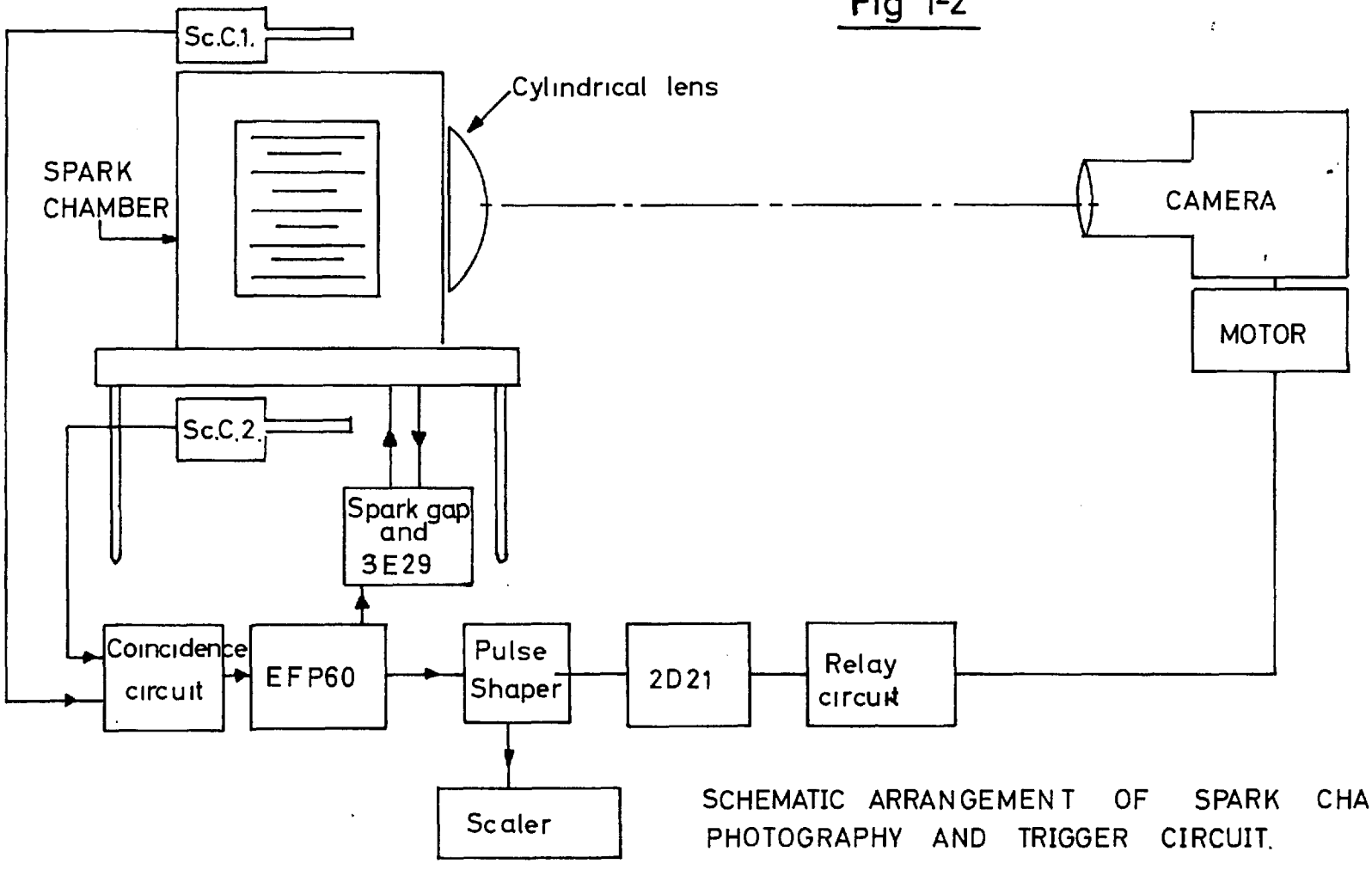
(i) To detect the passage of a particle through the chamber and apply a high voltage pulse within a $\frac{1}{4}\mu$s.

(ii) To wind on the film in the camera.

The first part of the trigger circuit which was designed by Dr. D.M. Binnie is shown in Fig. 1.3. Outputs from a Scintillation counter telescope, covering the sensitive area of the chamber, were fed into a Garwin Coincidence circuit which produced a positive signal when a coincidence was recorded. When the voltage on the grid of the EFP60 reached the threshold value, it fired, giving an output independent of the trigger. Due to the high secondary emission dynode inserted between the suppressor grid and the anode, and the feedback mechanism, the EFP60 was capable of giving far more current output in a shorter time than a conventional pentode.

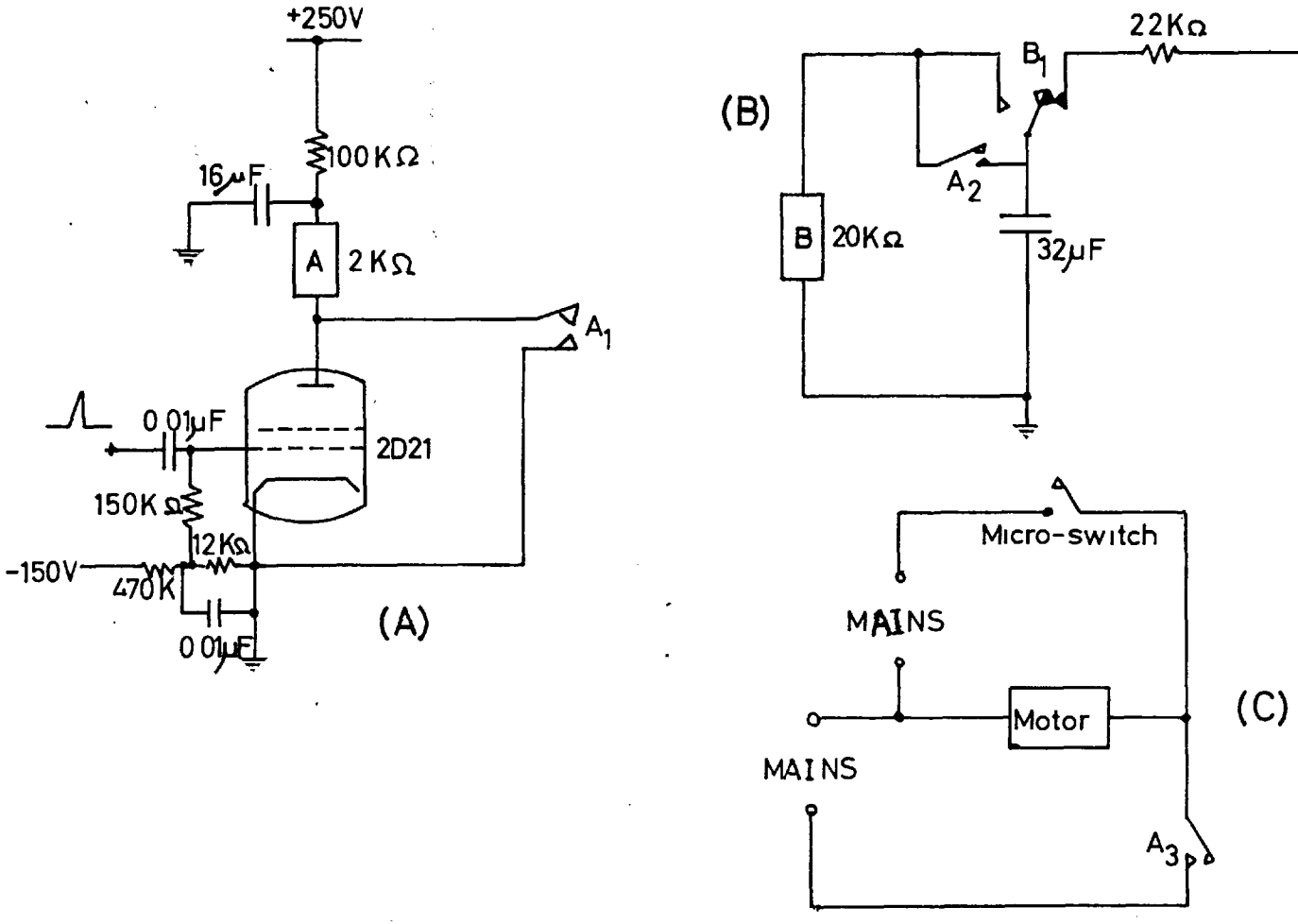
The +750V pulse, taken from the dynode was used to trigger the 3E29, (see Fig. 1.4) a double tetrode capable of carrying 10 amps with a working anode voltage of 5kV. The anode was capacity coupled to the middle sphere of a three-sphere spark gap, the centre of the spheres being in a line.

Fig 1-2



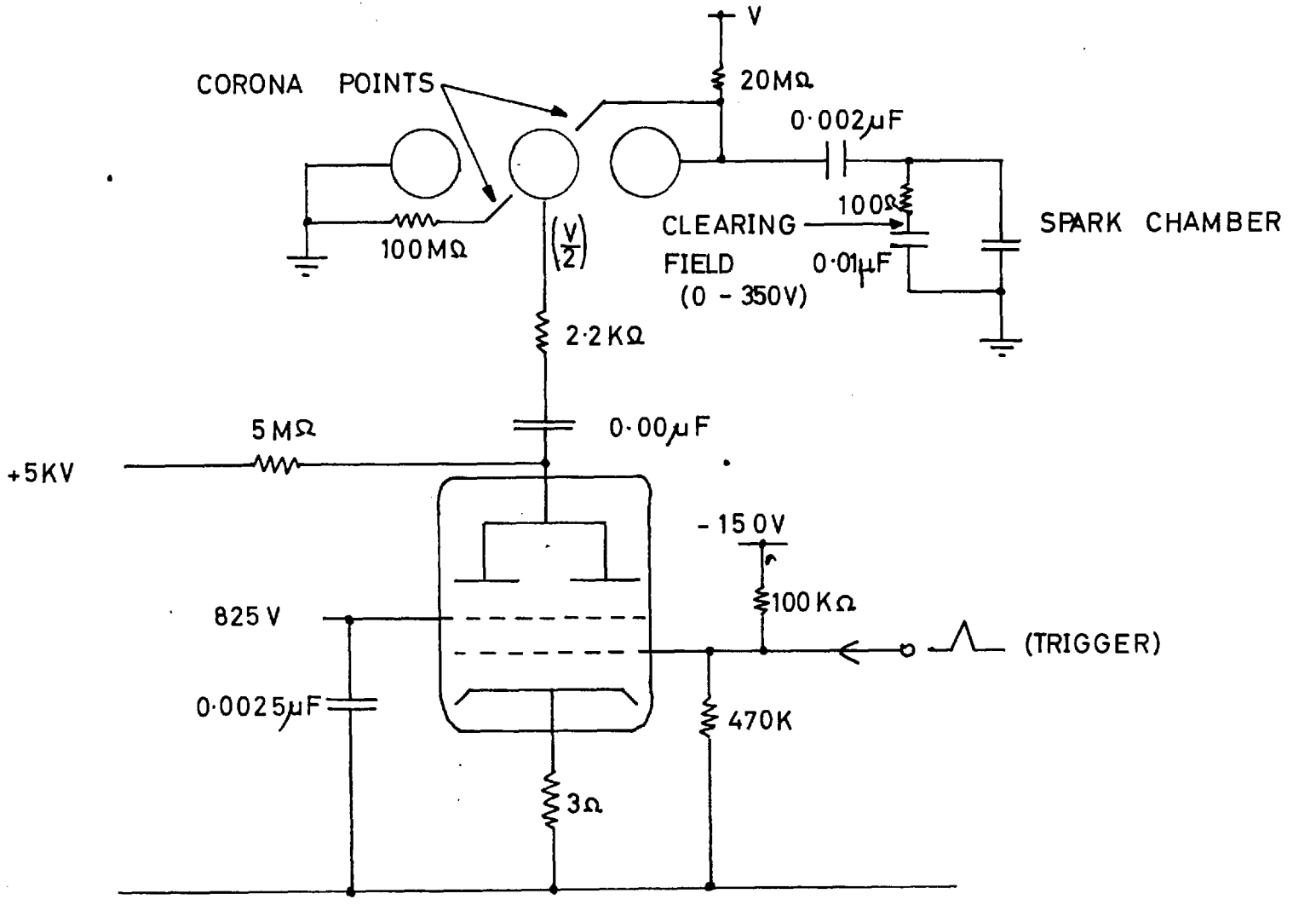
SCHEMATIC ARRANGEMENT OF SPARK CHAMBER PHOTOGRAPHY AND TRIGGER CIRCUIT.

Fig 1-3



DETAILS OF THE RELAY CIRCUITS

Fig 1-4


V
20MΩ
CORONA POINTS
0·002μF
100Ω
CLEARING FIELD (0 - 350V)
0·01μF
SPARK CHAMBER
100MΩ
(V/2)
2·2KΩ
5MΩ
0·00μF
+5KV
-150V
100KΩ
825V
(TRIGGER)
0·0025μF
470K
3Ω

The gaps between the spheres were so arranged that they were in equilibrium with the potential difference between the end spheres being about 20kV with the middle sphere at about 10kV.

The -5kV pulse on the middle sphere disturbed the potential equilibrium of the gaps which cascaded in breakdown. The 2000 pf storage condenser then discharged through the chamber with a time constant of about 200 n.s.

The total time delay between the passage of the particle and the application of the high voltage pulse was about 250 n.s. The calculated rise time of the high voltage pulse on the chamber was about 25 n.s., calculated on the basis of the inductance of the spark gap and the chamber.

To trigger the camera motor, part of the EFP60 pulse went through a pulse-shaper to trigger a 2D21 hydrogen filled thyratron. Relay A in the anode load of the thyratron was energised and three of its contacts were used: a) A_1 for quenching the thyratron b) A_2 for closing relay B to put a -150V bias on the EFP60 for 3 seconds c) A_3 for switching the mains across the camera motor, which switched itself off, when one frame had been moved, with the help of a micro-switch.

Photography of cosmic ray tracks was carried out using a motor driven camera with 7" focal length lens at f/11. As the film was moved on receiving a signal from the trigger circuit, no shutter was necessary. To obtain sparks of uniform width, a cylindrical lens was used on the window of the chamber.

(b) Variation of Efficiency with Gap Separation

This experiment was the fortuitous outcome of a technical mistake in the assembly of the Spark Chamber plates. The result was that the gap separation was not uniform and manifested itself in the lower efficiency of some of the gaps. A systematic check of gap separation was made which showed some correlation with the efficiency. It was found that the larger gaps tended to have a lower efficiency than the smaller ones (please see Fig. 15).

Efficiency here, has been defined as the number of sparks that occur in a gap divided by the total number which should have occurred. In Fig. 1.5 the efficiency of various gaps has been plotted as a function of their mean separation.

Within the statistical limits of the experiment, a variation of $\pm$ .0025" or $\pm$ 1% in the gap separation seems an acceptable figure. It may be pointed out here that this is applicable only when one storage condenser is used for several gaps in parallel.

After the gap separation had been made much more uniform (to $\pm$ .002") the efficiency of each gap was found to be $\sim$98%.

(c) Measurement of Sensitive Time

The efficiency of the chamber for a single track was defined as:-

$$\text{Efficiency} = \frac{\text{No. of sparks observed along track}}{\text{Total No. of gaps}} \times 100\%$$

and the sensitive time was defined as the time, from the instant of the passage of the particle through the chamber, during which the efficiency fell to $\frac{1}{e}$ (or $\sim$30%).

Fig 1-5

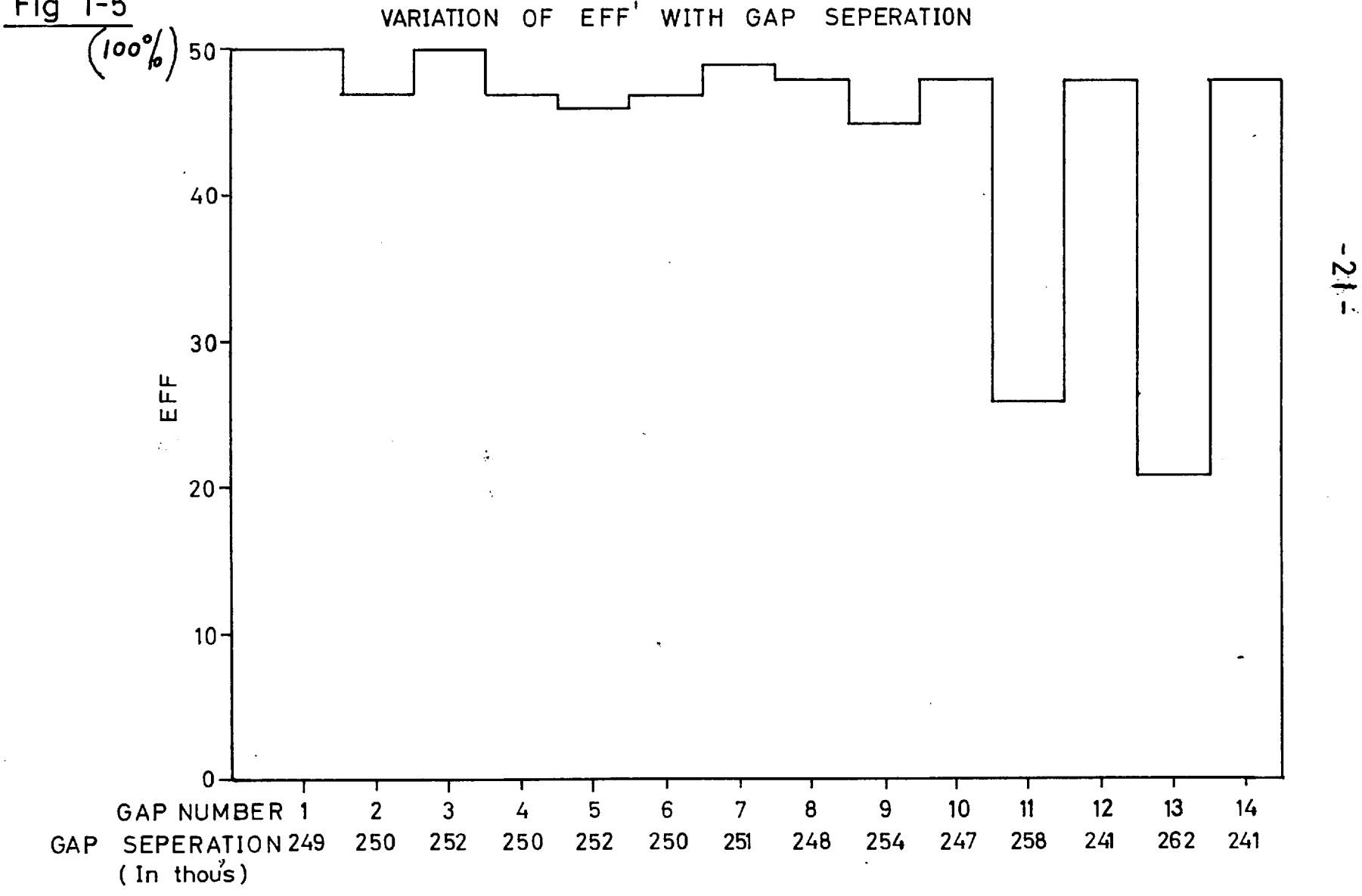

VARIATION OF EFF' WITH GAP SEPERATION
(100%)
50
40
30
20
10
0
EFF
GAP NUMBER 1 2 3 4 5 6 7 8 9 10 11 12 13 14
GAP SEPERATION 249 250 252 250 252 250 251 248 254 247 258 241 262 241
(In thou's)

Table 1.2

Clearing Field		$\frac{E}{p}$ (Volts per cm per mm Hg)	Drift Time (Klema & Allen)	Observed Sensitive Time
0	Volts	0	-	10.5 μsec.
5	"	.011	4 μ sec	4.05 "
25	"	.055	2 "	1.06 "
50	"	.11	1.5 "	0.73 "
100	"	.22	0.85 "	0.43 "
150	"	.33	0.75 "	0.42 "
200	"	.44	0.54 "	0.42 "
250	"	.55	0.54 "	0.41 "
350	"	.77	0.60 "	0.59 "

A constant amplitude high voltage pulse was applied across the chamber, which was filled with commercial grade Argon, with a variable delay, and for several different values of the clearing field. The results are shown in Table 1.2 and the derived results on the sensitive time are shown in Fig. 1.6.

For comparison, the second curve in Fig. 1.6 has been drawn using values of electron drift velocities in 99.6% pure Argon, for various values of E/p, as found experimentally by Klema and Allen[11]. The rather simple assumption has been made that the sensitive time is equal to the time taken by an electron to cross the gap under the applied clearing field. In view of the fact that commercial grade argon was used as a filling it is not surprising to find a shorter sensitive time then Klema and Allen. This is because Nitrogen is a very likely impurity which also tends to increase the drift velocity.

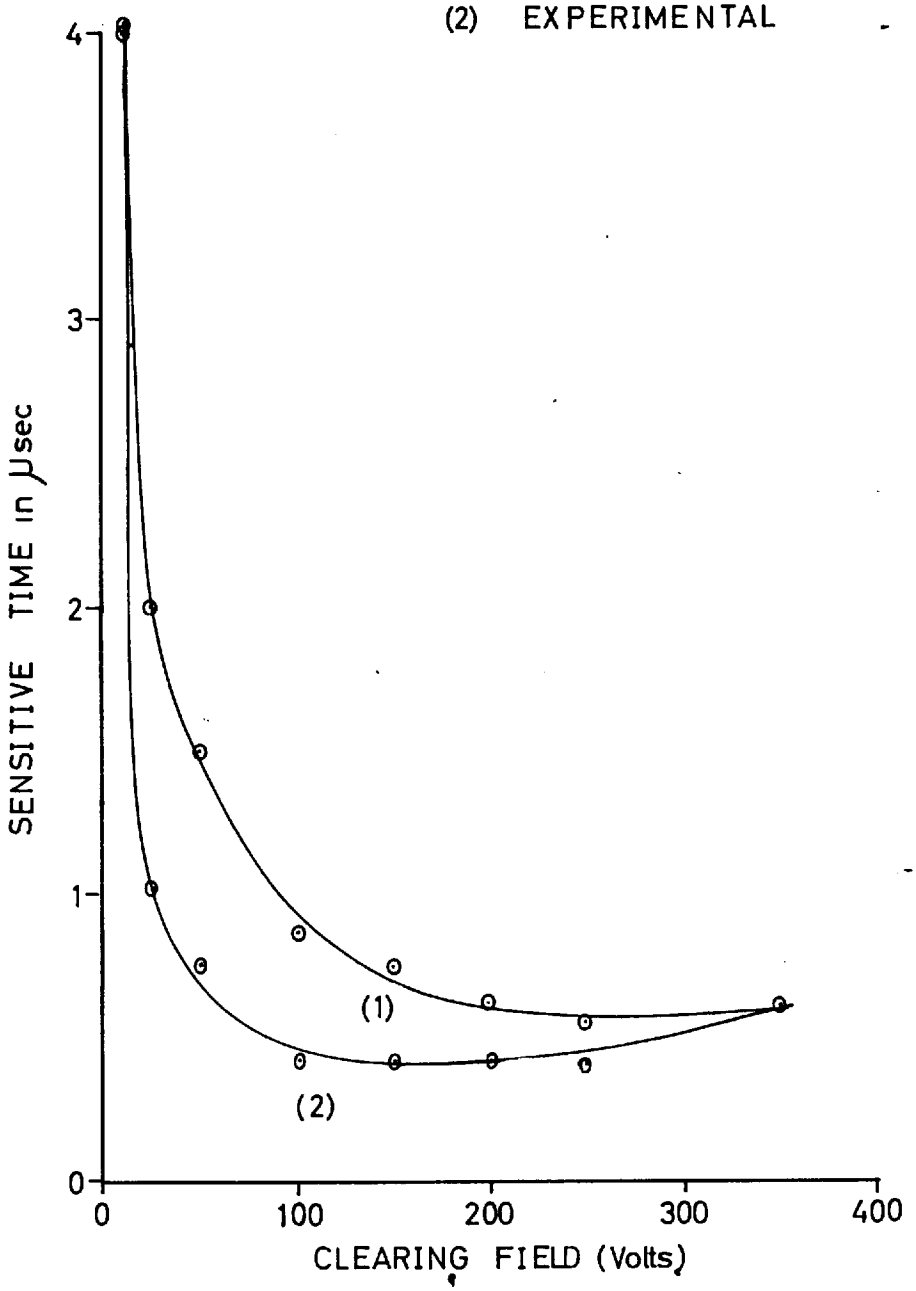
1.4 Conclusions

The special properties of a spark chamber, some of which have been discussed above, make it very effective in certain experiments involving the detection of nuclear particles. This thesis is concerned mainly with the design and construction of spark chambers, efficient in the detection of electrons and in distinguishing charged pions from electrons very accurately. This problem arose in connection with the study of the 2-particle decays of the π^0-meson which imposed special requirements on the Spark Chambers, discussed in the next chapter.

Fig 1-6

VARIATION OF SENSITIVE TIME WITH CLEARING FIELD

(1) THEORETICAL
(2) EXPERIMENTAL



CHAPTER 2

Experimental Background of the Study of ω^0-Decays

2.1 Introduction

A proposal to study the decay

$$\omega^0 \longrightarrow e^+ + e^-$$

and the interference effects between the two decays

$$\omega^0 \longrightarrow \pi^+ + \pi^- \text{ and } \rho^0 \longrightarrow \pi^+ + \pi^-$$

with the help of Spark Chambers was made by the Imperial College - Manchester University group[12].

The theoretical interest in the $\omega^0 \to e^+ + e^-$ decay stems from the fact that if it is compared to the $\phi^0 \to e^+ + e^-$ decay, it is possible to have a measure of the electromagnetic mixing between the ω and the ϕ-mesons. The ω-ϕ mixing is, at present required by the SU(3) theory to explain the masses of the two mesons[13]. A theoretical estimate for the branching ratio of $\omega^0 \to e^+ + e^-$ has been made by Ketley[14] who finds a value of 0.7%. A similar estimate for the branching ratio $\rho \to e^+ + e^-$ is 0.07%

The ρ meson is produced in comparable numbers in any reaction producing the ω-mesons, as it has the same quantum numbers and only a slightly lower mass (750 MeV). The ρ-meson decays into $\pi^+\pi^-$ via strong interactions while for the ω this process is allowed through a second order electromagnetic process. The prediction regarding the ω-ρ interference is that it will show up in the $\pi^+\pi^-$ sprectrum as a broad ρ-peak centred at 750 MeV and a sharp ω peak at 780 MeV[15].

A list of the ω^0-decay products is given in Table 2.1.

Table 2.1

ω^0 Decay Products	Branching Ratio	References
$\pi^+\pi^-\pi^0$	$\sim$ 80%	16,17,18
$\pi^+\pi^-$	$<$ 2%	19,20
$\pi^0\gamma$	10-20%	21,22
e^+e^-	$<$ 1%	14,23,24,25
$\mu^+\mu^-$	$<$ 1%	14

2.2 Production of ω^o-mesons

It is proposed to produce ω^o's by the reaction

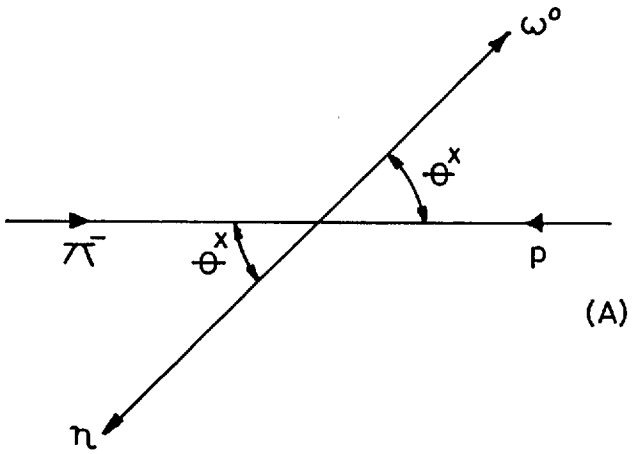
$$\pi^- + p \longrightarrow \omega^o + n \qquad (1)$$

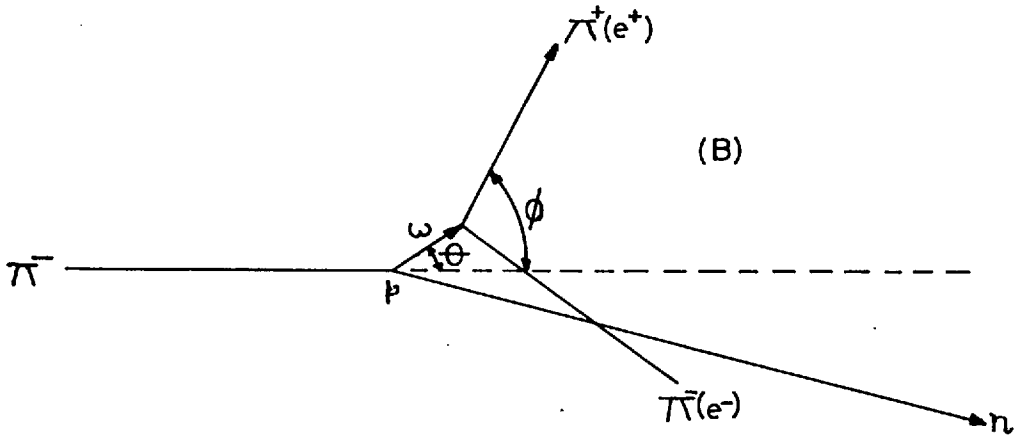
where the momentum of the π^--meson is adjusted accurately ($\Delta p_\pi \pm .5\%$) to be just above threshold for the process (1). The ω's are selected by measuring the momentum of the incoming π-meson and the time of flight of the neutron. The ω^o and the neutron are produced almost at rest in the C.M.S. of the π-meson and the proton (Fig. 2.1). Transforming back to the Laboratory system both the ω^o and the neutron go forward, at small angles to the incident π^-.

The neturon is detected in one of the six neutron counters, arranged as shown in fig. 2.2, at about 3 metres distance from the Hydrogen target. The neutrons are expected to have approximately the same velocity as the C.M.S., which provides with an effective "gating" criterion for the neutron counters. The estimated time of flight of the neutrons is 20 n.s. and the proposed gating time 3 n.s. Taking into account the geometrical factor for the neturon counters and their detectron efficiency, preliminary calculations show that $\sim$ 10% of the neutrons will be detected.

The principle of counter selection for ω's is a coincidence between the two beam counters S_1, S_2 and a suitably delayed neturon count, together with 'no' count from A_1 and A_2. The anti-coincidence counter A_1 reduces the probability of an interaction outside the Hydrogen target being selected, or a beam particle triggering one of the neutron counters. A_2 prevents charged particles coming from the Hydrogen target from

Fig 2-1





PRODUCTION OF ω-MESONS IN :-

(A) C.M.S. SYSTEM
(B) LABORATORY SYSTEM

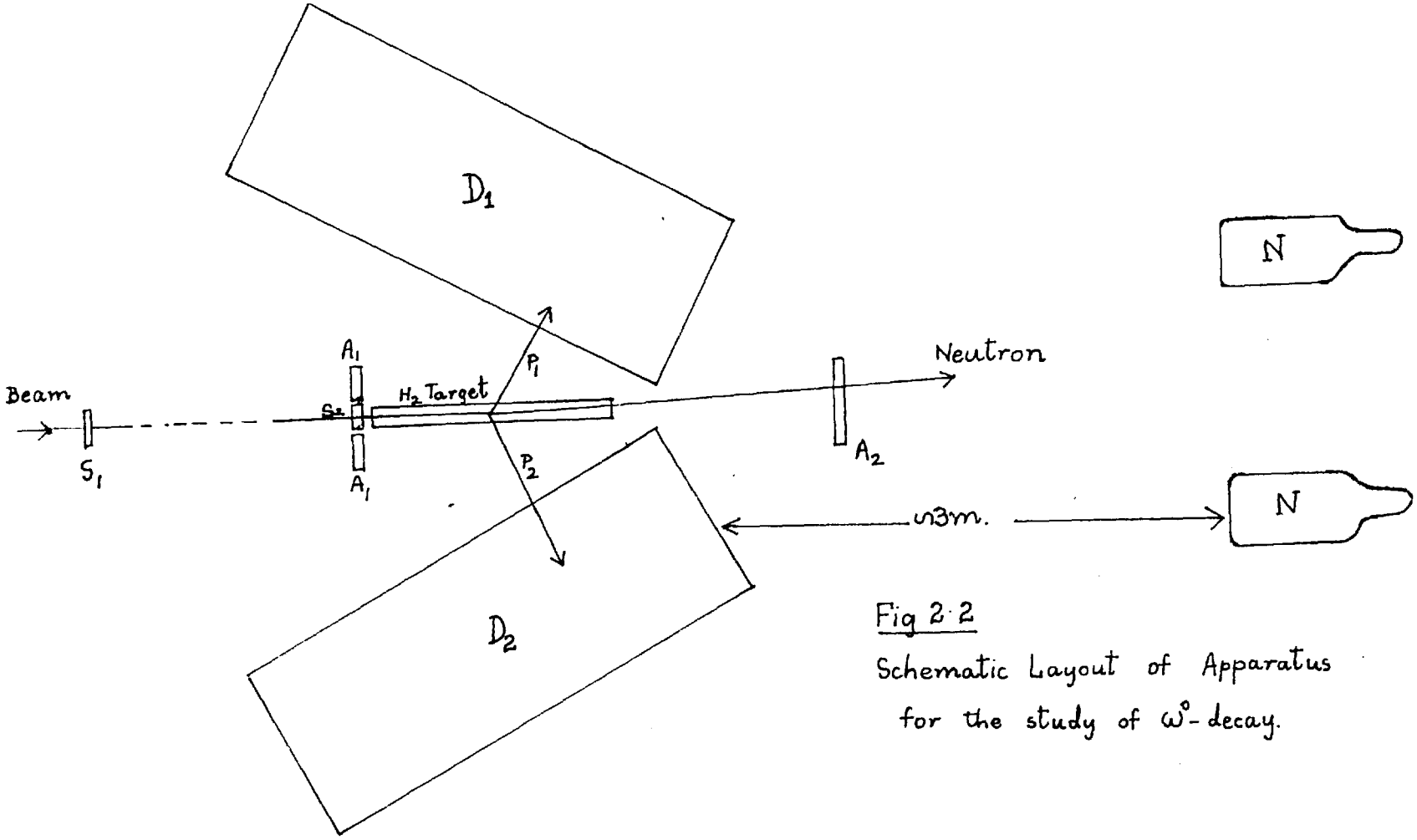


Fig 2·2

Schematic Layout of Apparatus for the study of ω°- decay.

triggering the Neutron counters. In short, the counter selection is

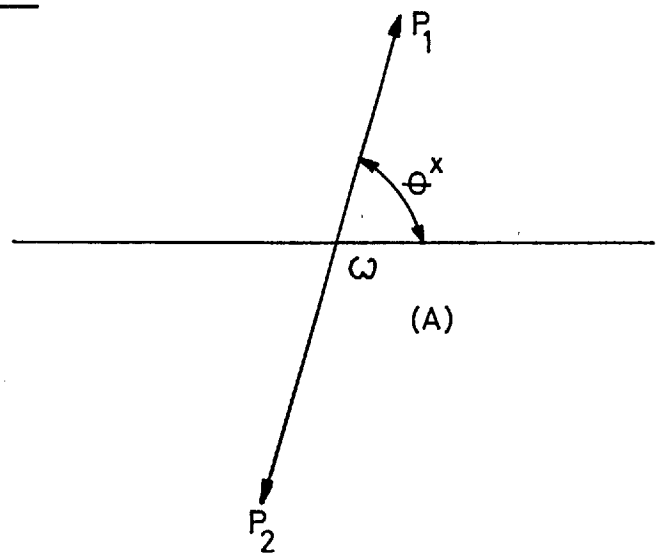
$$S_1 S_2 \bar{A}_1 \bar{A}_2 \, N_{delay} \text{ (within gate)}$$

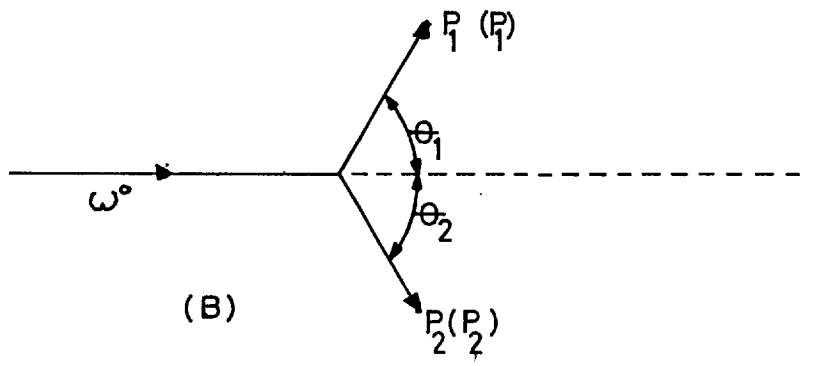
2.3. Kinematics of the $\omega^0 \to \pi^+\pi^-$ and $\omega^0 \to e^+e^-$ Decays

A knowledge of the kinematics of the ω-decay helps considerably in the design of the detection system for the decay particles. The two most important factors are the angles of the decay and the momentum of the decay particles. For low values of p^x ($\lesssim 100$ MeV/c) the Laboratory momentum of the ω varies between 400-600 MeV/c. Tables 2.2 and 2.3 show the variation of the decay angle (see Fig. 2.3) and the momentum as a function of the C.M.S. angle of decay θ^x, of the $\omega^0 \to e^+ + e^-$ and the $\omega^0 \to \pi^+ + \pi^-$ decay, respectively.

A preliminary design envisaged D_1 and D_2 as Spark Chambers covering an angle π in the vertical plane and $\sim 20^\circ - 110^\circ$ in the horizontal plane (from the centre of the hydrogen target; see Fig. 2.4). They would consequently subtend a solid angle on the hydrogen target sufficiently large to cover θ^x from about 30°-90° (i.e. $\sim 25\%$ of the 2e or 2π decays would fall in the chambers). From the Tables 2.2 and 2.3 it can be seen that this would cover events with momentum ranging from $\sim$ 300-600 MeV/c. The opening angle of the decay particles ($\theta_1^0 + \theta_2^0$) varies from $\sim 100^\circ$-130°.

Fig 2-3

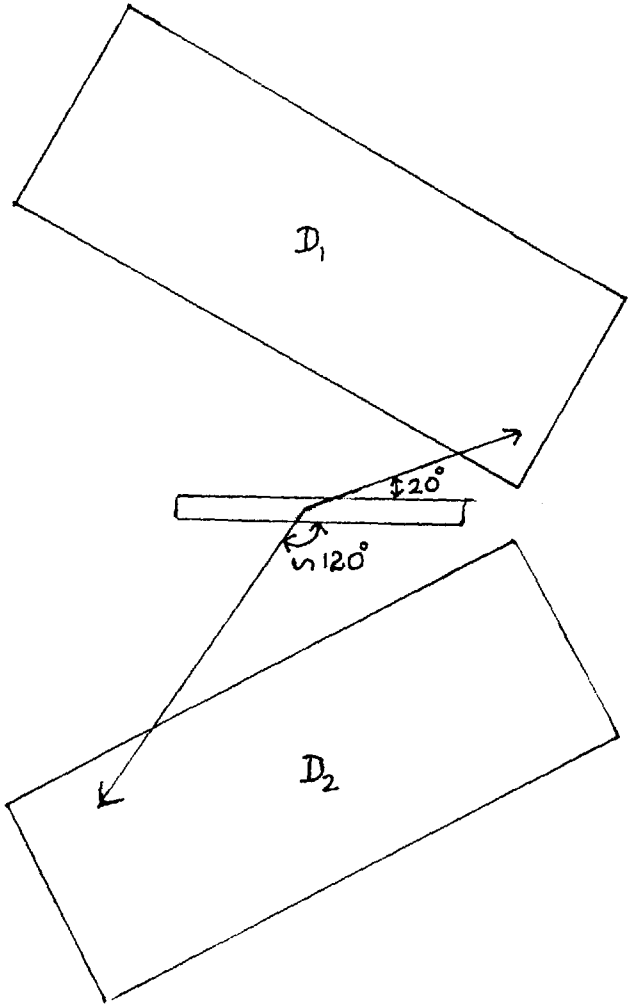




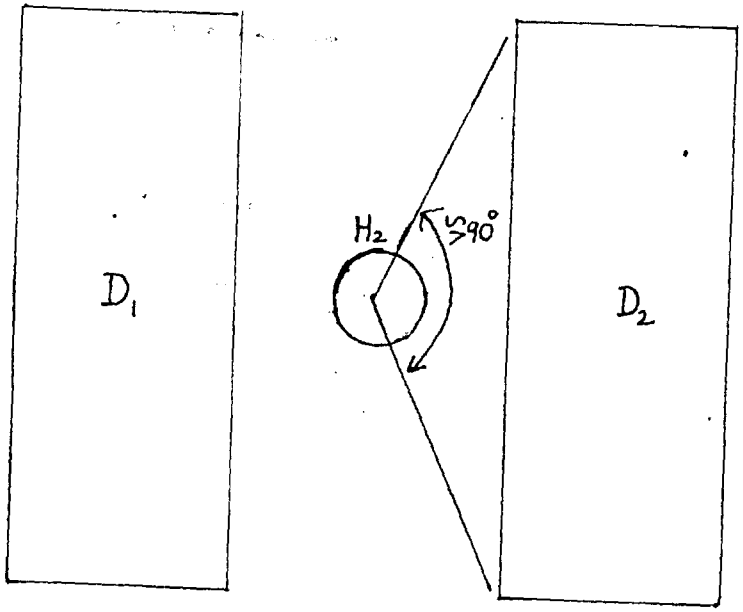
DECAY OF AN ω-MESON IN :-

(A) C.M.S. SYSTEM

(B) LABORATORY SYSTEM



(a) Plan



(b) Elevation

Fig 2·4

Spark Chamber Geometry

Table 2.2 $\omega^0 \longrightarrow e^+ + e^-$

P_ω = 400 MeV/c

θ^*	P_1(MeV/c)	P_2(MeV/c)	θ_1^0	θ_2^0
0°	639	239	-0°	0°
30°	612	266	18.6°	132.7°
60°	539	339	38.9°	93.1°
90°	439	439	62.9°	62.9°

P_ω = 500 MeV/c

θ^*	P_1(MeV/c)	P_2(MeV/c)	θ_1^0	θ_2^0
0°	714	214	-0°	0°
30°	680	247	16.7°	127.8°
60°	589	339	35°	86.9°
90°	464	464	57.4°	57.4°

P_ω = 600 MeV/c

θ^*	P_1(MeV/c)	P_2(MeV/c)	θ_1^0	θ_2^0
0°	793	193	-0°	0°
30°	753	253	15°	122.9°
60°	643	343	31.8°	81°
90°	493	493	52.5°	52.5°

Table 2.3 $\omega^0 \rightarrow \pi^+ + \pi^-$

P_ω = 400 MeV/c

θ^x	P_1(MeV/c)	P_2(MeV/c)	θ_1^0	θ_2^0
0°	610	210	-0°	0°
30°	585	240	18.2°	130.4°
60°	514	316	38°	90.9°
90°	416	416	61.3°	61.3°

P_ω = 500 MeV/c

θ^x	P_1(MeV/c)	P_2(MeV/c)	θ_1^0	θ_2^0
0°	683	183	-0°	0°
30°	651	221	16.3°	124.5°
60°	564	318	34°	84°
90°	443	443	55.6°	55.6°

P_ω = 600 MeV/c

θ^x	P_1(MeV/c)	P_2(MeV/c)	θ_1^0	θ_2^0
0°	760	160	-0°	0°
30°	722	208	14.6°	118.4°
60°	617	324	30.8°	77.6°
90°	473	473	50.6°	50.6°

2.4 Rate of ω^0-Production and Background Processes

An estimate of the rate of production of ω^0's can be made on the basis of the experimental data of Toohig et al[26], who have measured the cross-section for ω-production at a higher energy than envisaged in the present experiment. Assuming an s-wave production of ω's, the cross-section turns out to be

$$\sigma = 5 p^x \quad \mu b.$$

For an average value of $p^x \simeq 50$ MeV/$_c$, $\sigma \sim 250$ μb. The background events which could simulate the production of an ω are listed in Table 2.4. Column 4 gives an estimate of the fraction of the events which are likely to produce a neutron within the gating interval of the neutron counter. The background events caused by ρ^0-production are far more difficult to separate, as the ρ^0-mass overlaps the ω^0-mass. A rough estimate based on bubble chamber results shows, however, that the ratio of ω's to ρ^0's counted will be $\sim$ 8:1.

The signal to background ratio can be estimated by comparing the cross-section for ω^0-production with the sum of cross-sections of the background processes (Table 2.4) for $p^x \leq 100$ MeV/$_c$, as only neutrons with a low p^x value are selected. The ratio of ω^0-events to background events would therefore be expected to be 1.5:1.

The relative rates of 2e decays and the $\pi^+ \pi^-$ background events set an important restriction on the detection system of the ω^0-decay particles. The ratio of $\pi^+ \pi^-$ events to e^+e^- events is estimated to be $\sim$ 50:1. Setting a conservative limit, the number of π-mesons which simulate electrons, should, therefore be $\lesssim$ 1%. With this value, the

Table 2.4

No.	Reactions	Total Cross-Sections	Cross-sections for $p^x_{\pi} < 100$ MeV/c
			Estimated from Phase Space Calculations
1	$\pi^- p \rightarrow \pi^+ \pi^- n$	10 mb	80 μb
2	$\pi^0 \pi^0 n$	5 mb	40 "
3	$\pi^0 \pi^0 \pi^0 n$; $\pi^+ \pi^- \pi^0 n$	$\sim$ 2 mb	20 "
4	$n^0 n$	12 "	negligible

Total Cross-section for events with $p^x_{\text{neutron}} < 100$ MeV/c

= 140 μb.

number of $\pi^+ \pi^-$ events which are likely to simulate a 2e decay are $\sim$.01% (remembering that it is necessary for both π's to simulate electrons). The other ω-decay products are discussed in Chapter 3.

2.5 General Requirements on the ω-Decay Particle Detection System

(i) The number of π's simulating electrons should be $\lesssim$ 1%.

(ii) The efficiency of electron detection should be high.

(iii) The solid angle covered by the detection system should be as large as possible.

(iv) A good efficiency for photon detection would be an asset, as it would give a measure of the $\omega^0 \to \pi^0 + \gamma$ branching ratio.

CHAPTER 3

Feasibility of Employing Spark Chambers in the ω-Decay Experiment

Part 1

3.1 Choice of Detector for the ω-decay products

At the end of the last chapter, several requirements were mentioned in connection with the detectors for the ω-decay products. One of the more important of them, which is repeated here, was the ability of the detector to identify electrons, (300-600 $\frac{\text{MeV}}{c}$) and to distinguish them very accurately from the π mesons in the same momentum range. Three possible detectors are considered briefly here, but only one, the spark chamber, is considered in some detail, as it is found more suitable.

(i) Cerenkov Counters

The disparity in the velocities of the electrons and pions in the energy range considered (β =1 and < 0.95 for an electron and pion respectively) immediately suggest the use of a threshold Cerenkov Counter. The counter could be set to reject particles with $\beta < 0.975$ which would eliminate all charged π and μ-mesons.

There is however, a very serious drawback with a Cerenkov counter, in that it covers a very small solid angle, requiring a much larger number of ω-events to detect a given number of electron decays. This difficulty could be partially overcome by arranging a matrix of Cerenkov counters near the hydrogen target. This would, however, increase the complication in the electronics and the expense considerably so as to make this technique less attractive.

(ii) Bubble Chambers

The possibility of using a Heavy Liquid Bubble Chamber is only mentioned in the passing, as it is fundamentally a different technique. It can not be used in the experimental arrangement described in the last chapter, but can be considered as an alternative method for the study of ω^0 -decays.

The solid angle available for the study of the ω^0-products is very good (4π) and in the presence of a magnetic field, the distinction of π^-s from es does not present any problems. The serious drawback in this case is the large number of photographs which have to be scanned to pick out a rare event like the $\omega^0 \to 2e$ decay. Further, a study of $\omega - \rho$ interference would be impossible due to the large spread in the "Missing Mass Spectrum".

(iii) Spark Chambers

Finally, a Spark Chamber detection system is considered. As mentioned in the last chapter, a preliminary design of a Spark Chamber system was considered which showed that about 25% of the two-particle ω^0-decays would be covered by the solid angle subtended by the chambers. This figure is not comparable to the one obtained with Bubble Chambers, but some other advantages make up for this shortcoming.

The most attractive feature is the relative simplicity in construction and operation of Spark Chambers, and unlike a Bubble Chamber it can be triggered for only selected events, reducing the scanning problems considerably. Spark Chambers also have some drawbacks, one of them

being the uncertainty in the accuracy of distinguishing π-mesons from electrons.

3.2 Discussion on a Spark Chamber Arrangement

From these preliminary considerations it was decided to choose Spark Chambers after a satisfactory test on the π/e distinction had been carried out. It was expected to identify electrons by their characteristic showers, which they produce when traversing matter. This meant the insertion of some high density material plates between chambers in which the shower could develop and be detected in the chambers. A charged π-meson (300-600 MeV/c) can not produce a shower unless it has a nuclear interaction with the production of energetic photons. The most likely way this can happen is by the decay of a π^0 (neglecting the process $\pi^- + p \rightarrow n + \gamma$, which occurs with only $\sim$ 2% frequency of the charge exchange reaction, $\pi^- + p \rightarrow \pi^0 + n$) produced in a charge exchange reaction.

It is simple to obtain an order of magntiude value of the expected π/e distinction ratio in spark chambers. Suppose lead is chosen as the material in which the electrons are allowed to develop a shower. The typical distance an electron travels to produce a shower is $\sim$ 1 radiation length, i.e. 0.6 cm. On the other hand the interaction length for a π -meson is $\sim$15 cms, the ratio of the two lengths being about 25:1. Considering that not all nuclear interactions result in the emission of a π^0, the quoted distinction ratio ($\sim$ 1%) seems a reasonable figure.

Some aspects of the ω^0-decay experiment are again considered here

to find out how a spark chamber could be used more efficiently in the experiment. The processes likely to be observed in the chamber are the Λ^0-decay products (Table 2.1) and the accompanying background reactions (Table 2.4). The processes are considered mainly from the $\Lambda^0 \rightarrow 2e$ simulation point of view.

(i) $\pi^+ \pi^- \pi^0$

This process would not fulfill the co-planarity requirement between the incident π^--meson and the other two observed charged particles, as there are three particles in the final state. Consequently it should be easy to reject these events.

(ii) $\pi^+ \pi^-$

As considered previously (Chap. 2), this process required a further test for the accuracy in the distinction of πs from es.

(iii) $\pi^0 \gamma$

As the π^0 decays into 2γ in a very short time ($\sim 10^{-16}$sec.), both the π^0 and the γ will apparently produce a cascade shower in the Spark Chambers. However, the fact that the shower will be initiated by neutral particles can be used to distinguish this decay from the 2e decay. If very little material is present between the hydrogen target and the first spark chamber (see Fig. 2.2), reducing the probability of materialization of the photons, no charged particle will be observed in the first chamber. Less than 1% of the π^0s decay as $\pi^0 \rightarrow e^+ + e^- + \gamma$. These electrons, can, in general, be rejected, as they do not satisfy the

co-planararity requirement. It may be possible to identify $\pi^0\gamma$ decays and measure the branching ratio of ($\omega^0 \to \pi^0\gamma$).

(iv) $2\pi^0$

These events can also be rejected on the same criterion as (iii), i.e. initiation of shower by neutral particles, or non-coplanarity of decay electrons.

(v) $\mu^+\mu^-$

As μ-mesons do not interact strongly, nearly all μ-decays would appear as charged particles going straight through (except Coulomb scattering) the spark chambers. It is not expected to be possible to distinguish μ-mesons from π-mesons, but due to the small number of μ-decays expected, the statistics on 2π events will not be affected.

(vi) e^+e^-

The kinematics of this decay have already been discussed in the last chapter. It is expected that electrons would show up as a singly charged particle in the first chamber followed by multiplication in the subsequent chambers.

From the preceding discussion as well as from Chapter 2, several important points concerning the Spark Chambers emerge, which can be summarised as follows:-

(i) The Spark Chambers should have a high detection efficiency for electrons in the range (300-600 MeV/$_c$).

(ii) It should be possible to distinguish πs from es very accurately,

viz. less than ~1% of the πs should look like electrons.

(iii) The chambers should be as near the hydrogen target as possible, and there should be a minimum amount of material between the hydrogen target and the first gap.

(iv) The first few gaps of the chambers (adjacent to the H_2 target) should be very efficient.

(v) The size of the chambers should be as large as possible to cover a large solid angle. In addition, with larger chambers, it is possible to use a longer hydrogen target, increasing the rate of collection of events.

In order to attain the highest possible efficiency for the detection of electrons with spark chambers, it is necessary to have a closer look at the development of electron showers. This helps to determine the amount of material required, and its position with respect to the chambers.

Part II

3.3 Features of Electron Showers[27]

Qualitatively speaking, an energetic electron can lose energy by a) collision and b) radiation. The energy lost by collisions is spent mainly in exciting and ionizing atoms, hence dissipated. This loss is only important for lower energy electrons. High energy electrons lose most of their energy by Bremsstrahlung, i.e. radiation of photons. The spectrum of the radiated photon's energy extends from zero to the

energy of the incident electron. The photon in turn can lose energy, by a) Compton Scattering and b) Pair Production. The former is significant only for photon energies $<$ 10 MeV, above which the latter is predominant.

It is simple to combine the processes mentioned above, to understand the formation of a cascade shower when an energetic electron travels through matter. Initially, the electron loses energy mainly by radiation, resulting in a large number of low-energy and a few high-energy photons. The low energy photons are more likely to lose energy by Compton scattering, whereas the high energy photons are more likely to produce electron pairs. The electrons from Compton scattering would have very low energy which would be dissipated due to collisions, etc. effectively removing them from the rest of the shower. The energetic secondary electrons would further radiate photons, and the process repeats itself - producing more and more particles with lesser average energy. When the energy of the electrons gets below a certain value, (7 MeV in lead) they lose most of their energy by collisions which is effectively dissipated and the shower dies out.

Several features of the showers are important from the spark chamber detection point of view, and are as follows:

(i) The Angular Spread

From the angular spread involved in the shower production, the required size of the chambers can be estimated.

As mentioned above, the two significant processes in shower formation are bremsstrahlung and pair production. According to Stearns[28], the root mean square angle of emission of a photon of energy E' by an initial electron of energy E in the vicinity of a nucleus of charge Z is given by

$$\langle \theta_R^2 \rangle_{av.}^{\frac{1}{2}} = q(E, E', Z) \frac{m_e c^2}{E} \log \frac{E}{m_e c^2}$$

where $q \sim 1$. For an incident electron of energy 100 MeV,

$$\langle \theta_R^2 \rangle_{av.}^{\frac{1}{2}} \simeq 1.5^\circ$$

The expression for the opening angle of a pair of electrons produced by a photon of energy E is given by[28]

$$\langle \theta_p^2 \rangle_{av.}^{\frac{1}{2}} = q(E, E', Z) \frac{m_e c^2}{E} \log \frac{E}{m_e c^2}$$

where θ is the angle between the incident photon and one of the pair of electrons, whose energy is E'. As before, for an incident photon of 100 MeV,

$$\langle \theta_p^2 \rangle_{av.}^{\frac{1}{2}} \simeq 1.5^\circ$$

It is apparent that if pair production and brensstrahlung were solely responsible for the development of the shower, the angular spread and consequently the lateral spread would be very small, viz. about 1 cm after developing for about 30 cms. However there are two factors which increase the effective size of the shower. Firstly, Compton Scattering, which is important for low energy photons, could produce an electron at a larger angle and secondly, multiple scattering at all stages of the

shower tends to spread it out. The former is important only in so far as the single Compton Scattered electron is considered, as it does not propagate the shower. Multiple scattering depends on the momentum of the particle; taking a 100 MeV/$_c$ electron as an example, the multiple scattering in one radiation length of lead would be:

$$\langle\theta^2\rangle^{\frac{1}{2}}_{\text{Mult. Scattering}} \simeq 10^{\circ}$$

Obviously, the multiple scattering angle would go on increasing as the shower progresses due to the lower energy of the particles involved. However, the smaller angle scatters earlier in the shower are also important as they change the direction of the "cone" of the shower.

(ii) The Average Behaviour of Showers

Some results on the average behaviour of a 500 MeV/$_c$ electron shower in lead are quoted here from a computation by Crawford and Messel[29]. The object of quoting these results is that they give an idea of the number of electrons and photons present at the various stages of the development of an average shower. The momentum 500 MeV/$_c$ is chosen arbitrarily as it lies within the range (300-600 MeV/$_c$). As reported later, this was the momentum at which the π/e distinction tests in Spark Chambers were carried out.

Several intrinsic quantities of an average shower have been computed by accounting for the relative probabilities of the following mechanisms:

a) Bremsstrahlung

b) Pair Production

c) Compton Scattering

d) Multiple Coulomb Scattering

e) Collision Losses

The procedure was to follow each electron in the given material (lead) until

a) it reached the maximum depth considered.

b) it travelled backwards i.e. at an angle $> 90^{\circ}$ to the primary electron.

c) its energy dropped to below 10 MeV.

The details of the results are given in Table 3.1, while Fig. 3.1 shows the average number of electrons at various depths of the shower. Several important conclusions can be drawn from these results. Firstly, the maximum development of an average shower occurs at a depth of 2-3 radiation lengths, and most of the multiplication is contained between 1-4 radiation lengths. Secondly, it is not of great value to follow a shower to depth $>$ 10 radiation lengths. Thirdly, it should be stressed that Fig. 3.1 represents only electrons with energy $>$ 10 MeV. From Table 3.1 it is clear that there are a large number of electrons with energy 10 MeV which, if present in a spark chamber should be detected along with the higher energy electrons.

3.4 Special Requirements on Spark Chambers

The detection of electron showers imposes several special requirements on the construction and operation of Spark Chambers which are discussed in this section. However, the relevant features of electron

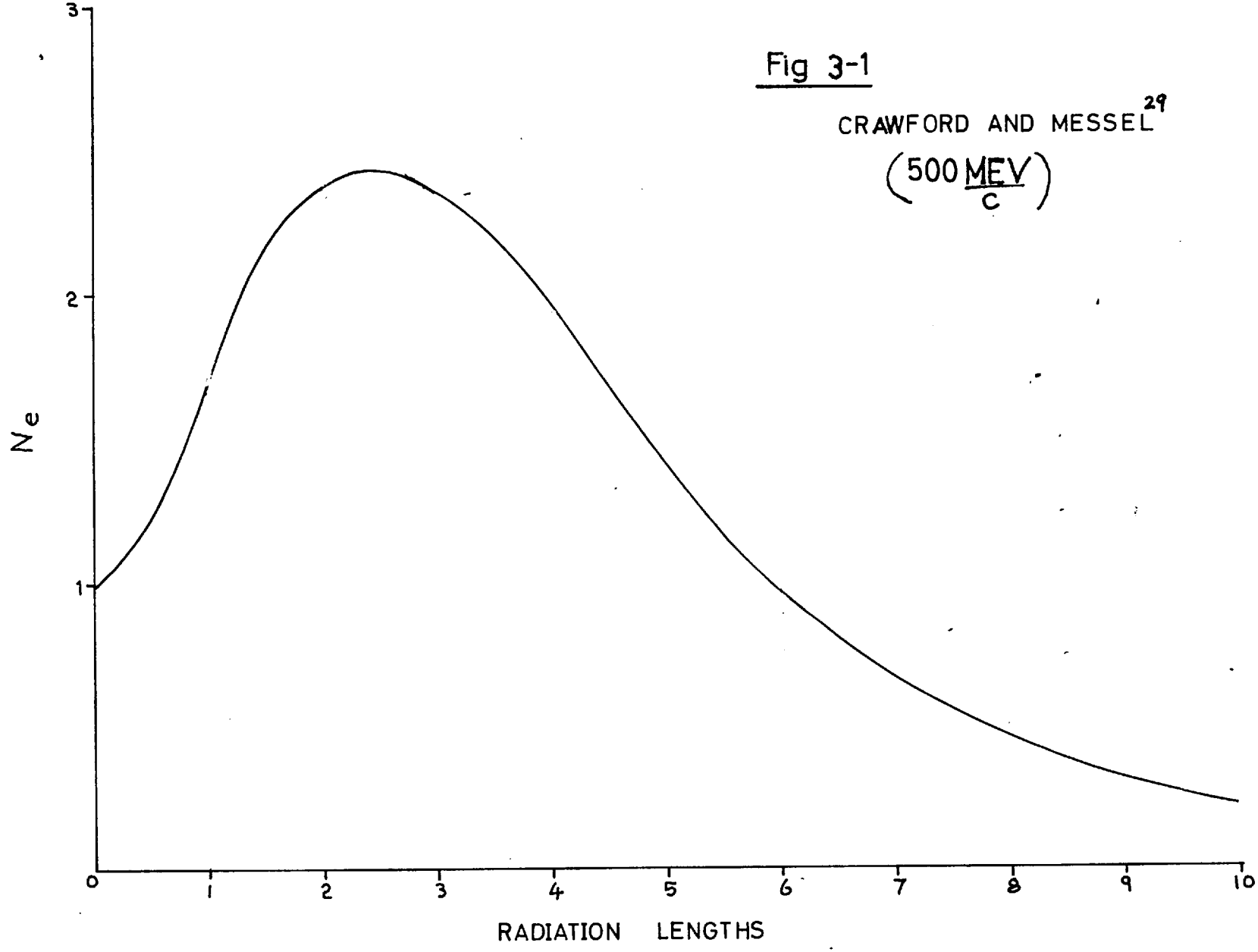

Fig 3-1
CRAWFORD AND MESSEL[29]
(500 MEV/C)
N_e
3
2
1
0
1
2
3
4
5
6
7
8
9
10
RADIATION LENGTHS

Table 3.1

Details of a 500 MeV shower in Lead.[29]

Depth (Radn. Lengths)	Number of Electrons <10MeV	Number of Photons <10MeV	Number of Electrons >10 MeV	Number of Photons >10MeV	Total Energy of electrons and photons (>10MeV)
1	0·5	8·7	1·8	2·9	468 MeV
2	1·3	13·7	2·4	4·7	408 "
3	2·0	15·6	2·5	5·2	330 "
4	4·2	29·2	2·0	5·0	250 "
5	3·8	21·5	1·4	4·4	184 "
6	3·0	16·1	1·1	3·7	135 "
7	2·6	11·8	0·7	3·0	97 "
8	2·0	8·1	0·5	2·3	68 "
9	1·5	5·5	0·3	1·8	48 "

showers which impose these restrictions are summarized first.

(i) From a single electron the shower develops to a maximum number of electrons (2-6) in a few radiation lengths of lead. The linear separation of these electrons may be as small as ~ 1 cm.

(ii) Quite a large number of photons of varying energies are present in the shower which materialize in the lead plates.

(iii) The shower proceeds in the direction of the incident electron in a cone of small angle.

The requirements imposed by (i) can be split up into two parts, (a) a high multiple particle efficiency for the spark chambers, and (b) the ability to record precisely, the information supplied by the chambers.

(a) Multiple Particle Efficiency

Obviously, one of the most important requirements is for the spark chambers to have a high multiple particle efficiency, to be able to record most of the shower particles. There are some encouraging results which were obtained by Faissner et al[30], in an attempt to measure the multiple particle efficiency of Spark Chambers filled with a Neon Helium mixture. The procedure adopted, was to allow the passage of several minimum ionizing particles almost normally through the chambers, and to measure the efficiency of each gap as a function of the number of particles crossing the gap. The efficiency measured was very high and even for 12 particles it did not drop below 90%. Two of their important

conclusions may be quoted here. Firstly, the wider gaps tended to have a lower efficiency than the narrower ones. (One storage condenser pulsed a pair of gaps). Secondly, although the overall efficiency of the chambers with a Helium filling was constant with the number of particles, it was lower than with a Neon-Helium mixture.

The second observation would confirm Miyamoto's theory of multiple particle efficiency[31], which requires more "seeding" electrons (electrons which initiate the spark discharge) for a higher efficiency. The number of primary electrons produced by a minimum ionizing particle per cm. is 8 for He and 20 for a 70:30 mixture of Neon Helium. Another point from Miyamoto's theory is that a fast risetime high voltage pulse on the chamber plates improves the multiple efficiency.

In practical terms, the first conditions implies that Argon would be a more suitable filling than Neon or Helium, as it produces more ion pairs per cm(40). However, it has not proved very successful in the past[32]. In addition it has a higher breakdown potential than Neon which introduces new problems of insulation from spurious breakdown.

The second condition implies that the electrons produced in the chamber by the incident particle, should not be lost due to diffusion, drift or attachment in the delay time of the high voltage pulse. The loss of electrons due to diffusion can be neglected compared to the loss due to the drift velocity. The electrons possess a drift velocity because a small D.C. potential ($\sim$ 100 Volts) is applied across the gap to clear it of unwanted ions from previous tracks. The D.C. potential

is usually adjusted so that the efficiency of the chamber drops to zero at $\sim 1\mu$ second from the instant of the passage of the particle. As the drift velocity of electrons in Neon is a very sensitive function of the impurities present, and it is usually higher with impurities, it is important not to have any impurities in the gas.

The third process due to which electrons may be lost is by attachment with oxygen, whose probability is high for low-energy[33] ($\sim$ few eV) electrons. It is very important therefore to exclude oxygen as much as possible from the gas filling.

Lastly, a doubt may be expressed at taking Faissner's results for multiple particle efficiency too seriously in the present context, as they were obtained for particles well separated from one another ($\sim$ tens of cms). In the present instance where particles are close together ($\sim$1 cm) the "robbing" effect may be much more significant. In addition, as it would depend largely on the technical specifications of the chamber and its triggering circuit, it was felt that a practical test was essential for a conclusive result.

(b) Efficient Recording of Showers

It was decided to employ photography to record the events in the spark chambers. This provides with several auxilliary problems, assuming the chambers to have a high multiple efficiency. The central problem is simply being able to record several sparks close together in any part of the chamber. The sparks on the film, should, of course, appear well resolved.

As mentioned above, a spark chamber could expect to have anything from 0-6 sparks in each gap. This immediately requires enough energy to be pulsed in each gap to photograph six sparks. A test is required to find out the minimum power required by a spark to enable its photography at a suitable aperture. The aperture is rather important because of the large depth of focus required in the chambers, which were envisaged to be $\sim$ 1 metre^2. Another related factor is the photographed width of each spark which presumably varies with the energy pulsed into it. Previous measurements (Chap. 1) had shown that a spark width $\sim$ 1 m.m. was normal. A measurement for higher power sparks however, is needed.

3.5 Construction of Spark Chambers

The restrictions imposed by showers on the operation of spark chambers were discussed in the preceding sections. There are also some details of showers, which help in deciding the method of construction of the spark chambers. Before discussing the details, it may be mentioned that it was decided to use Spark Chambers constructed with Aluminium foil electrodes glued to perspex frames. The details of construction are discussed elsewhere; here only the decision to use this method is discussed.

(i) Flexibility

As the amount of matter present in the Aluminium foils of the spark chamber is negligible, it can be assumed that the presence of the

chambers do not affect the development of the shower. It would be a simple matter to vary the amount of lead between chambers, to enable the shower to be sampled at any stage of its progress. It would also be quite simple to substitute another material for lead, if so required.

(ii) Reduction of Noise Sparks

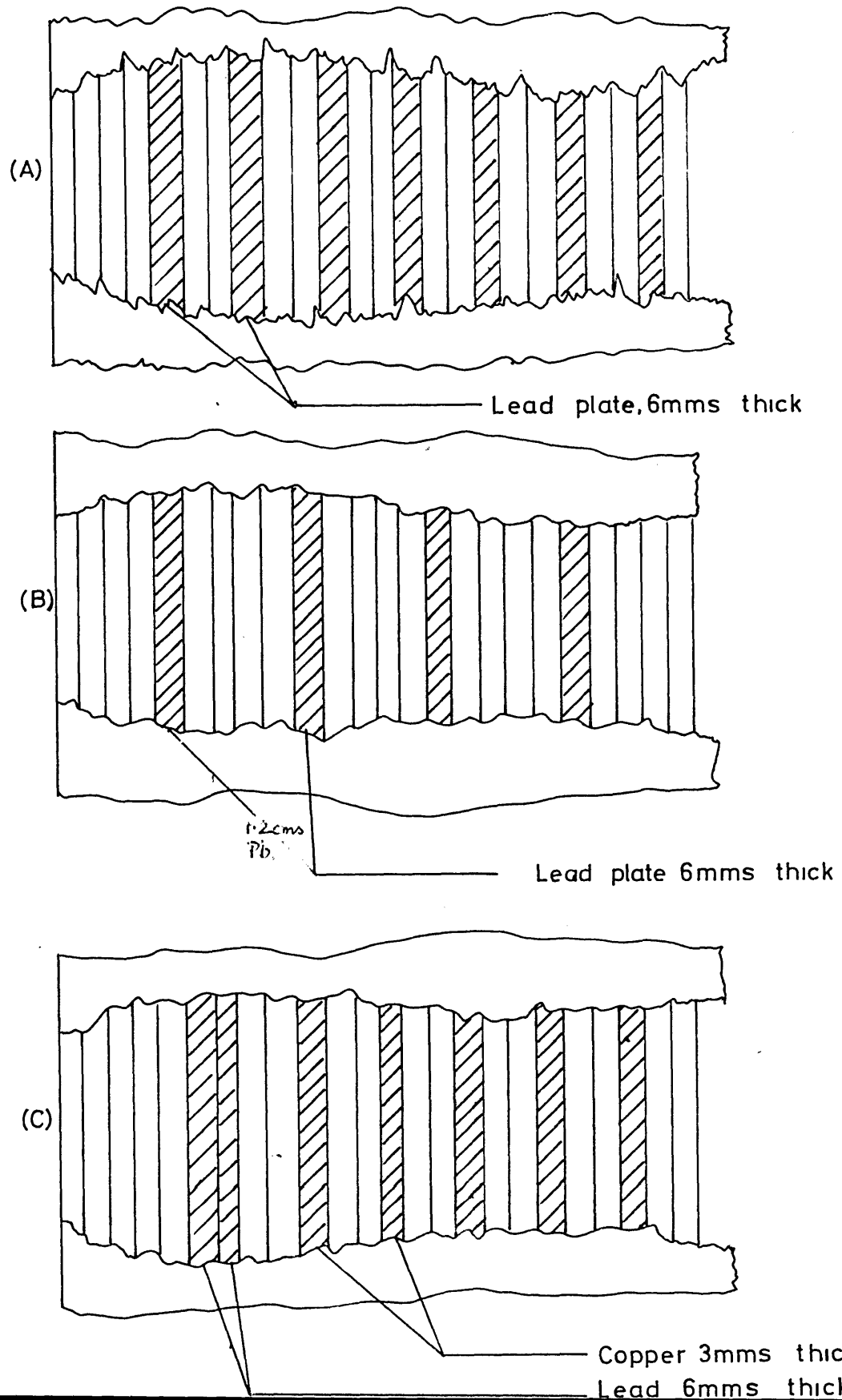
Due to the small amount of matter presented by the chambers, it should be possible to follow even a low energy electron through several successive gaps of the chamber. Consequently, an isolated spark could be counted as a spurious spark. This means that there should be several gaps between lead plates for a better identification of electrons.

A further test would be required to find out if an Aluminium foil electrode could stand up to the high powered sparks in the chamber without puncturing or distortion. It may be pointed out that the power going in a single spark could be twelve times the "normal" power required for photography if only one particle was present in the chamber which was pulsed with sufficient power for six sparks, and one gap failed to fire.

3.6 Spark Chamber Systems for Electron Detection

From the preceding discussions on electron showers, specially the average behaviour of showers, it is possible to propose two simple spark chamber systems for the detection of electrons (Fig. 3.2). Each shaded section corresponds to one radiation length of lead (0.6 cm) and the unshaded gaps represent the spark chambers. The main difference

Fig 3-2


(A)
Lead plate, 6mms thick
(B)
1·2cms
Pb
Lead plate 6mms thick
(C)
Copper 3mms thick
Lead 6mms thick

between the two arrangements is that in (b), the amount of lead used is roughly half that used in (a), and there are four gaps between lead plates instead of only two. The idea of increasing the number of gaps is to find out if it is easier to identify a shower in this case. The object of using less lead is to find out if a smaller fraction of π-mesons simulate an electron (due to the correspondingly smaller number of nuclear interactions).

A look at Table 3.1 shows that there are a large number of low energy photons present in the shower. The method described here for detecting electrons relies on the detection of these low-energy photons by their Compton scattered electrons. The electron is allowed to pass through two radiation lengths of lead where it can generate low energy photons in a small forward cone. Next two-gap Spark Chambers are separated by thin (3 mm thick) copper plates in which the photons can undergo Compton scattering. The choice of copper is dictated mainly by two facts, (a) it has nearly the same electron density as lead, i.e. Compton scattering cross-section would be about the same and (b) the multiple scattering angle is much less in copper than in lead, enabling a larger fraction of electrons to be observed in the chambers.

$$\sqrt{\frac{\langle\theta^2\rangle_{Pb}}{\langle\theta^2\rangle_{Cu}}} \simeq 1.6$$

Part III

3.7 Features of π-Interactions

This section is included mainly to estimate the behaviour of πs(500 MeV/$_c$) in lead to help in their identification later. The nuclear interaction cross-sections help to give an estimate of the fraction of pions which can simulate electrons. The processes considered here are

(i) Single and Multiple Coulomb Scattering

(ii) Diffraction Scattering

(iii) Nuclear Interactions (including inelastic scattering)

(i) The maximum value for a single Coulomb scatter is given by

$$\theta_{max} \sim \frac{\lambda\!\!\!^{-}}{r_n}$$

where r_n = radius of the Lead nucleus, and

$\lambda\!\!\!^{-} = \frac{\hbar}{p}$, p being the momentum of the π-meson.

Substituting p = 500 MeV/$_c$,

$r_n = 1.4\ (206)^{\frac{1}{3}} \times 10^{-13}$ cm,

$\theta_{max} \sim 3^{\circ}$

The multiple coulomb scattering in one radiation length of lead is given by

$$\langle \theta^2 \rangle = \left(\frac{21}{500}\right)^2 1$$

or $\langle \theta^2 \rangle^{\frac{1}{2}} \sim 2^{\circ}$

It is clear that in one radiation length of lead, single and multiple coulomb scattering is not significant for angles $> 5^{\circ}$.

(ii) The differential cross-section for diffraction scattering[34] calculated from the Optical Model (in the Black Sphere Limit) is plotted in Fig. 6.1 of Chapter 6, as a function of the angle of scattering. The maximum angle of diffraction scattering is $\sim 12^{\circ}$.

(iii) Several experiments have been done to study the inelastic scattering of π-mesons on lead and nuclear emulsions roughly in the energy range considered[35-41]. The results described here have been chosen mainly because the π-meson energy was the closest available to the energy under consideration ($p_{\pi} = 500$ MeV/$_c$, K.E. $\simeq$ 380 MeV). The experiment consisted of measuring the inelastic cross-sections for π-mesons in lead (plates) with the help of a cloud chamber. The cross-sections for the inelastic processes was as follows

σ (total) = 2200 mb

σ (stars and stops, including charge exchange) = 1600 mb

σ (inelastic scattering, with $\Delta E > 45$ MeV) = 550 mb

The energy and angular distributions of the inelastically scattered π-mesons are also presented. The mean energy with which a π-meson emerges from the lead nucleus was found to be 90 MeV. This large energy loss is explained on the basis of multiple collisions between the π-meson and nucleons inside the nucleus. The angular distribution of the inelastically scattered π-mesons was anisotropic with the forward and backward scattering being predominant. From the differential

scattering cross-section curve it is apparent that $\left(\sigma_{0\text{-}90^\circ}\right)$ inel. = $\frac{1}{2}\left(\sigma_{0\text{-}180^\circ}\right)$ inel., a figure which can help to estimate the fraction of π°s produced in the forward ($0\text{-}90^\circ$) direction.

A very elementary estimate for the cross-section of π° production can be made (Lederman[35]) using π-Nucleon cross-sections for the given energy. If R is the ratio of the charge exchange cross-section to the nuclear scattering cross-section,

$$R = \frac{Z\sigma(\pi^- p \to \pi^\circ n)}{Z\sigma(\pi^- p \to \pi^- p) + N\sigma^-(\pi^+ p \to \pi^+ p)} \qquad \because \sigma(\pi^- n) = \sigma(\pi^+ p)$$

Putting in the cross-sections[42,43],

$$R = 0.28$$

From Ignatenko[36] $\sigma_{\text{inelastic}} \simeq 550$ mb

σ (charge exchange) $\simeq$ 150 mb

and σ(charge exchange, $0\text{-}90^\circ$) $\simeq$ 75 mb, assuming that π°s have a similar angular distribution to π^-s. From this assumption, it can be stated that if all the π°s produce a shower and the π^-meson is counted as an electron, then 0.1 - 0.2% of the π's would simulate an electron in each radiation length of lead. This derivation gives only an approximate figure and cannot be expected to be very accurate.

No important restrictions are imposed on the spark chambers to detect π^-mesons. However, there are three points which arise in connection with the detection of π^-mesons.

(i) As a π-meson track does not contain any non-ionizing links (like the γ's in an electron shower) the track should appear continuous. It would be easier to recognize π's if the efficiency of the chambers were high and no breaks appeared in the track.

(ii) In a nuclear interaction, low energy (hence heavily ionizing) secondaries are expected to be produced. It is not known if the heavier ionizing track would 'rob' the lower ionizing track of its energy. Evidence[44,45] at the moment appears to favour such a possibility.

(iii) π-mesons traversing the chambers at large angles to the normal ($\sim 45^{\circ}$) may produce multiple sparks per gap, increasing the probability of electron-simulation. This clearly requires a test to find the maximum acceptable angle.

CHAPTER 4

Preliminary Tests with Aluminium Foil Spark Chambers

4.1 Introduction

The special requirements on Spark Chambers to detect electron showers and π^0-mesons in the study of the ω^0-decays were described in the last chapter. Tests with the chambers can be broadly classified into two categories:

(i) Tests involving single spark chambers

(ii) Tests involving complete spark chamber arrangements (i.e. with lead, etc.) to find the efficiency of electron detection and percentage of pions simulating electrons.

Only the tests with single spark chambers are described in this chapter, the tests consisting of:

(i) Construction of the chamber and trigger circuit.

(ii) Measurement of single-particle efficiency of the chamber

(iii) Tests involving photography (a) Power required in a spark

(b) Photographed width of sparks

(c) Depth of Focus

(iv) Power tests to test puncturing in Aluminium Foils of various thicknesses

(v) Tests on multiple sparking for large angle tracks

4.2 Construction of the Spark Chamber and Trigger Circuit

The construction of the chamber was fairly conventional[46] with

.0005" thick stretched Aluminium foil stuck on perspex frames ($\frac{1}{4}$" thick) which also acted as spacers. The Aluminium foil which was prestressed, was mirror flat, and as the perspex frames were accurately machined to $\pm$ .001", the gap separation was expected to be very uniform. There was a total of four gaps in the chamber with common manifolds for inlet and outlet of the gas which was flushed continuously. A mixture of Neon-Helium (ratio 65:35) was used for all the tests described.

Each pair of gaps in the chamber was pulsed by separate storage condensers. The electronic circuits used for triggering the chamber were practically identical to the ones described in Chapter 1 with one difference - a modified version of the Spark Gap was used for the present tests.

In principle, the Spark Gap had three electrodes enclosed under pressure in an atmosphere of nitrogen. A figure of a section of the Spark Gap illustrates the main features of construction (Fig. 4.1). The high-voltage electrode A was made out of a cylindrical metal piece with a rounded end. The earth electrode B was hollowed out along its length to allow the insertion of the trigger electrode C which was $\sim$ 1 mm in diameter. The trigger electrode was insulated from the earth electrode except near the end. The gap between B and C was .005" and the main gap which was adjustable was $\sim$1". It was possible to adjust the pressure of nitrogen in the gap up to 20 lbs/sq.in.

Tests were made to measure the breakdown time of the spark gap for two pressures. The time delays which are plotted in Fig. 4.2 represent

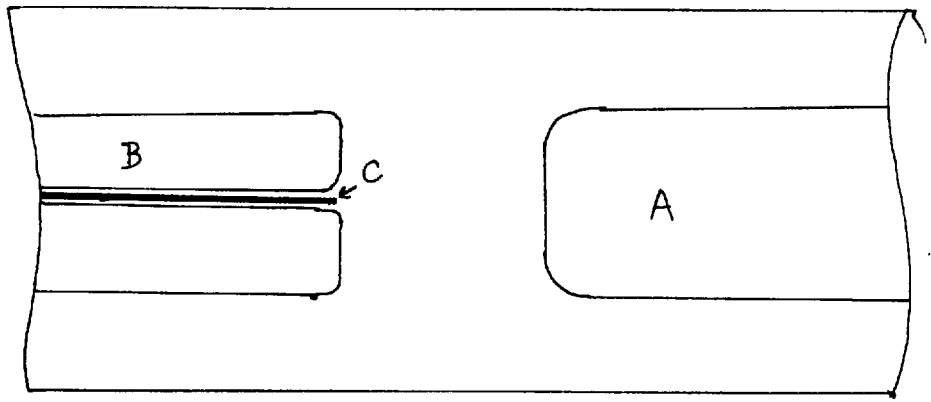
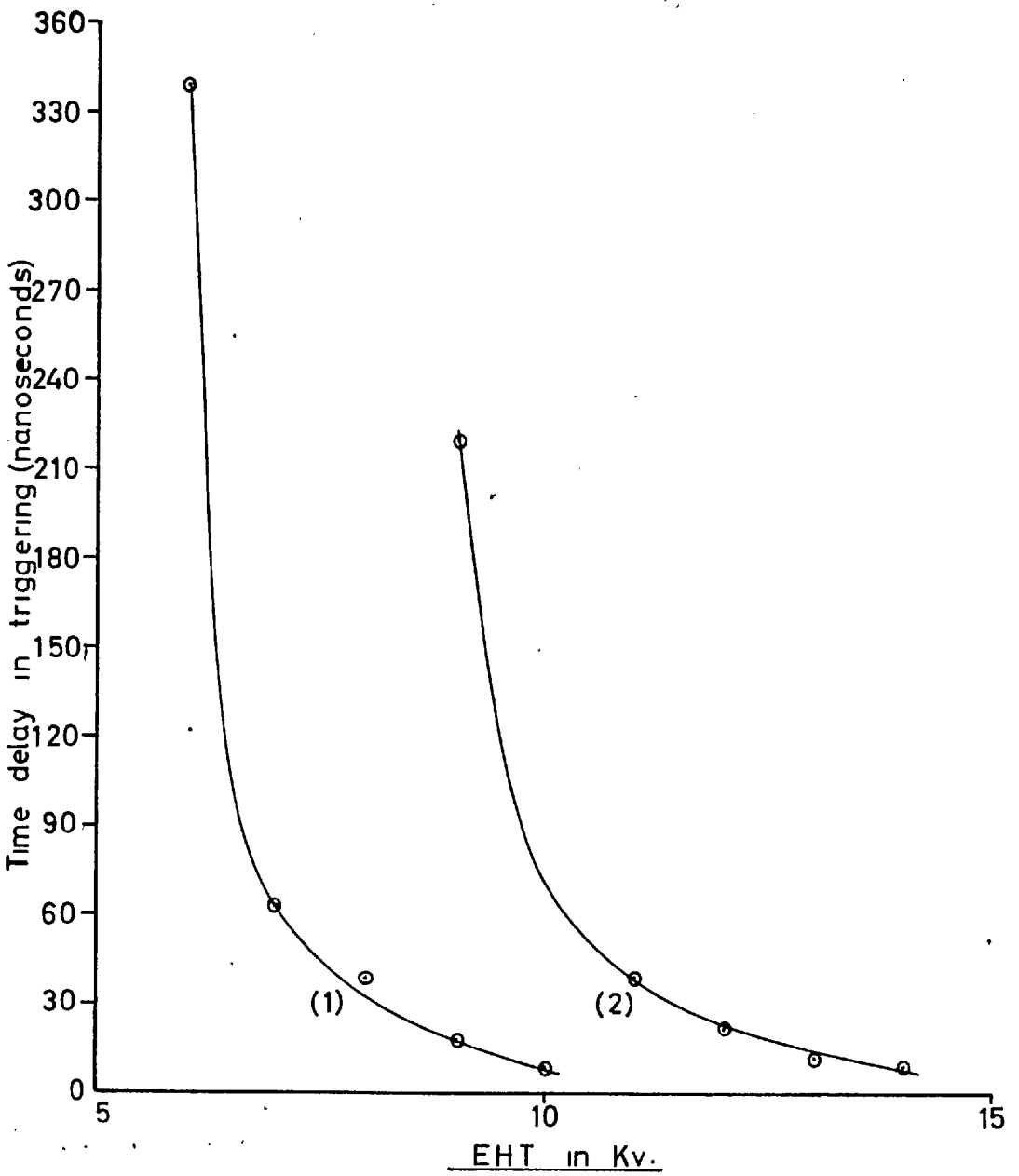


Fig 4·1

Spark Gap (Section)

Fig 4-2

TIME DELAY IN TRIGGERING THE SPARK GAP AT (1) 2lbs/sq inch
(2) 10lbs/sq inch



the time interval between the maximum voltage of the trigger pulse and the instant of breakdown in the gap. One fact that emerged from these measurements was that if the voltage on the gap was set at ~ 1 kV below the spontaneous breakdown level, the time delay in breakdown was ~ 10 n.s.

4.3 Measurement of Efficiency for Cosmic Rays

Cosmic Rays were used to measure the single particle efficiency of the chamber. The method of measuring the efficiency was the same as described in Chapter 1, i.e. it was the ratio of the number of sparks observed, to the total number of sparks that could have occurred.

The capacity of each pair of gaps was 120 pfs and the storage condenser was chosen as 180 pfs which gave rise to a voltage attenuation ratio of 0.6. The chamber was operated at 6 kV (i.e. the Spark Gap at 10 kV) which meant that if all the gaps fired singly for a track, the power going into a single spark would be 2.7 mj. Photography was carried out on Tri-X film at an aperture of f/11.

The efficiency was measured for various clearing fields and delay times. The results are summarised in Fig. 4.3 where the sensitive time of the chamber is plotted as a function of the clearing field. The sensitive time, defined as before, is the time after which the efficiency drops to $\frac{1}{e}$ of its original value. The results are in good agreement with other experiments[47]. The minimum in the sensitive time occurs at about 100 volts when the sensitive time is $\frac{1}{2}$ μs. Fig. 4.4 is included

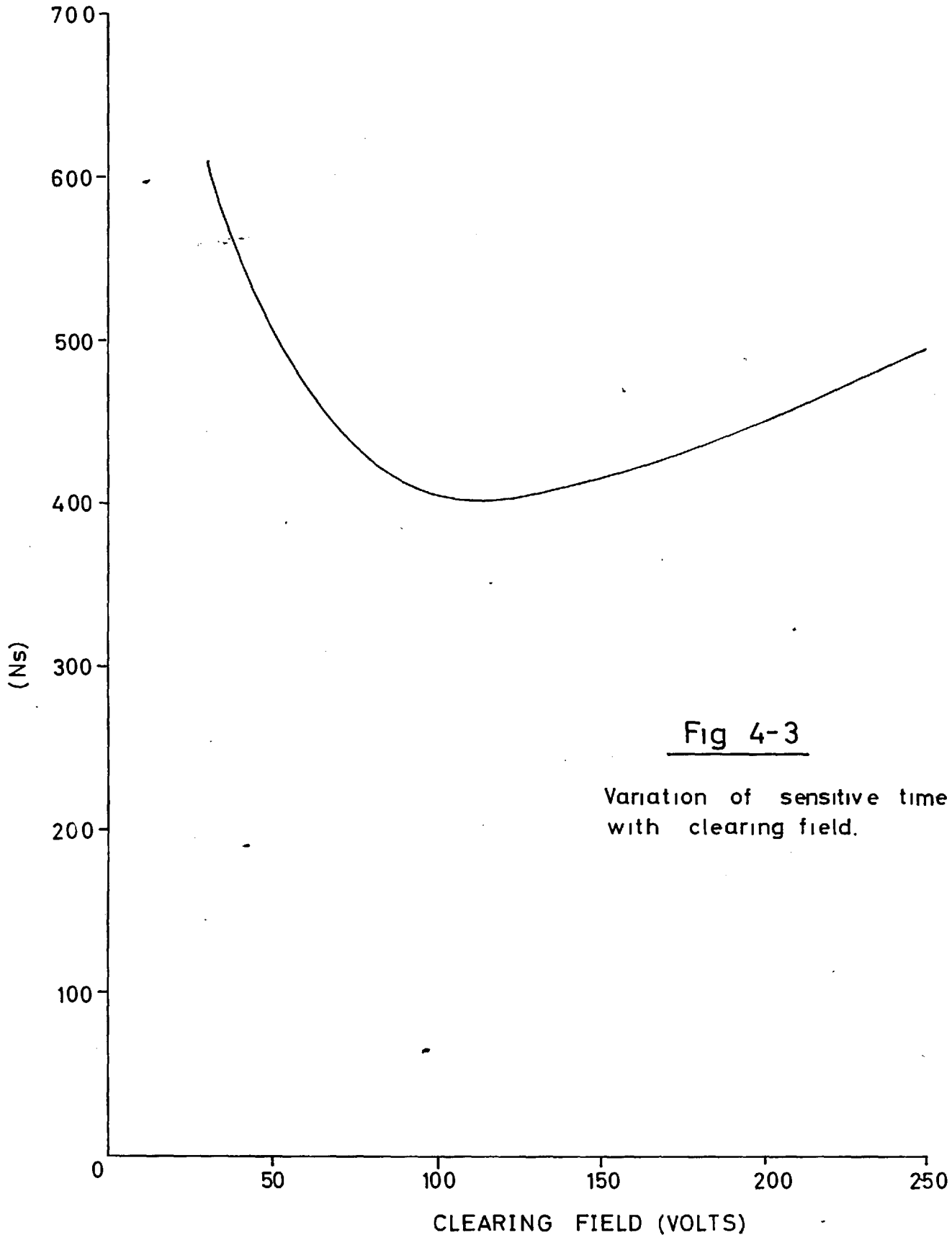
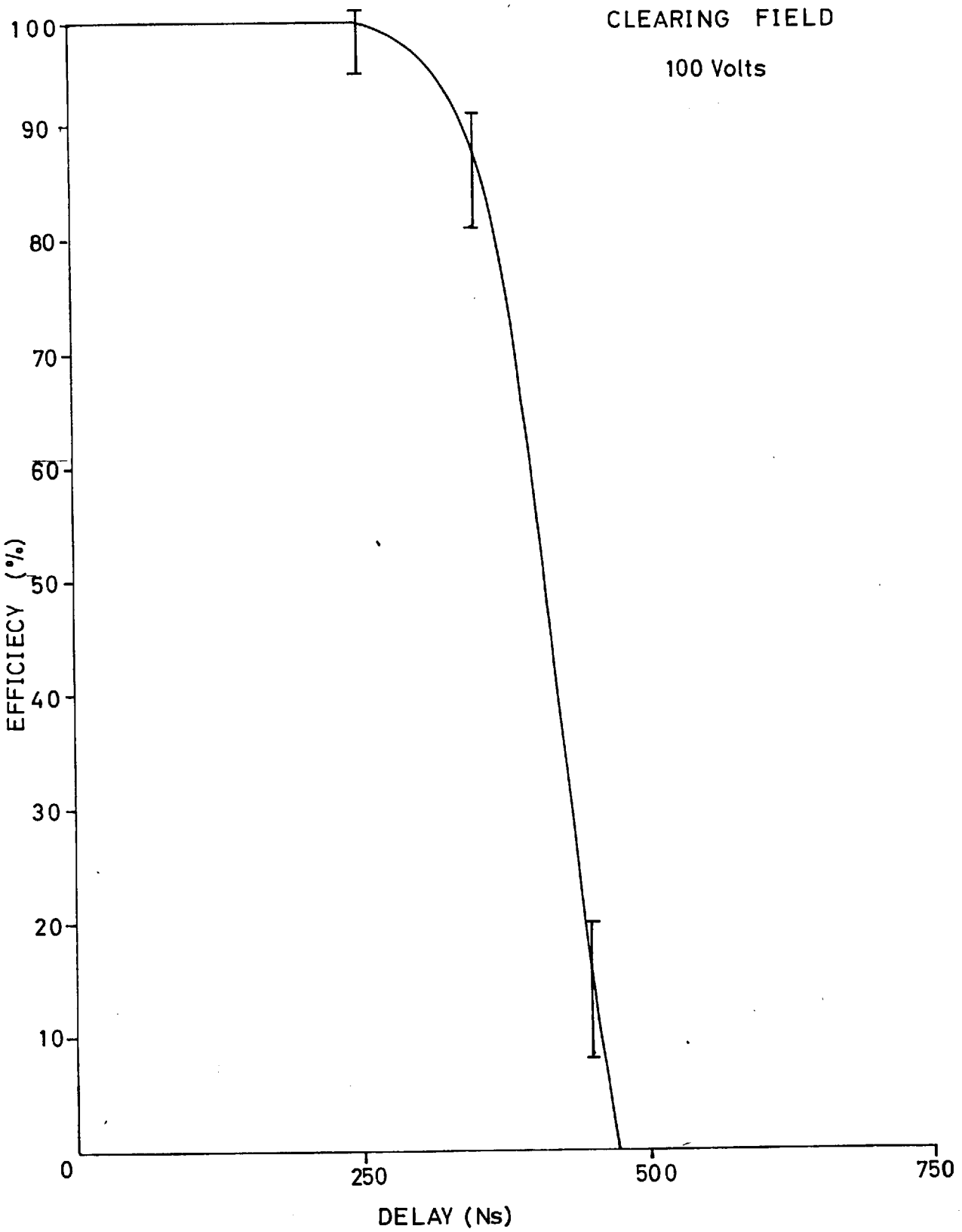


Fig 4-3

Variation of sensitive time with clearing field.

Fig 4-4


CLEARING FIELD
100 Volts
EFFICIECY (%)
100
90
80
70
60
50
40
30
20
10
0
250
500
750
DELAY (Ns)

to illustrate the variation of the Spark Chamber efficiency as a function of the delay in triggering for a 100 volts clearing field.

4.4 Photography

A reasonable figure for the power needed to photograph sparks at f/11 was found to be 3 mj. With this power the sparks appeared about 1 mm wide (as projected back in the chamber) on the film. The width of the spark appeared to increase with the power in the spark, presumably due to halation in the film, etc. It was found, for instance, that with an 18 mj spark the width was ~ 2 mms.

The increase in the width of the spark with power introduces a new problem in the detection of electron showers which is as follows: If a gap is pulsed with sufficient power for six sparks and only two occur close together, would it be possible to distinguish them, or would they appear as a single thick spark? It may be recalled that it is necessary to pulse the chamber with high power to enable the recording of electron showers (Chapter 3) and that in electron showers the several particles in the chamber are expected to be close to each other (Chapter 3). Photographs of electron showers in Chapter 6 illustrate the nature of the problem.

4.5 Power Tests

The strength requirements of the Aluminium foil are clear from the preceding discussion on the power needed to photograph a single spark and the maximum number of sparks likely to be present in a gap simultaneously.

Assuming that the maximum number is 6, the gap should be pulsed with ∿ 18 mj in every trigger. As one storage condenser is used to trigger a pair of gaps, in the event of one gap not firing, the maximum power input in the other one would be ∿ 36 mjoules which sets the minimum strength requirements on the Aluminium foil.

Three spark chambers were constructed using Aluminium foil of different thicknesses ($\frac{1}{2}$, 1 and 2 thousandth of an inch). The chambers were connected to high voltage pulsers which triggered at a predetermined rate. The energy being pulsed could be varied by a choice of storage condenser and the voltage. A radioactive source was pointed towards the chambers (emitting particles normal to the gaps) and its position was so adjusted that on the average, one spark occurred in the chamber for each trigger. The area covered by the radioactive source was about 10 sq.cms. of the chamber.

Table 4.1 shows the results of the experiment, from which, somewhat roughly, the maximum power inputs into chambers of different thickness Aluminium foils can be deduced as

.0005"	Al. foil	P_{max}	∿	30 m.j./gap
.001"	"	P_{max}	∿	80 m.j./gap
.002"	"	P_{max}	∿	150 m.j./gap

From these figures it seemed safe to use .001" thick Aluminium foils in Spark Chambers for the present tests.

Table 4.1

Number of Triggers 10^4

Thickness of Foil	Power in Sparks (m-joules)	Effects
.0005"	20	None
	30	None
	80	Bad pitting
	240	Punctured
.001"	80	Very slight pitting
	120	Slight pitting
	160	Pitting
	200	Punctured
.002"	80	None
	120	None
	160	Very slight pitting
	200	Pitting

4.6 Measurements on Angular Tracks

When a charged particle traverses an efficient chamber normal to the plates, it produces a spark in every gap, the sparks being normal to the plates. When the particle travels at an angle to the normal, however, there is some probability that it would produce more than one spark in a gap. (These remarks do not apply to the "special" chambers[48] where the sparks are made to follow the trajectory of the particle). A theoretical estimate of the number of sparks per gap as a function of the angle of the incident particle to the normal can be made with the help of the theory of spark formation. The theory has been specially applied to this problem by Fuku[49].

Consider a gap (Fig. 4.5) through which a charged particle passes at an angle θ to the normal with two electrons liberated at A and B, the distance AB = ℓ cms. When the electric field is applied across the gap, the electrons produce an avalanche in which the electrons are concentrated in the front semi-sphere whose radius is given by

$$r = \sqrt{4Dt}$$

where

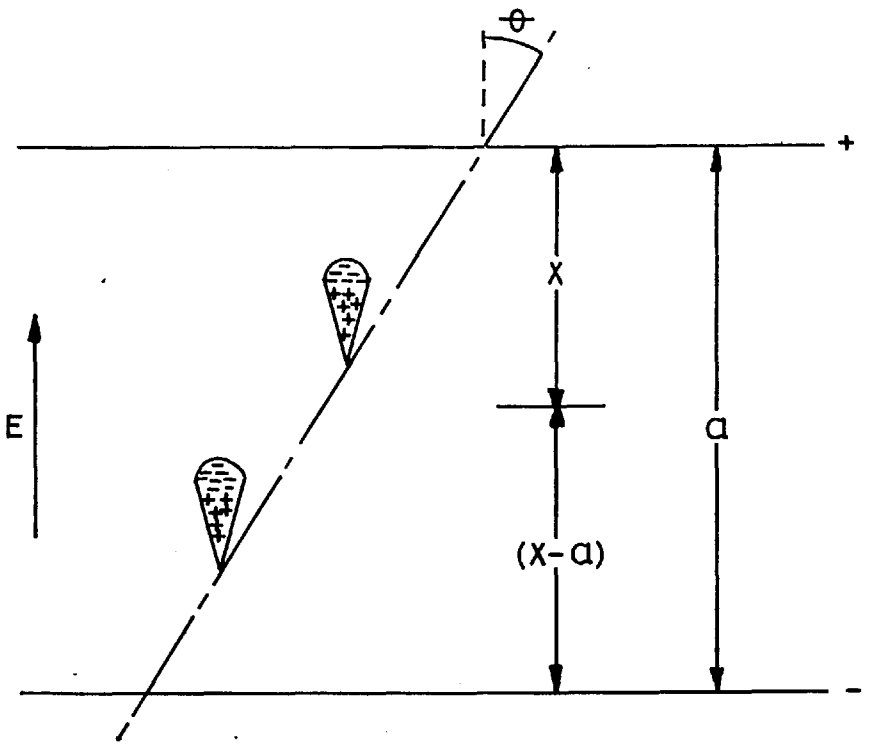
D = the coefficient of diffusion for the electrons in the gas, and

t = the time during which the electrons are allowed to diffuse.

In Neon, with an electric field 10 kV/cm, the coefficient of diffusion is 81. 10^2 cm^2 per second[50,33]. Another way of expressing t is,

$$t = \frac{\text{distance travelled by the avalanche}}{\text{drift velocity of electrons}}$$

Fig 4-5 and 4-6



SPARK FORMATION IN A LARGE ANGLE TRACK.

Since the Breakdown condition is, approximately[51]

$\alpha d \geq 20$ (α = Townsend's First Coefficient)

and for Neon with an electric field of 10 kV/cm,

$\alpha = 70$

$d = 3$ mms

Substituting the drift velocity of electrons, = 14×10^6 cms/sec,

$\ell \simeq 0.25$ mm

According to Fukui, if $\ell < 3\ell$, the space-charge field between the avalanches is strong and the streamer forms along the space charge field. If $\ell > 3\ell$, the externally applied field is stronger and the two avalanches develop into two sparks.

In Fig. 4.6, if the gap width is represented by 'a', and the insensitive volume of the gap by x, multiple sparks should be expected for

$(x-a) \cos\theta \geq 1$ mm

i.e. $\theta \geq 20^\circ$ ($x-a = 3$ mms)

According to Fukui, the number of sparks in a gap is given by the relation

$$N = \frac{A}{\cos\theta}$$

where A depends on the operating conditions of the chamber but is usually $\simeq 1$.

Experimental tests on angular tracks were carried out with the Spark Chamber described earlier in this Chapter. The main object was

to find a relation between spark multiplicity and the angle of the track, and a secondary object was to find out the appearance of a single particle track at various angles.

The chamber was triggered on Cosmic Ray particles at large angles to the normal to the plates. The geometry of the counters was so chosen that the particles made a large angle to the normal in one plane, while the angle was $\lesssim 10^{\circ}$ in the plane at right angles to the first. Photographs were taken only in the first plane, with a 7" focal length lens at f.11 using Tri-X film. A typical large angle track is shown in Fig. 4.7.

The experimental results are shown in Figs. 4.8 and 4.9. The former shows the percentage of multiple sparks as a function of the angle of the track. It is apparent that the fraction of multiple sparks increases rapidly with the angle and at 60° about half the sparks are accompanied by a "sattelite" spark. Another parameter measured was the distance between the sparks under question. Fig. 4.9 shows the percentage of sparks which appear to be spaced apart by 1 mm or more as a function of the angle of the track. (When more than two sparks were present, separation was measured between the extreme sparks only). It appears that a larger number of widely spaced sparks is obtained with larger angle tracks, as would be expected.

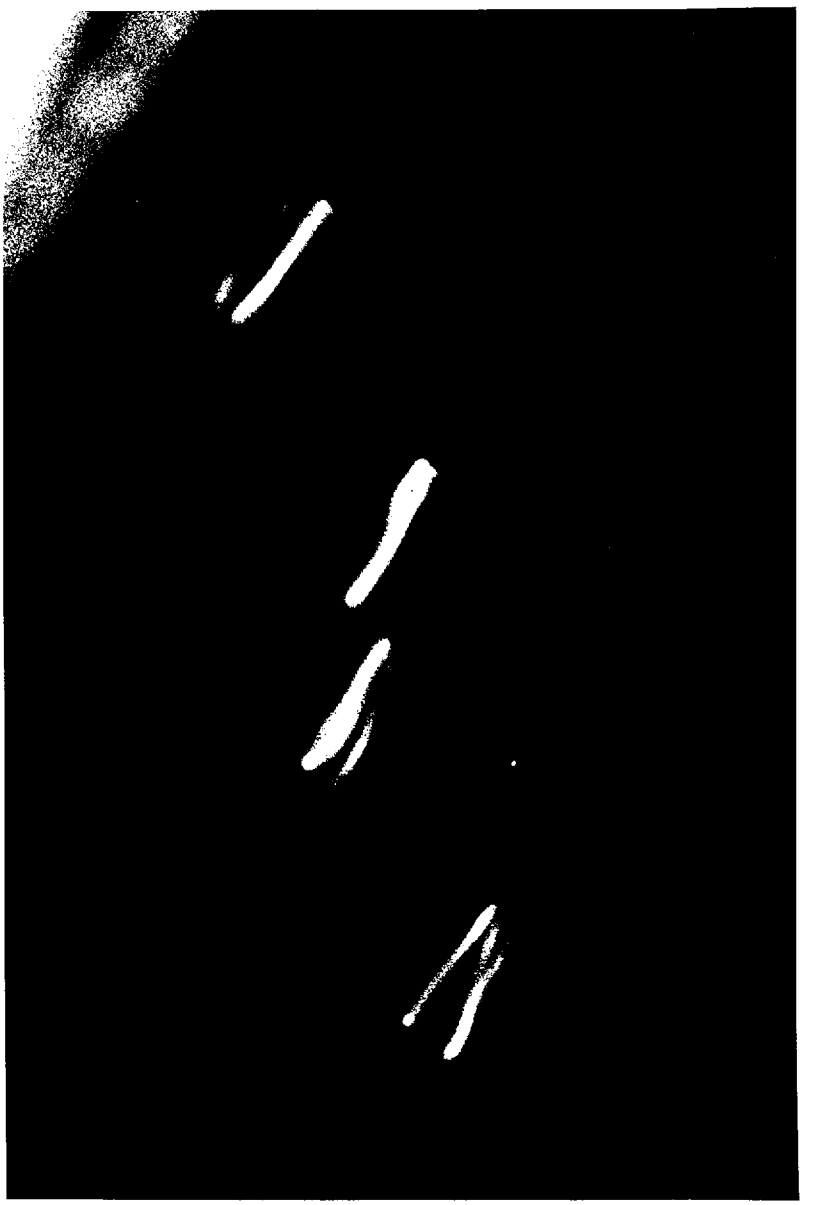


Fig 4.7

Fig 4-8

PERCENTAGE OF MULTIPLE SPARKS AS A FUNCTION OF THE ANGLE OF THE TRACK.

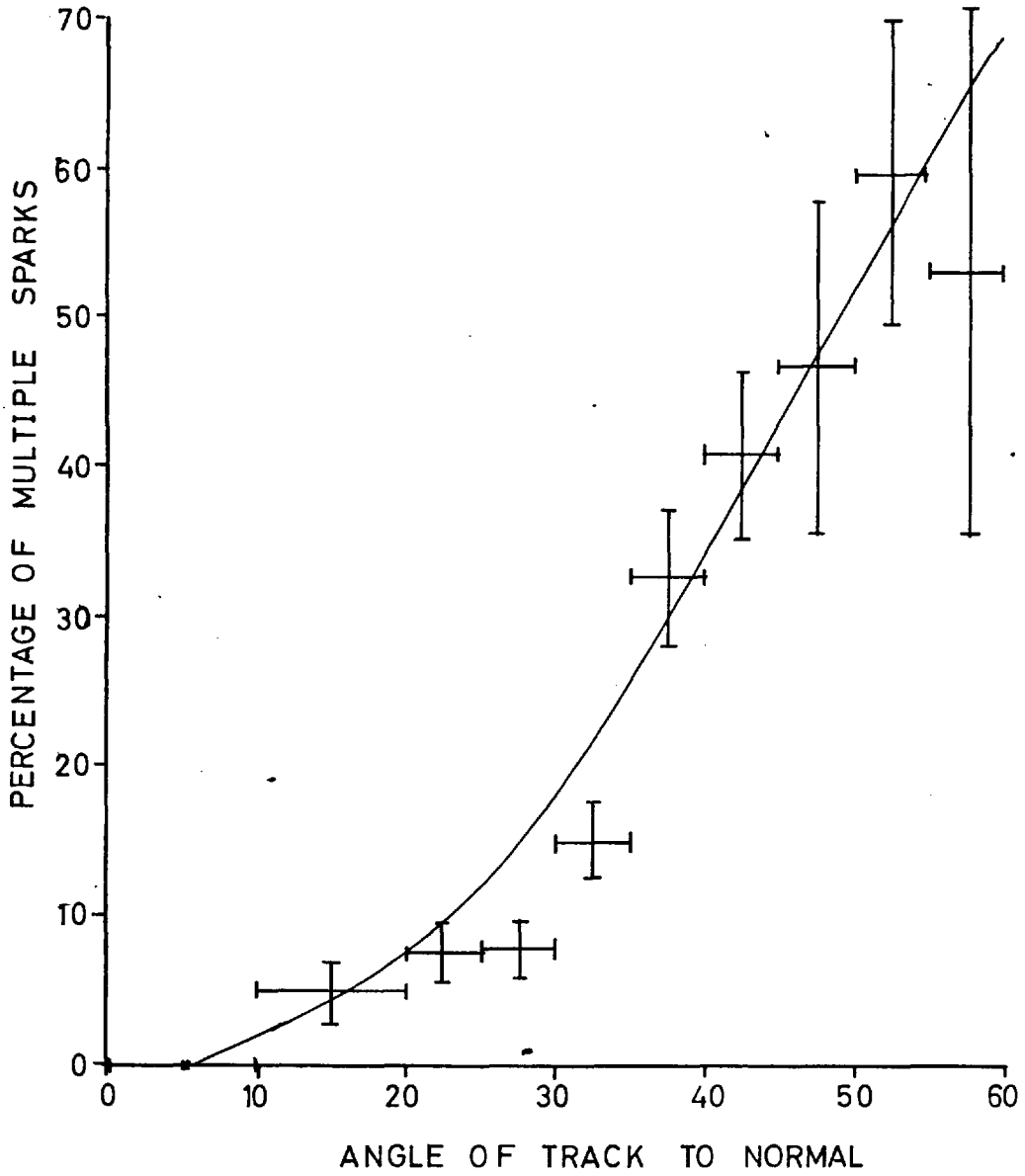
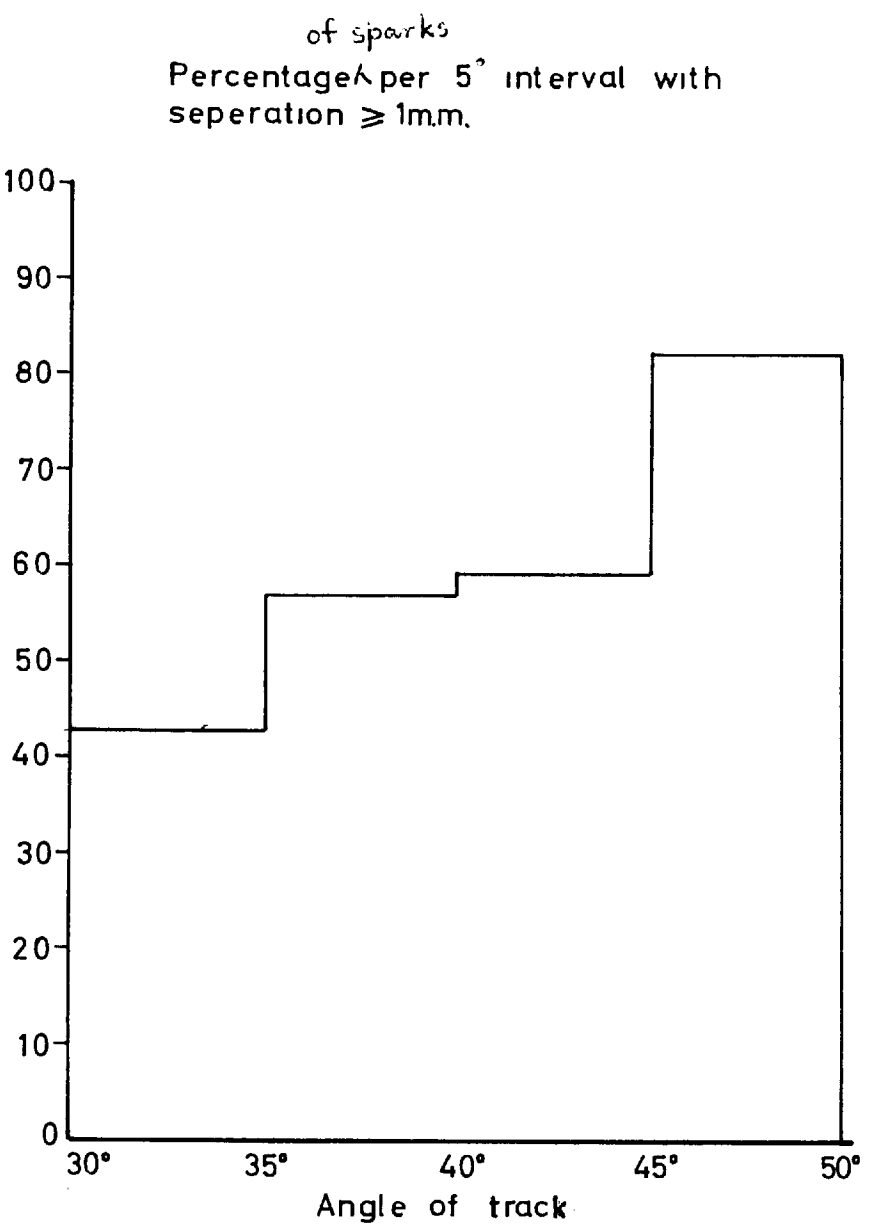


Fig 4-9


of sparks
Percentage per 5° interval with
seperation ≥ 1m.m.
100
90
80
70
60
50
40
30
20
10
0
30°
35°
40°
45°
50°
Angle of track

CHAPTER 5

Description of Experimental Set-Up at N.I.R.N.S.

5.1 Introduction

The need to measure the percentage of π-mesons simulating electrons (π_s) at 500 MeV/$_c$, and the efficiency of electron detection (η_E) at the same momentum, was emphasized in Chapter 3. It may be recalled that these two factors are of vital importance in the study of β-decay. Most of this chapter is devoted to a description of the experimental arrangements used for determining π_s and η_E.

5.2 The Beam Composition

A focussed 500 MeV/$_c$ beam of negative π-mesons was obtained on the π-2 beam line at the 7 GeV Proton Synchrotron, NIMROD, at the National Institute for Research in Nuclear Science. The requirements on the beam were not very stringent as only one event per machine pulse could be photographed. The flux in the beam was $\sim 10^2$ particles per second.

The Cerenkov Counter (see Section 5.3) was employed to find the electron component of the beam and it was assumed that π-mesons and μ-mesons made up the remaining part of the beam. The fraction of μ-mesons was found (see Section 6.3) by scanning the ($\pi+\mu$) tracks and searching for nuclear interactions in the lead plates. The following results were obtained:

Percentage of electrons in the beam $\sim$ 30%

Percentage of ($\pi+\mu$)-mesons in the beam $\sim$ 70%

Percentage of μ-mesons in (π + μ)-mesons component 15%

Percentage of π-mesons in the beam 60%

Percentage of K-mesons in the beam 10%

To photograph π-mesons, the electron contamination of the beam was reduced by inserting a 3 mm. thick lead plate in the beam just before the last bending magnet. With the lead plate in position, the percentage of electrons was found to be $\sim$6%.

5.3 The Cerenkov Counter

The main purpose of the Cerenkov Counter was to detect electrons in the beam with a high efficiency. The Cerenkov Counter was used in coincidence with the beam counters to photograph electrons in the Spark Chambers. To photograph π-mesons, the Cerenkov Counter was used in anti-coincidence with the beam counters.

Cerenkov light is given off at an angle θ, by a charged particle travelling at a velocity c in a medium of refractive index n, according to the relation

$$\text{Cos } \theta = \frac{1}{\beta n} \qquad (1)$$

The number of photons emitted within the spectral region defined by the wavelengths λ_1 and λ_2 is[52]

$$N_{ph} = 2\pi\alpha d \left(\frac{1}{\lambda_2} - \frac{1}{\lambda_1}\right) \text{Sin}^2\theta \qquad (2)$$

where $\alpha = \frac{1}{137}$

Between the wavelength limits 3500-5000A$^{\circ}$, (the sensitive range for an Antimony-Caesium photocathode)

$$Nph = 400\, l\, \sin^2\theta \qquad (3)$$

The efficiency of the Cerenkov Counter for electrons of 500 MeV/$_c$ momentum, was measured indirectly by measuring the efficiency for π-mesons of 2.2 GeV/$_c$ momentum. The measurement was based on the assumption that the efficiency of the Cerenkov Counter was only a function of Nph (or θ), if the other factors, viz. light collection efficiency, gain of the photomultiplier etc. were kept constant. Fig. 5.1 shows the variation of Nph with the pressure of Arcton 12 in the chamber and Table 5.1 shows the variation of the measured inefficiency of the counter as a function of the Arcton 12 pressure. From these measurements it was decided to operate the Cerenkov counter at 55 p.s.i. for 500 MeV/$_c$ electrons. At this pressure, Nph = 321, therefore the percentage of electrons which failed to be recorded was expected to be $\lesssim$ 2% (See Table 5.1).

Due to the slight inefficiency in the Cerenkov Counter, it was expected that a small number of electrons would be selected as π's during the photography of π-mesons. This number was $\sim$ 0.1% which was obtained by multiplying the inefficiency of the Cerenkov Counter ($\sim$ 2%) with the electron contamination in the beam during the π-run ($\sim$ 6%).

The reverse problem, i.e. π-mesons being selected as electrons arises due to the possibility of a knock-on electron triggering the Cerenkov Counter. The number of knock-on electrons can be estimated as follows:

The probability of knock-on electron production (with energy $>$ E)

Fig. 5-1

PHOTON YIELD OF 2·2 Ge$^{V}/_{c}$ π^{-} MESONS IN ARCTON 12 FOR VARIOUS PRESSURES.

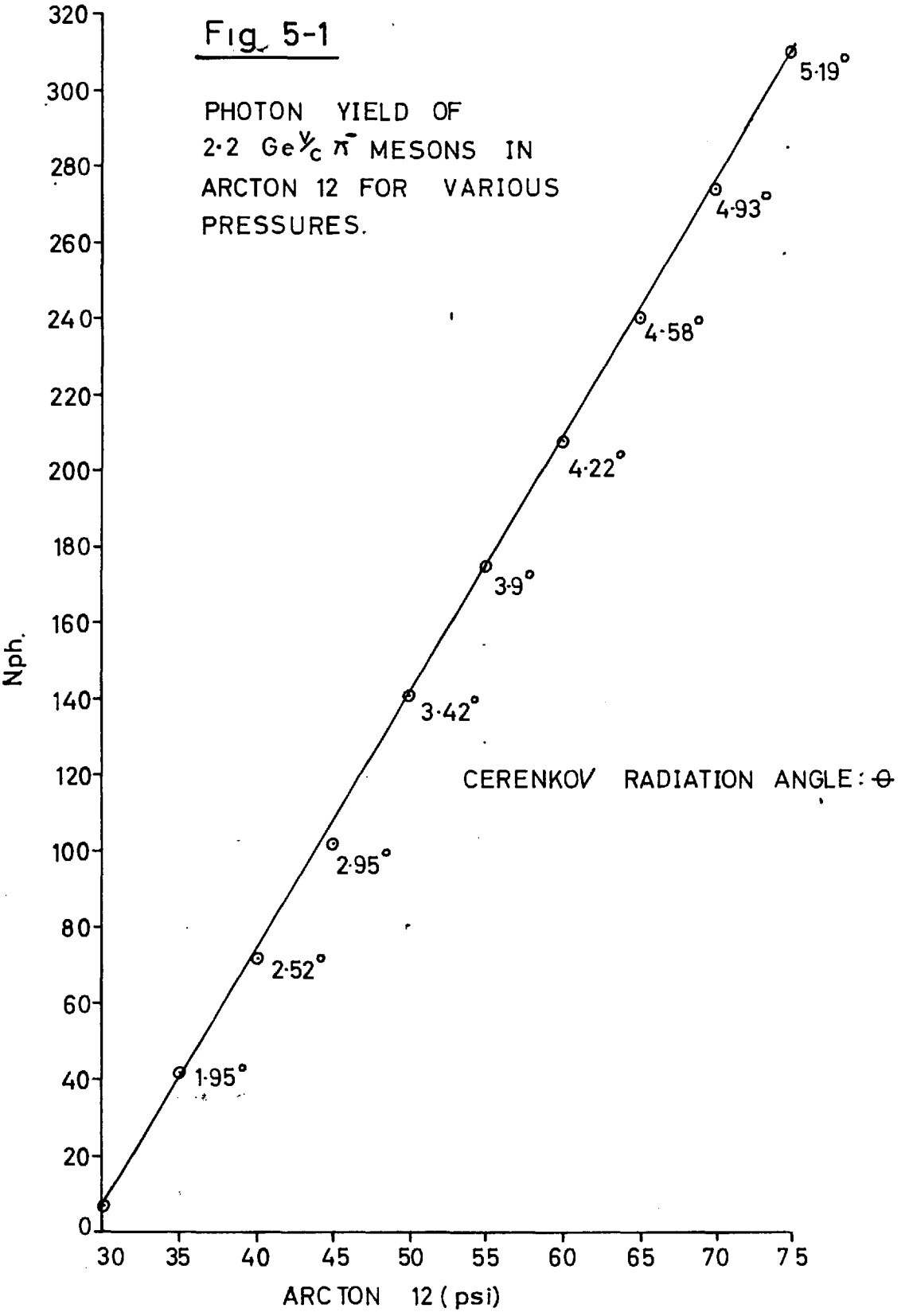


Table 5.1

Pressure (absolute) (p.s.i.)	$(n-1).10^5$	Nph.(calc.)	θ calculated	Percentage of particles not recorded (measured)
15	108	-	-	98.1 ± 3.1 %
20	146	-	-	95.1 ± 3.0 %
25	184	-	-	93.7 ± 3.0 %
30	220	7	.75°	58 ± 2.4 %
35	260	44	1.95°	39 ± 2.0 %
40	300	73	2.52°	30 ± 1.7 %
45	336	104	2.95°	26 ± 1.6 %
50	380	142	3.42°	21.4 ± 1.5 %
55	422	176	3.90°	14 ± 1.2 %
60	468	208	4.22°	7.2 ± 0.8 %
65	510	240	4.58°	5.8 ± 0.8 %
70	555	275	4.93°	3.5 ± 0.6 %
75	559	309	5.19°	1.7 ± 0.4 %

in a given medium is given by[53]

$$P(E)dE = W \frac{dE}{E^2} \tag{4}$$

where

$$W = 0.15 \frac{Z}{A} x \frac{1}{\beta^2} \quad \text{MeV} \tag{5}$$

x in $gms/_{cm^2}$ is the amount of matter traversed

β is the velocity of the incident particle

Z is the Atomic Number of the medium

A is the Atomic Weight of the medium

Integrating (4)

$$P(E_{min} - E_{max}) = \frac{W}{E_{min}} - \frac{W}{E_{max}} \tag{6}$$

where E_{min} = 5 MeV is the threshold for the production of Cerenkov radiation at the given pressure.

E_{max} = 11.5 MeV for a 500 $MeV/_c$ π-meson

Substituting E_{min}, E_{max} and W in (6)

$P(E_{min} - E_{max}) = .019$

∴ Number of π-mesons expected to be counted as electrons due to the production of knock-on electrons ~ 2%. This estimate is too high for the following reasons:

(i) During the "electron runs" the gain of the Cerenkov counter was lowered to reduce the efficiency to ~ 50%.

(ii) Some knock-on electrons would be produced near the end of the counter, reduing their chances of detection.

(iii) The efficiency of detection for electrons just above threshold will be low.

(iv) Some knock-on electrons will be given off at large angles to the incident particle and not be detected.

It is difficult to estimate (iii) and (iv), but putting in a factor 0.5 for (i) and 0.75 for (ii),

$P_{(\text{Knock-On Electron})} \simeq .007$

As only 30% of the beam consisted of electrons, 1.5% of the electrons would be expected to be really π -mesons counted as electrons.

5.4 The Spark Chamber Arrangements and Associated Electronics

The complete experimental arrangement is shown schematically in Fig. 5.2. The counters and the Spark Chambers were mounted on a trolley whose height was adjusted to the beam level. The description of the apparatus can be divided into two groups:

(i) Description of the Spark Chamber Arrangements, and

(ii) Description of the Counter Selection system and the trigger circuit.

The Spark Chambers were constructed to a standard size - the internal dimensions being (20 x 20) cms^2 and with a gap width of 0.6 cms. Except the first, all the chambers were two-gap modules constructed of 0.001" Aluminium foil and protected by Melinex foil on both sides. The first chamber had 4 gaps and was constructed with .0005" Aluminium foil. The method of constructing the chambers was the same as described in Chapter 4.

The Spark Chambers and the lead plates were mounted on a Dural

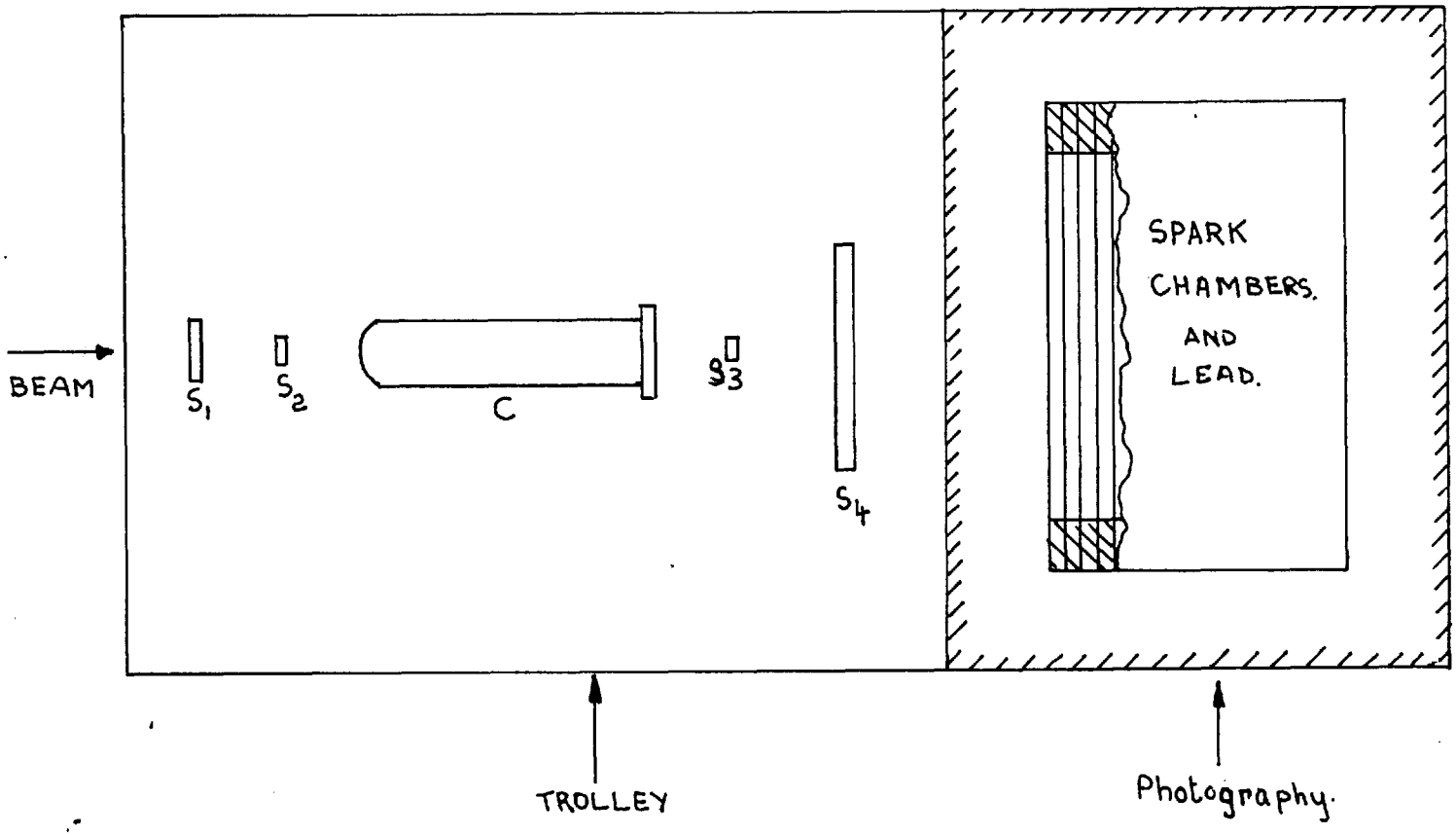


Fig 5-2

THE EXPERIMENTAL ARRANGEMENT.

base plate which was later attached to the trolley. It was a simple matter to swing the whole arrangement through 45°, to photograph π's and e's traversing the arrangement at 45°.

The chambers were flushed with a Ne-He mixture for several hours before the run and once they were operational, the flow rate was reduced to a minimum. The gas was supplied to the chambers from one cylinder with the help of a manifold, effectively putting them all in parallel. The flow was monitored constantly throughout the run to prevent "starvation" of any chambers.

Each chamber was triggered by an independent Slave Spark Gap with a 1000 pf storage condenser. (Except for the first 4-gap chamber, which was pulsed by two 1000 pf storage condensers.) The power pulsed in each gap of the chambers was $\sim$ 25 mj which was sufficient for $\sim$ 8 particles (See Chapter 4).

Photography of the Spark Chambers was carried out at f/8 using Kodak Tri-X 35 mm film, in two views; the firect view and at 90° (with the help of a plane mirror). The film was automatically advanced after each exposure with the help of a motor tirggered by the coincidence circuit.

Four Spark Chamber Arrangements were tested in all. Fig. 3.2 shows three of them, the fourth being the same as 3.2(a) except for the fact that the beam was incident at 45°.

(I) A 4-gap chamber was followed by a lead plate, 0.6 cm thick (= 1 Radiation Length). The rest of the arrangement consisted of a

succession of 2-gap chambers and Lead plates, one radiation length thick. In all 9 radiation lengths of lead was used. Photographs of π -mesons in this arrangement were labelled "F.1" and electrons, "F.2".

(II) The first 4-gap chamber was followed by a 1.2 cm thick lead plate. The rest of the arrangement consisted of two, 2-gap spark chambers and 0.6 cm. lead plate, repeated three times, i.e. in all 5 radiation lengths of lead were used. The π's and e's in this arrangement were labelled F.3 and F.4 respectively.

(III) As mentioned earlier, this was simply the first arrangement swung through 45°. The πs and es in this arrangement were labelled F.5 and F.6 respectively.

(IV) The first 4-gap chamber was followed by a 1.2 cm lead plate. After this there was a succession of 2-gap chambers and 3 mm thick copper plates, in all, 8 copper plates were used. The πs and es in this arrangement were labelled F.7 and F.8.

Figs 5.3 shows the counter selection system and the ancillary electronics schematically. Outputs from S_1, S_2 and S_3 were fed into CO1, the first coincidence circuit. The output from the large counter, (15 cms^2). S_4 was fed into CO2 through a Rationer whose function was to prevent a pulse getting through if there had been a pulse within the last microsecond. This was to prevent photography of a track in the presence of an 'old' track. The target pulse, received from the Main Control Room, opened a 'gate' for 100 m seconds ensuring that only

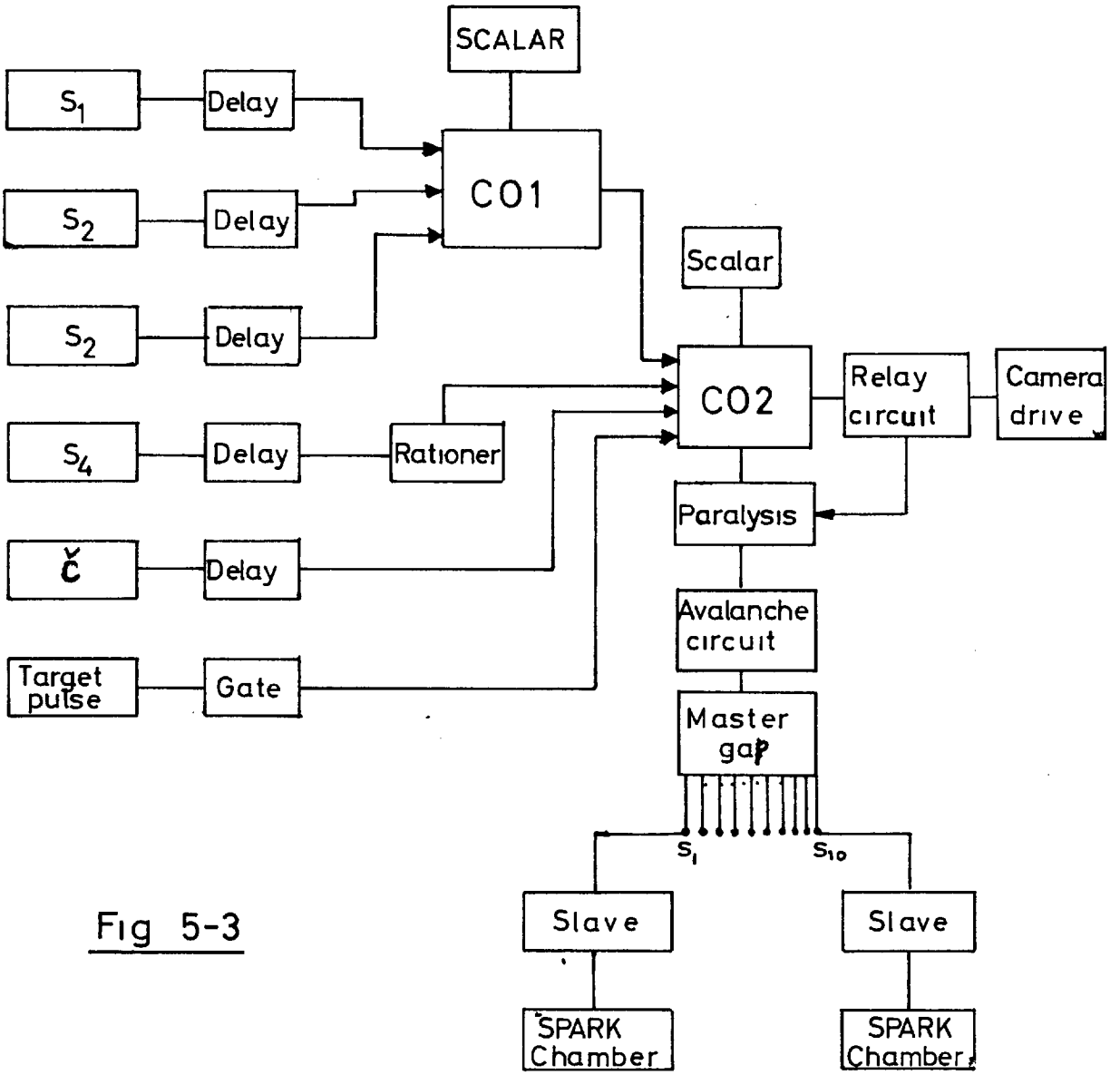


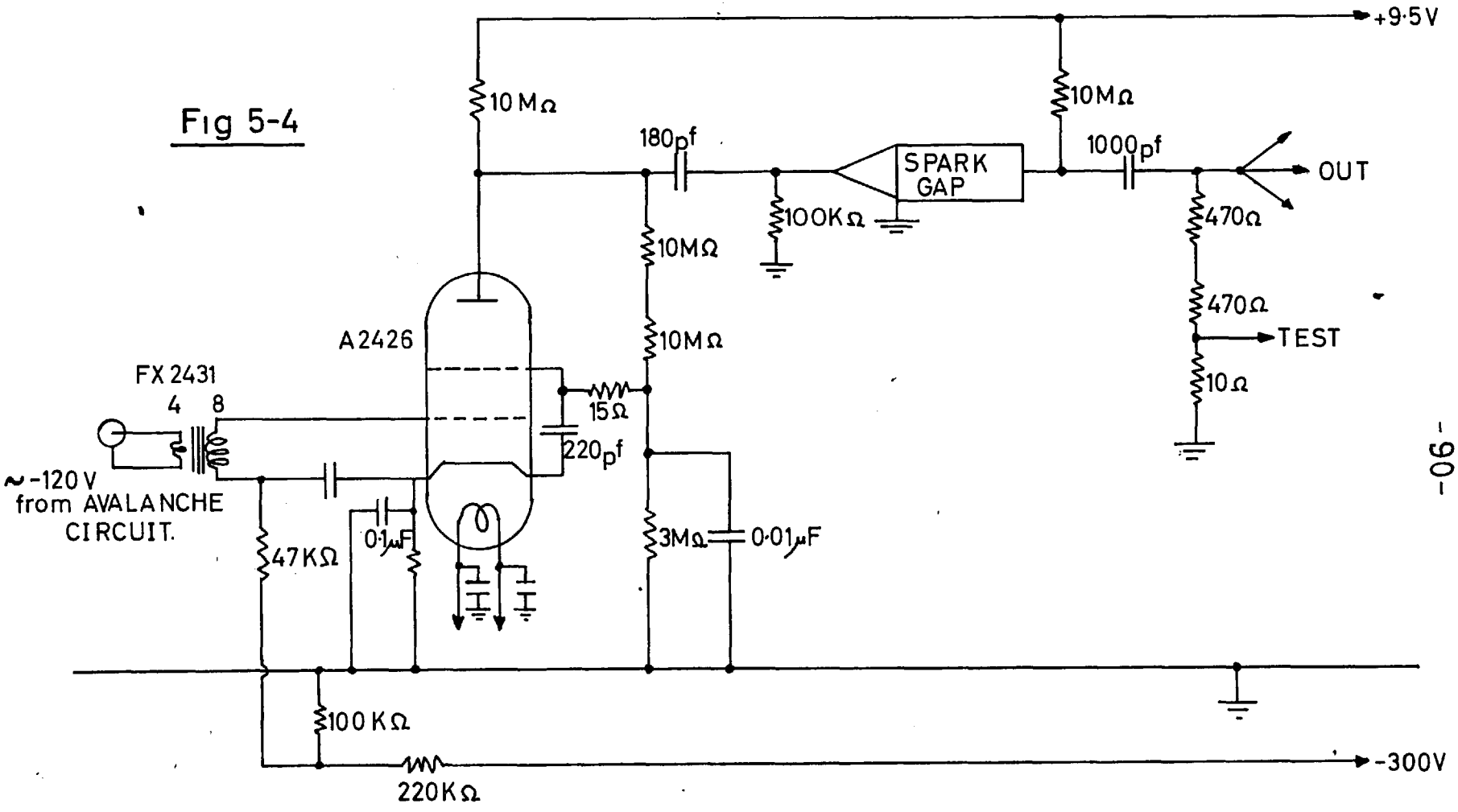
Fig 5-3

SCHEMATIC DIAGRAM OF COUNTER SELECTION SYSTEM AND TRIGGER CIRCUIT.

particles coming from the relevant target were considered. The outputs from CO1 and the Cerenkov Counter were also fed into CO2. To select pions, the Cerenkov Counter had to be changed to anti-coincidence. A slow output from CO2 was used to drive the camera relay circuit for advancing the film. The relay circuit also paralysed the fast output of CO2 for the duration of the film advance ($\sim$ 1 second).

The Paralysis, Avalanche Circuit and Master Gap circuits are shown in Fig. 5.4. The relay circuit on being triggered gave a +35 Volt output which biased a HD5000 diode and prevented the CO2 output pulses from triggering the Avalanche Circuit. In the absence of a bias, however, the Avalanche Circuit gave an output of -120 volts which was applied after inversion on a A2426 - a high-current tetrode. When the valve triggered, the anode, which was normally held at $6\frac{1}{2}$ kV fell to ground potential applying the voltage pulse on the trigger electrode of a spark gap (similar to the one described in Chapter 4). The spark gap was filled with nitrogen at 10 p.s.i. and its anode was held at +9.5 kV. The output from the Master Gap was fed into ten Slave Gaps through 100Ω co-axial cables. Each chamber had a separate Slave Gap with a storage condenser of 1000 pfs and with 1000 in parallel with the chambers which gave a 180 n.s. pulse length. There was provision for a clearing field which was set at +100 Volts (with polarity opposite that of the pulsed field).

Fig 5-4



MASTER SPARK GAP CIRCUIT

CHAPTER 6

Experimental Results

6.1 Introduction

The spark chamber arrangements described in the last chapter were used to photograph π mesons and electrons of 500 MeV/$_c$ momentum. In all, about 4000 π's and 2000 electrons were photographed, and the results are presented below.

6.2 Spark Chamber Performance

The single particle efficiency of all the chambers was measured by scanning pion tracks which did not have a nuclear interaction or scattering at angles $> 15^o$. Further, only those tracks were selected in which the first chamber (S_o) had at least three gaps out of four sparking along a track, with no other track present in it; the last chamber was required to have at least one of the two gaps sparking in line with the track (within reasonable limits of scattering). The results are shown in Table 6.1.

The efficiencies of chambers S_o - S_7 were reasonably high and at about the level expected from the preliminary tests (Chapter 4). The chambers S_8, and especially S_9, showed a low efficiency which could have one of many explanations. Firstly, as all chambers had independent Slave Trigger Spark Gaps, it is possible that due to maladjustment, the particular Slave gaps were inefficient in triggering the chambers. Secondly, the efficiency of S_9 may have been seriously impaired by an excess of Perspex Cement which was used in its construction instead of

Table 6.1

Chamber	Efficiency (%)
S_0	95 $\pm$ 0.5 %
S_1	95.4 $\pm$ 0.35 %
S_2	99 $\pm$ 0.35 %
S_3	98.5 $\pm$ 0.35 %
S_4	97.5 $\pm$ 0.35 %
S_5	93 $\pm$ 0.34 %
S_6	96.4 $\pm$ 0.35 %
S_7	95.5 $\pm$ 0.35 %
S_8	88.7 $\pm$ 0.32 %
S_9	71 $\pm$ 0.28 %

Araldite, which was used for the other chambers.

An annoying feature in the analysis of the photographs was the persistent spurious breakdown in some of the chambers. The breakdown occurred for nearly every trigger in the same region of the gap. It consisted of a large number of very low energy sparks and gave the impression of a 'glow discharge' across the gap. In the absence of a track, the breakdown appeared to be stronger. Examples of the breakdown can be seen in the photographs later in this chapter. As this type of breakdown was not encountered in the preliminary tests described in Chapter 4, and due to a shortage of time before the test run, nothing could be done to eliminate this breakdown. This handicap was partially overcome during the scanning of the photographs by accepting only those sparks for tracks which could be correlated in both gaps of the chamber and in both views (direct, and at 90°). This procedure proved rather cumbersome with some of the photographs, especially of electron showers, and perhaps introduced a bias in the scanning of multiple tracks.

Results

6.3 F.1. (π -mesons in Arrangement I)

The scanning of this film was done in more detail than the other π-films, with the following considerations in mind:-

(i) Efficiency of the Spark Chambers.

(ii) Nuclear Interaction cross-sections in Lead for π-mesons.

(iii) μ-meson contamination in beam.

(iv) Production of δ-Rays

(v) π-mesons simulating electrons

(ii) The first of these was discussed above. The main object of measuring the nuclear interaction cross-section was to estimate the μ-meson contamination in the beam. As discussed in Chapter 3, the combined Coulomb and diffraction scattering was not expected to exceed 15°. An experimental check was made on the differential scattering cross-section for small angles (shown in Fig. 6.1).

The inelastically scattered π-mesons were recognised by one of the following processes:-

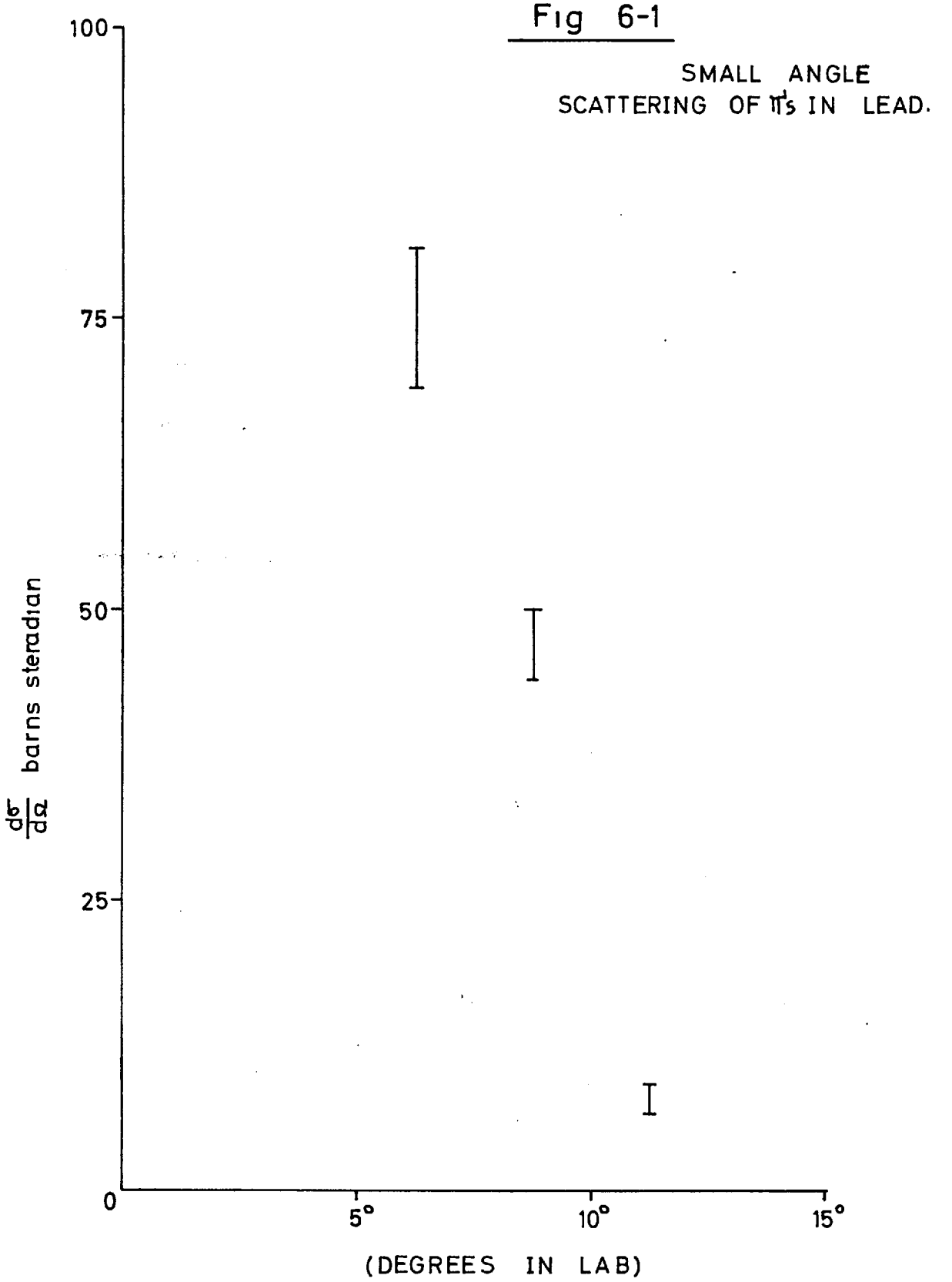
(a) Scattering at angles $> 15^{\circ}$

(b) Interactions, with more than one outgoing particle

(c) Stops

The angle of the outgoing particle was measured in (a) and (b), the more energetic particle only being measured in (b). The differential cross-section of inelastically scattered πs is shown in Fig. 6.2. There are two points in connection with this curve worth mentioning. Firstly, the cross-section is artificially depressed in the region 60°-120° due to the geometry of the chambers. Secondly, the cross-sections in the backward hemisphere see low (especially near 180°) compared to Ignatenko[36]. This may be due to either a low efficiency of the chambers for two particles, or scanning losses because the secondary particle went through the first chamber (S_o). Only those photographs were considered

Fig 6-1


SMALL ANGLE
SCATTERING OF π's IN LEAD.
100
75
50
25
0
dσ/dΩ barns steradian
5°
10°
15°
(DEGREES IN LAB)

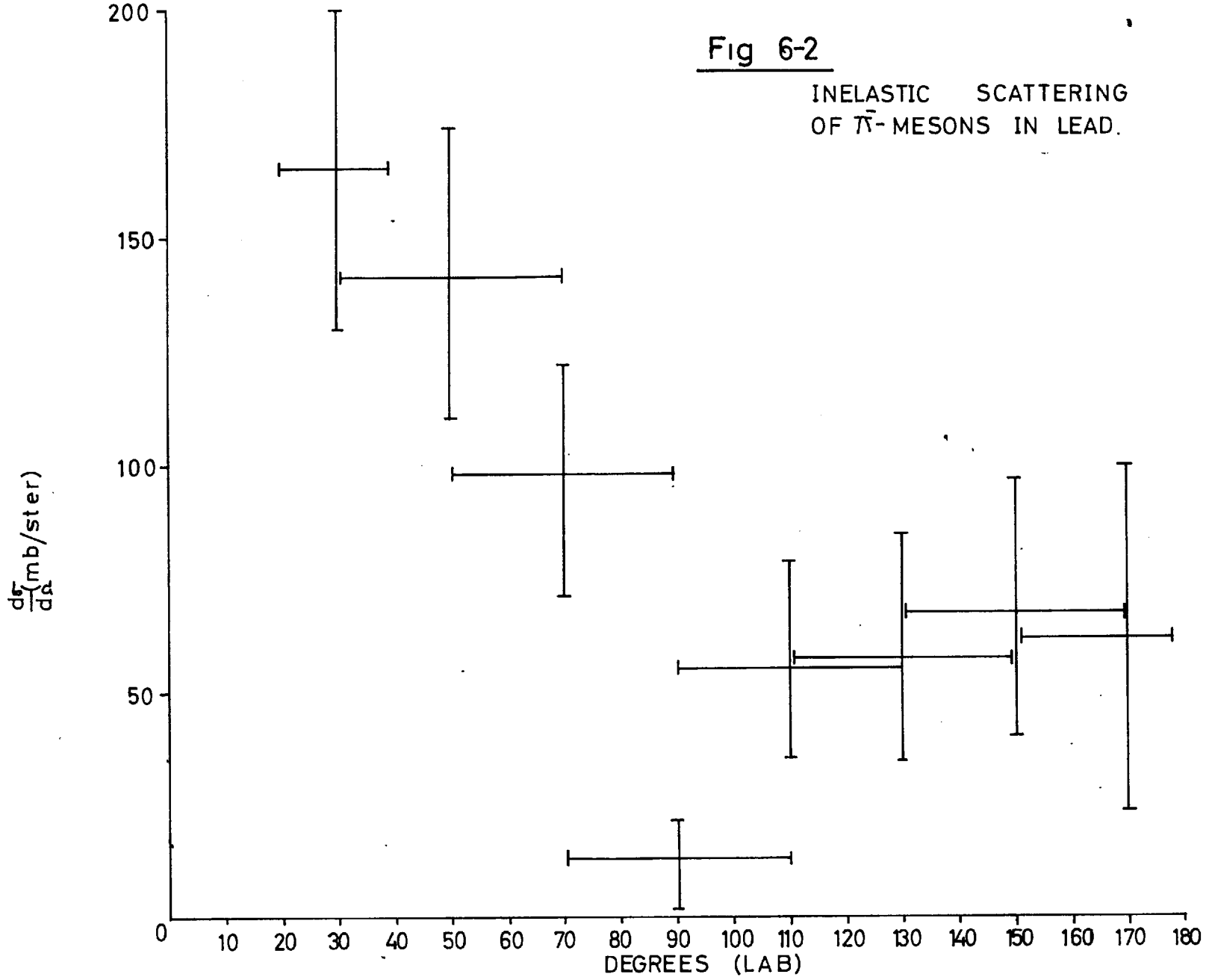


Fig 6-2

INELASTIC SCATTERING OF π^- MESONS IN LEAD.

which had only one particle in the first chamber, or if there were more than one particle, the others were obviously coming from an interaction. Some events may have been missed due to this criterion.

(iii) μ -Meson Contamination in the Beam.

It may be recalled that the counter system for selecting electrons and pions was based on the Cerenkov Counter which selected only electrons. Along with the pions, the μ-mesons, K-mesons etc. were also expected to be selected of which only the μ-mesons were expected to form a significant fraction. It is important to know this fraction in determining πs.

The principle of estimating πs was to calculate the ratio of the number of nuclear interactions which should be observed from the simple geometrical cross-section, to the number that were actually observed. All π-tracks which either stopped, had an obvious interaction, (more than one secondary particle) or were singly scattered at angles greater than 15° were counted as nuclear interactions. To this, the estimated number of nuclear scattering in the range $0\text{-}15^{\circ}$ was added. It turned out that the percentage of π-mesons was $\sim 85\%$ of the total particles selected as π's, from which the fraction of πs in the beam can be readily calculated.

(iv) δ-Rays.

The presence of δ-rays, along with the π track could be of significance if the π-meson subsequently interacts in one of the lead

plates. The object of counting the δ-rays produced in the π-run was to estimate the additional difficulty in preventing πs from simulating electrons. The following observations were made on the 600 photographs taken, considering only the first six radiation lengths of lead.

Number of single δ's observed = 66 i.e. 11%

Number of two single δ's per photograph = 6 i.e. 1%

Number of 2 δ's (in the same chamber, probably back-scattered in the following lead plate) = 6 i.e. 1%

(v) π-mesons simulating Electrons.

Some of the π-tracks which may have been mistaken for electrons are shown in Figs. 6.3 to 6.9. The question of forming a criterion for accepting or rejecting π-mesons is deferred to after the electron pictures analysis.

6.4 F.2 (Electrons in Arrangement I)

Nearly 300 photographs of electrons were scanned. As mentioned above, there was some difficulty in distinguishing particle tracks from spurious breakdown in some chambers. This difficulty is apparent in nearly all the electron shower photographs shown in Figs. 6.10 to 6.14. The discussion on electrons is divided into three sections:-

(i) Average Behaviour of Showers

(ii) Linear Spread of Showers

Arrangement I

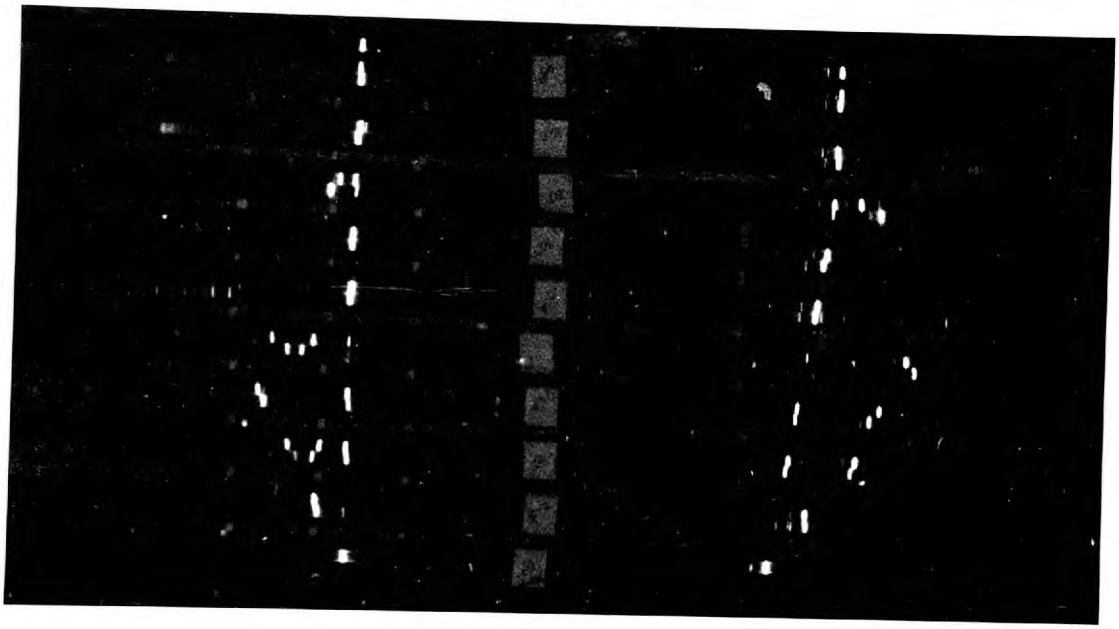


Fig. 6.3

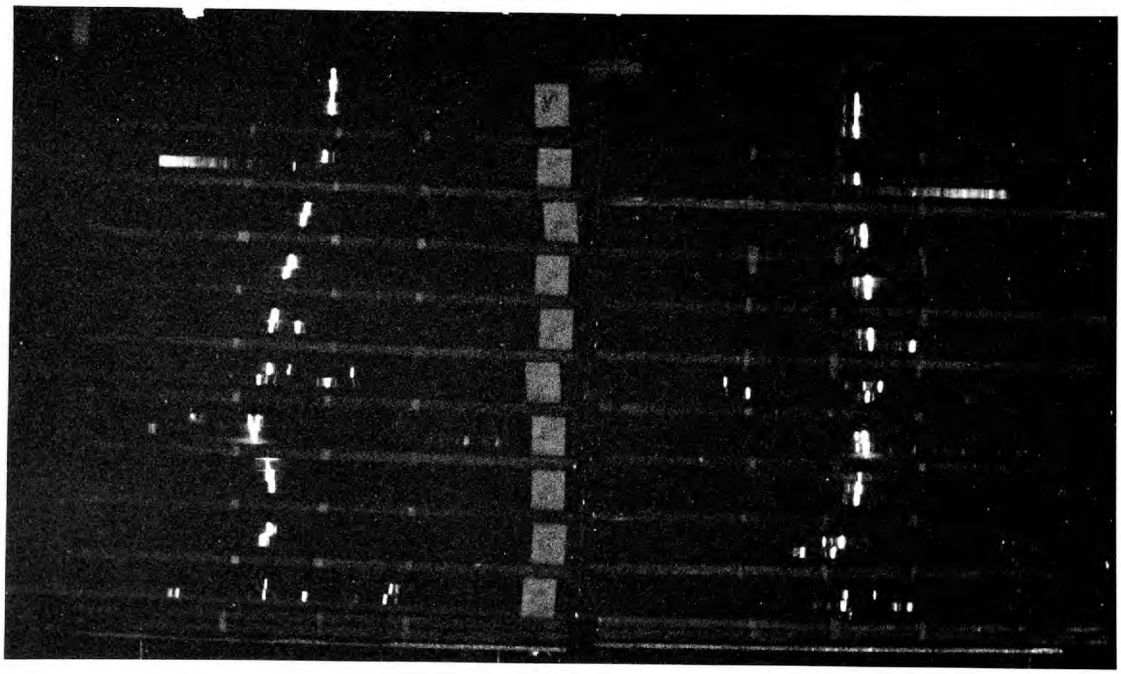


Fig. 6.4

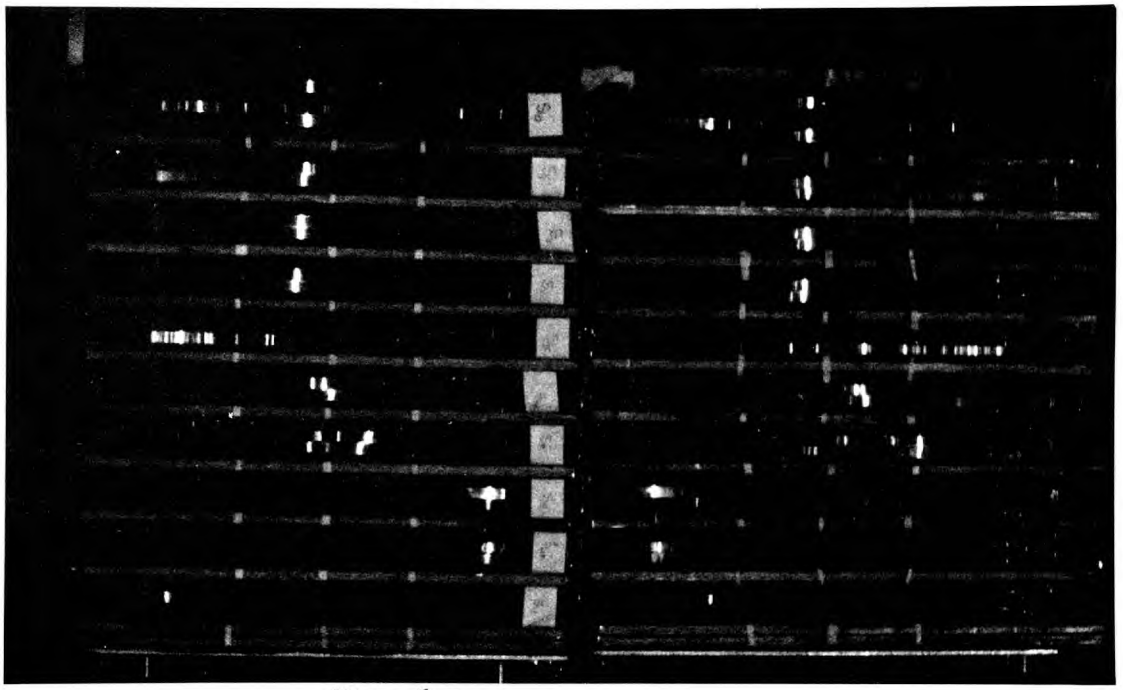


Fig. 6.5

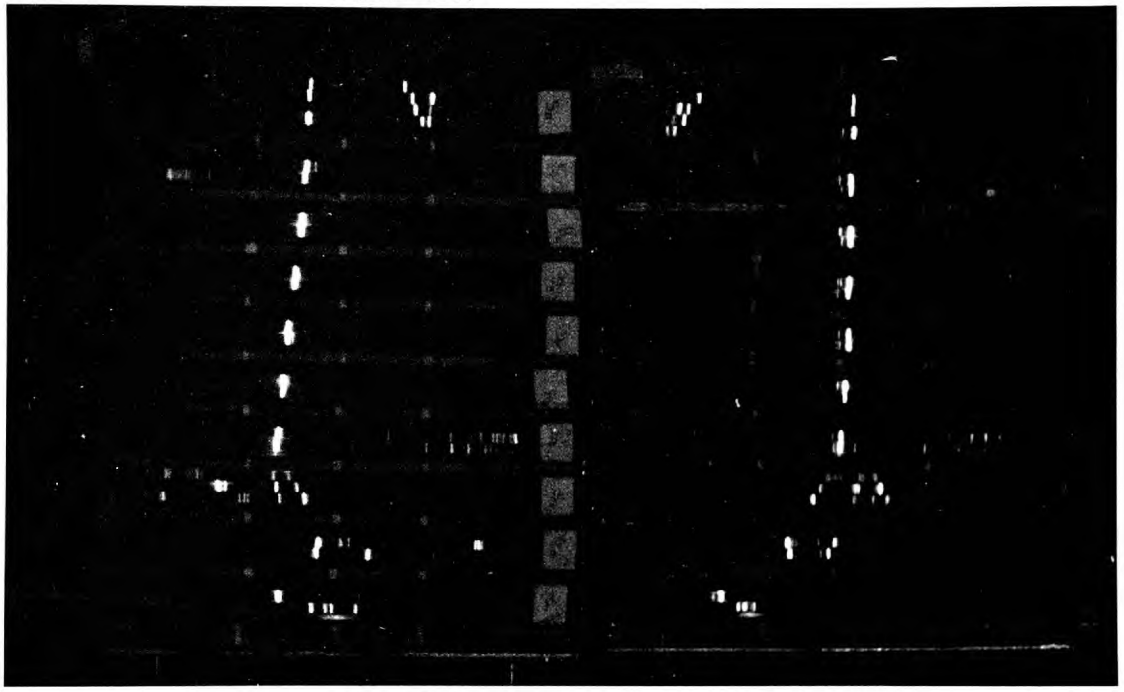


Fig. 6.6

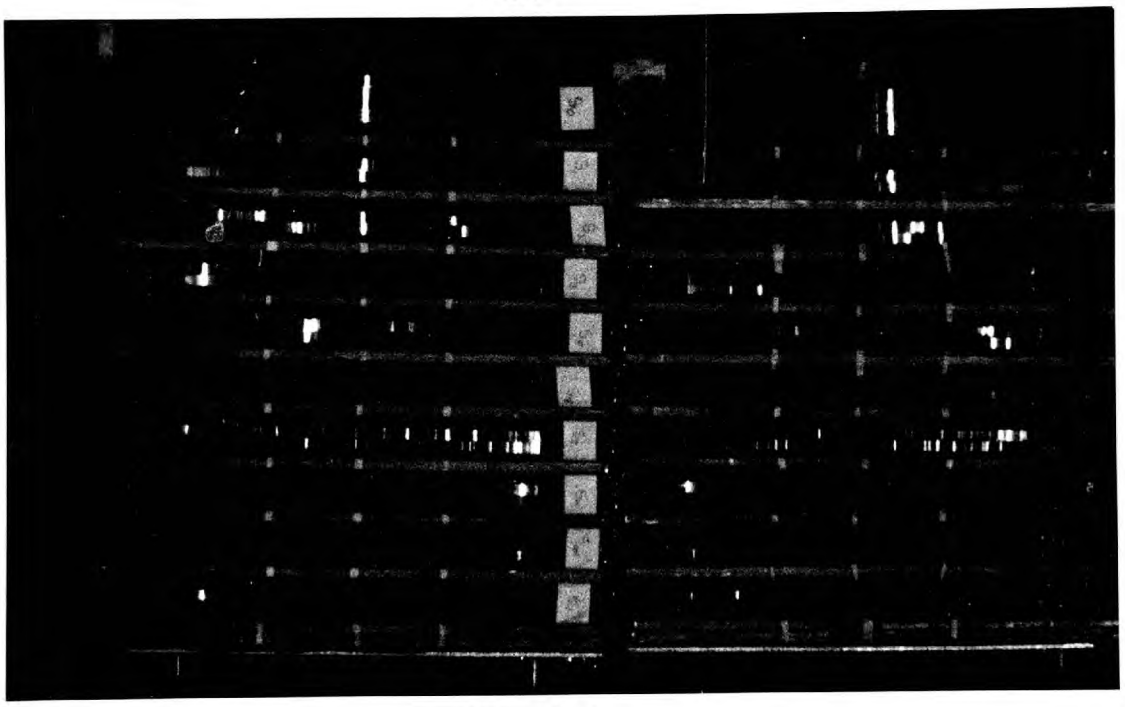


Fig. 6.7

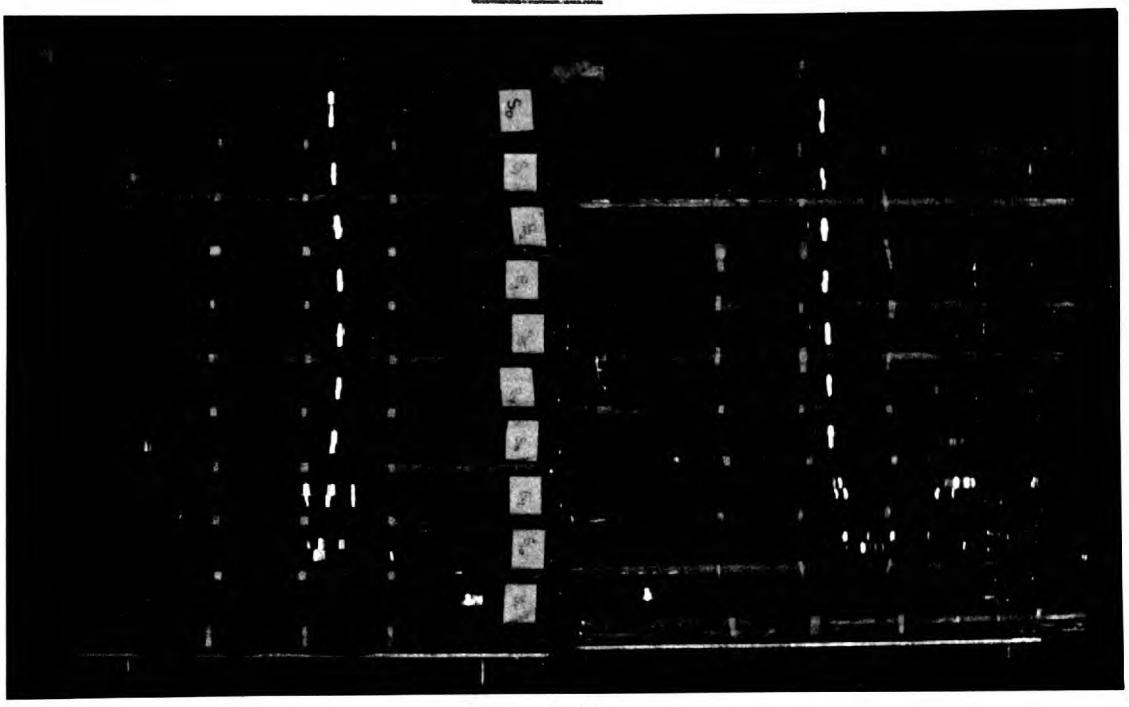


Fig. 6.8

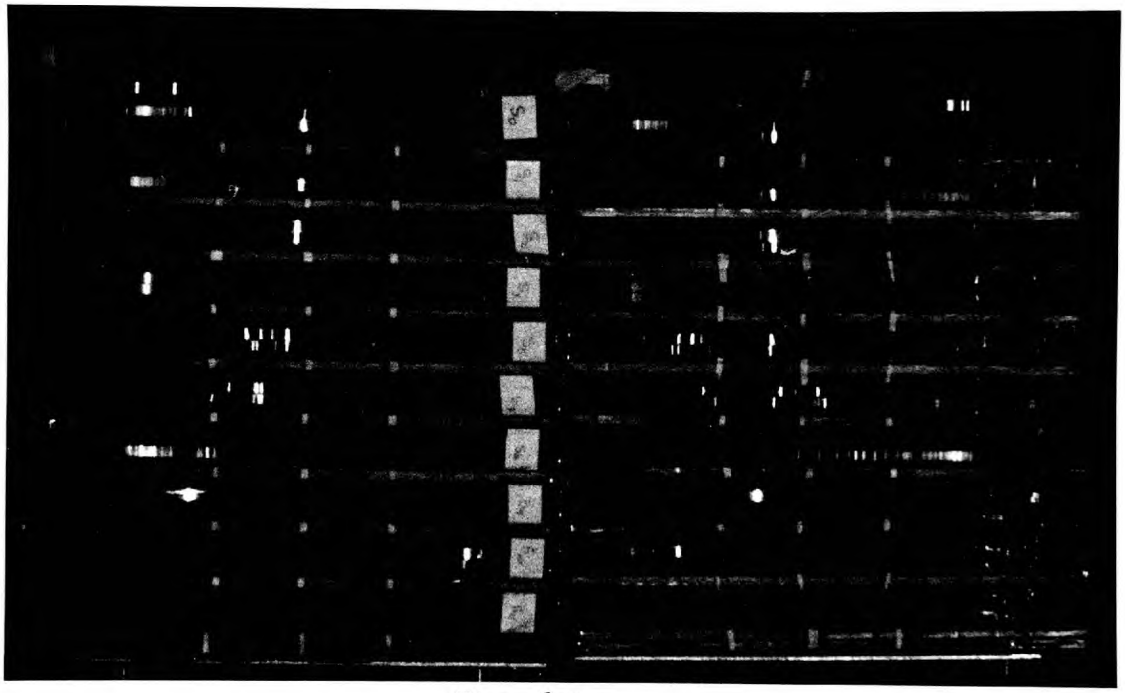


Fig. 6.9

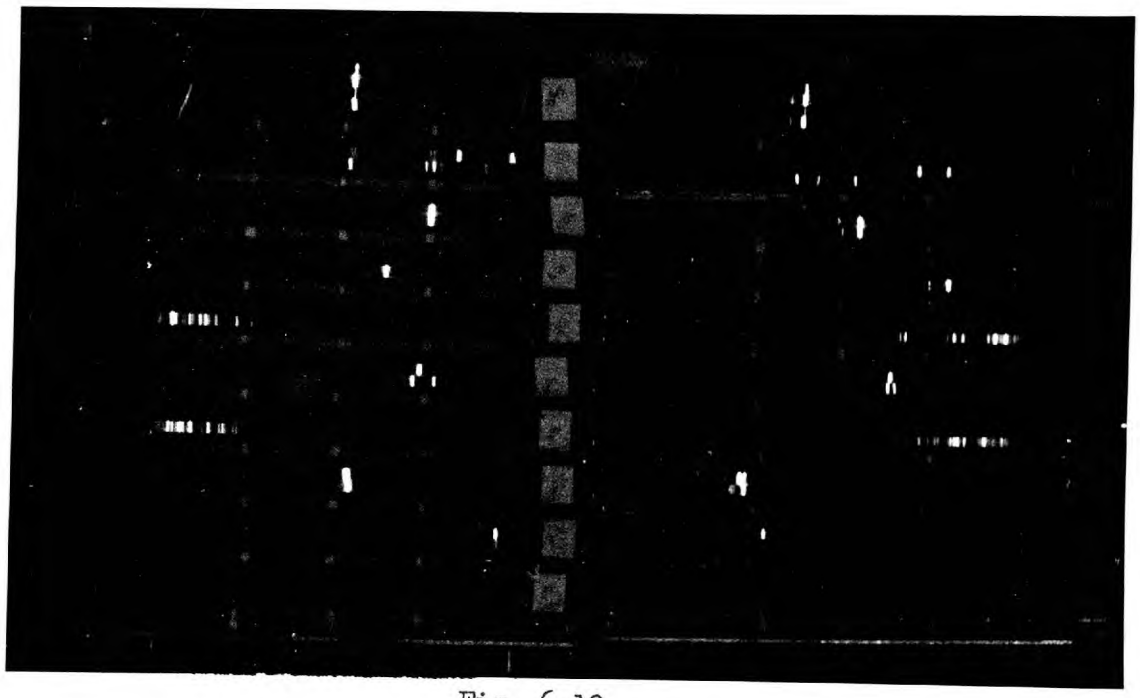


Fig. 6.10

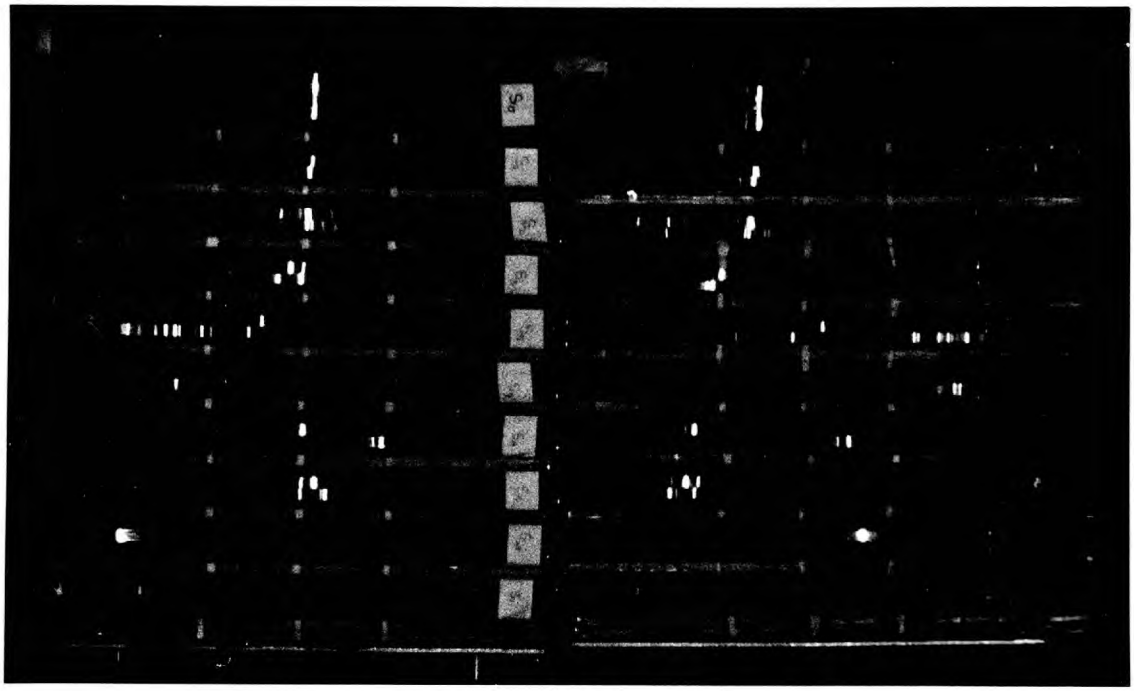


Fig. 6.11

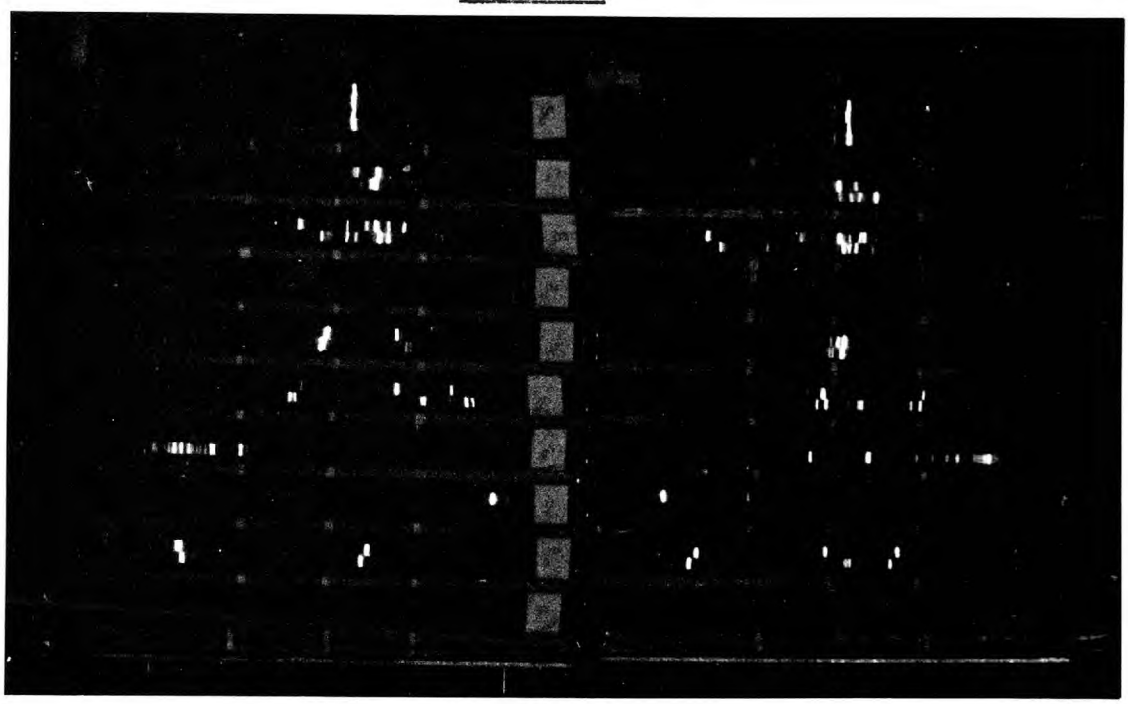


Fig. 6.12.

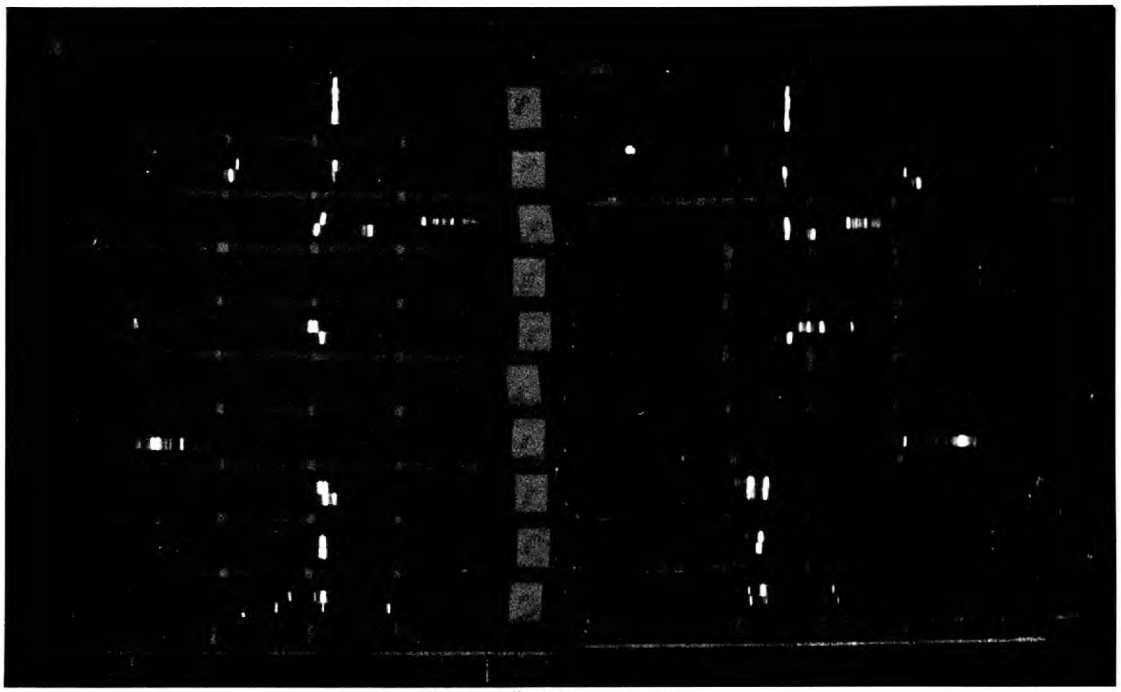


Fig. 6.13

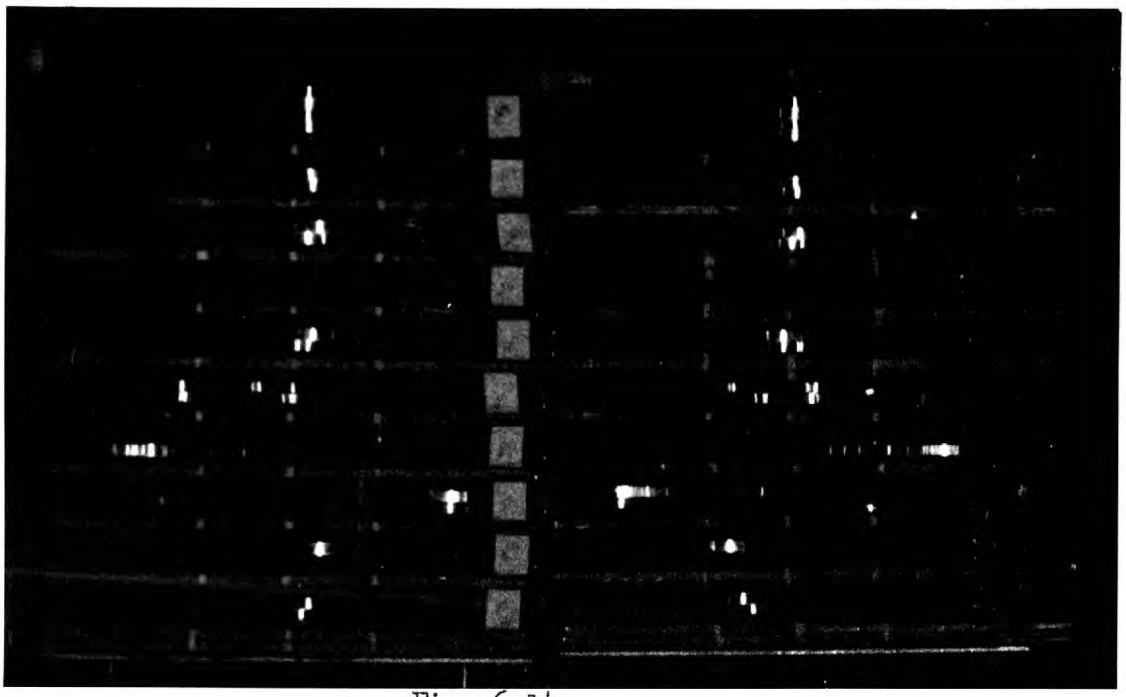


Fig. 6.14

(iii) Bad Electron events.

(i) Average Behaviour of Showers

The number of electrons in each chamber was counted to calculate the average number of electrons as a function of the depth of the shower, as shown in Fig. 6.15. The solid curve represents the computed value for the number of electrons with energy greater than 10 MeV[29]. In view of the fact that the computed curve includes only electrons with energy greater than 10 MeV, the agreement is surprising. On the other hand the scanning bias was in favour of reducing the number of electrons which might account for the relative agreement.

(ii) Linear Spread of Showers

For 72 electron tracks, the displacement of all electrons in the shower was measured from the axis, which was defined as the perpendicular distance between the shower electrons and the direction of the incident electron. Table 6.2 shows how the shower electrons are distributed spatially. Fig. 6.16 shows the same distribution graphically which helps illustrate the fact that most of the shower is restricted in a rather forward narrow cone. Fig. 6.17 shows the spatial distribution of electrons as a function of the depth of the shower (in radiation lengths). The first distribution (Curve No. 1) includes $(90 \pm 3.5)\%$ of the electrons present in the chamber and the second distribution includes $75 \pm 3)\%$ of the electrons. These numbers help in estimating the size of the spark chambers needed for shower detection.

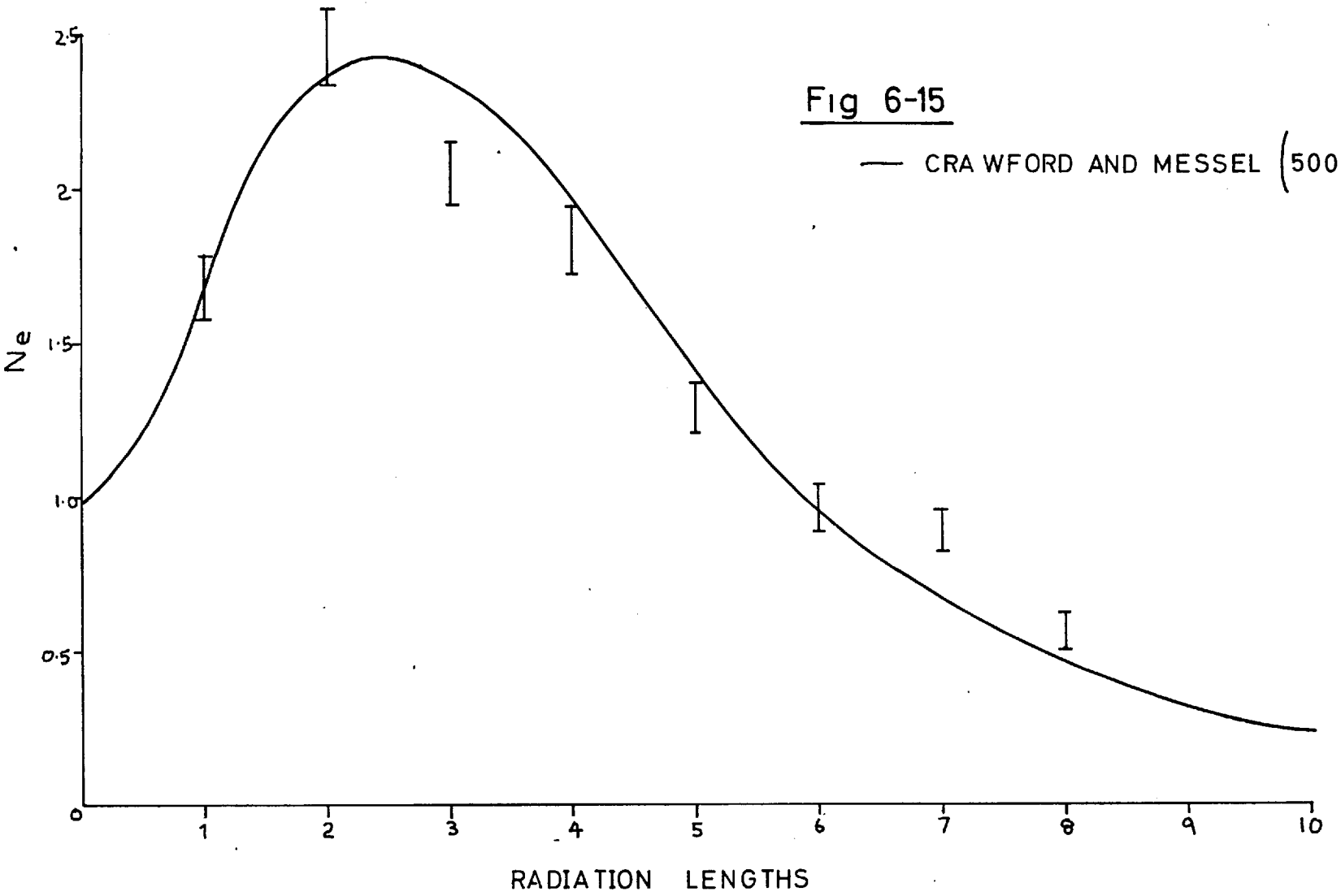


Fig 6-15

— CRAWFORD AND MESSEL $\left(500 \frac{MeV}{C}\right)$

Table 6.2

Total Number of Photographs = 72

Displacement (Projected) (cms)	Number of Electrons	Percentage in the Interval	Integrated Percentage
0 - 0.5	325	41.2	41.2
0.5 - 1.0	120	15.4	56.6
1.0 - 1.5	71	9.1	65.7
1.5 - 2.0	52	6.7	72.4
2.0 - 2.5	39	5.0	77.4
2.5 - 3.75	56	7.2	84.6
3.75 - 5.0	64	8.2	92.8
5.0 - 7.5	41	5.3	98.1
7.5 - 12.5	12	1.5	99.6
	Total 780		

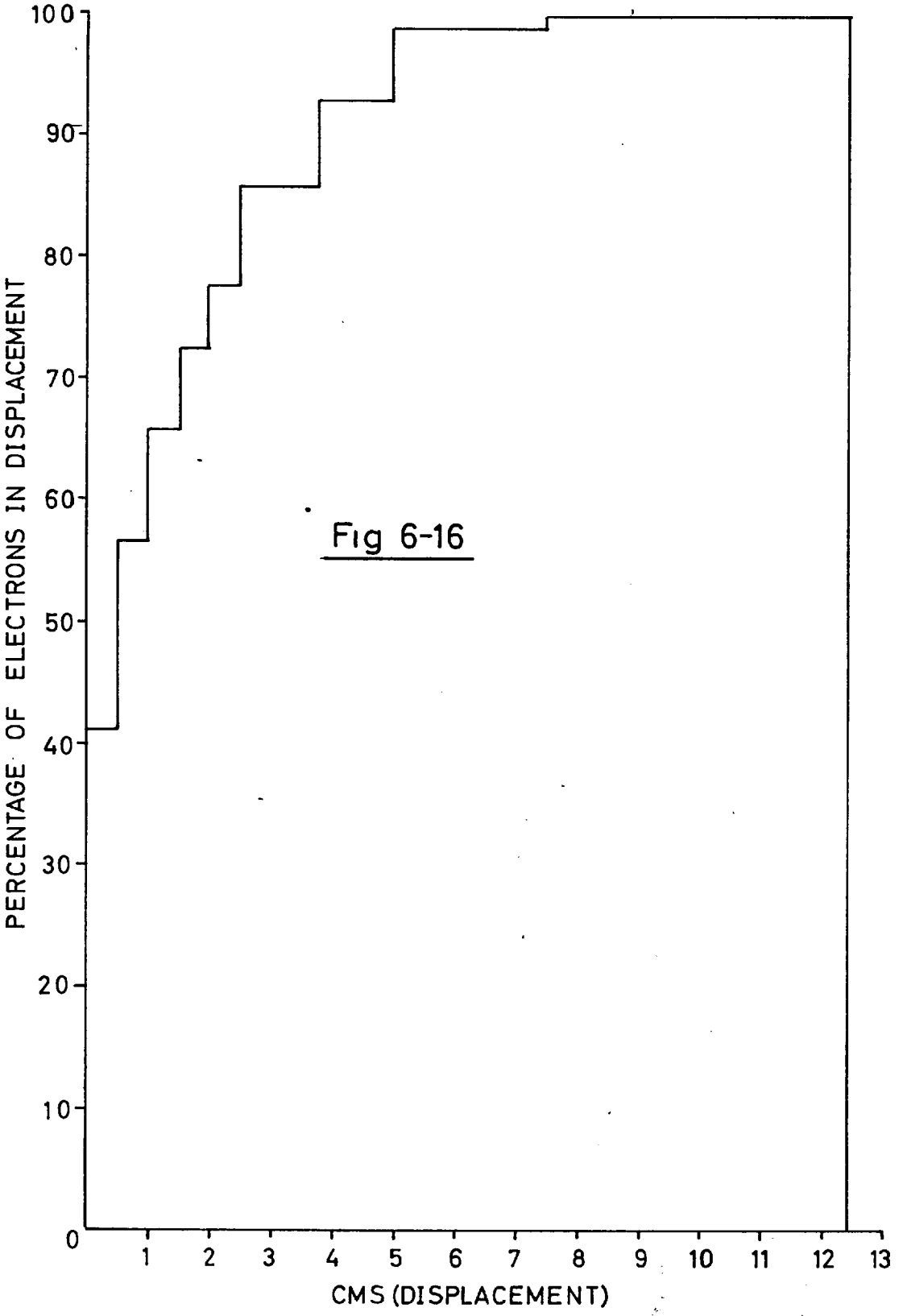

100
90
80
70
60
50
40
30
20
10
0
PERCENTAGE OF ELECTRONS IN DISPLACEMENT
1
2
3
4
5
6
7
8
9
10
11
12
13
CMS (DISPLACEMENT)

Fig 6-16

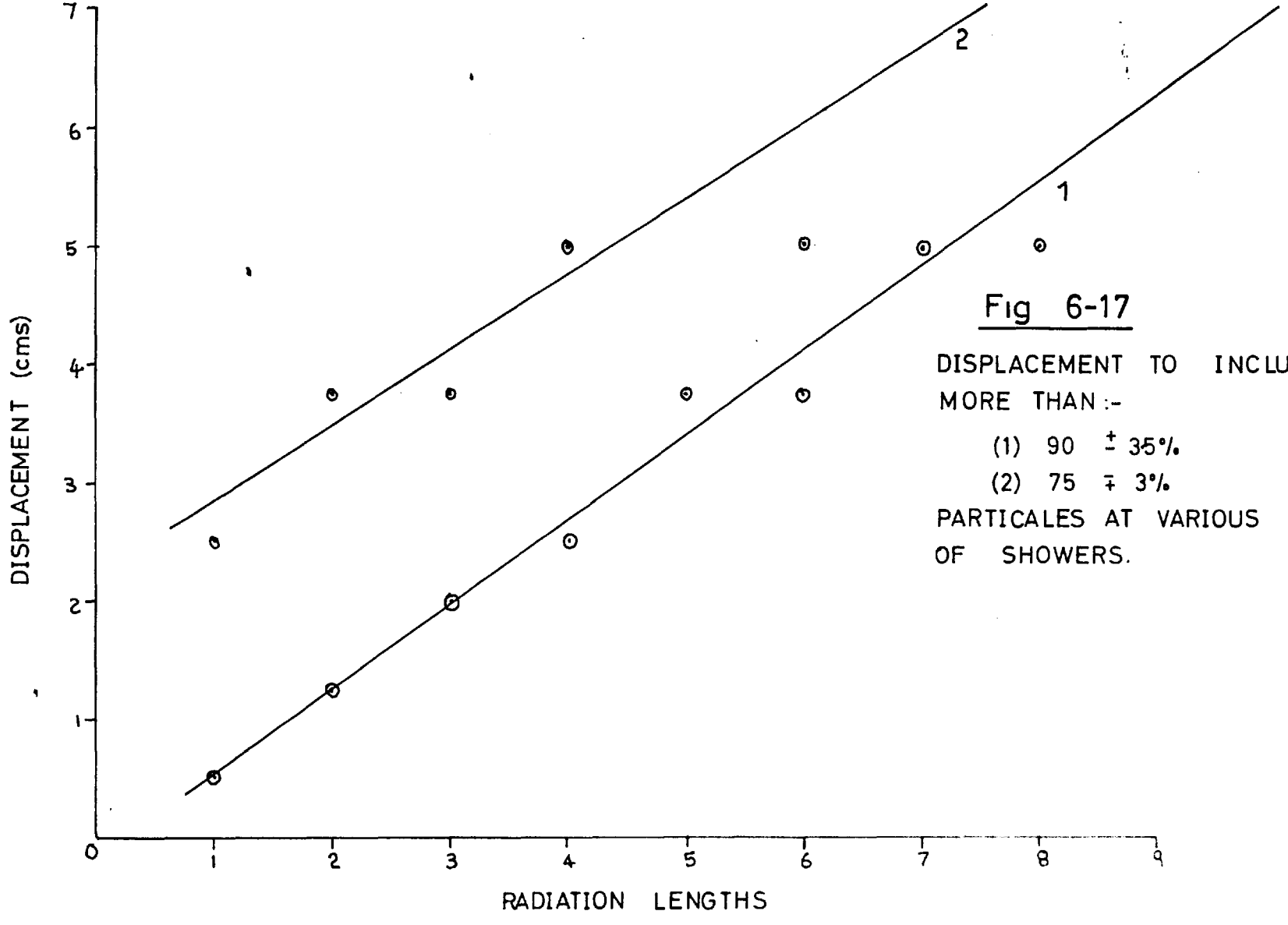


Fig 6-17

DISPLACEMENT TO INCLUDE MORE THAN :-

(1) 90 $\pm$ 35%

(2) 75 $\mp$ 3%

PARTICALES AT VARIOUS STAGES OF SHOWERS.

(iii) Bad Electron Events

Among the electron events shown in Fig. 6.10-6.14, except the electron in Fig. 6.12, all the other electrons are not positively identifiable. Several criteria for recognizing electrons were formed to find an optimum value for πs and η_E, and they are discussed below.

6.5 Criterion No. 1

The most obvious characteristic of the electrons observed in the photographs is the multiplication within the first few lead plates. This criterion requires the number of particles observed in chambers S_1-S_4 (i.e. in the first four radiation lengths) to be ≥ 6 for identifying an electron. The same criterion is applied to πs to find out the probability of electron simulation (πs) with the reservation that the multiplication does not occur in an obvious nuclear interaction. (See for example Fig. 6.13.) The results obtained are:

Efficiency for Electron Detection (η_E) = 88.5 $\pm$ 5.7%

Percentage of πs simulating electrons (πs) = 1.66 $\pm$ 0.56%

The main criticism of this criterion is that it increases πs quite unnecessarily by including obvious δ-rays. It may be pointed out that only two δs are needed in the first four chambers for a π to simulate an electron. In addition one δ, backscattered in the following lead plate is sufficient by itself to simulate an electron. From the results in 6.3 (iv) the following effects would be expected:

Number of 2 single δs in 4 Lead Plates $\sim$ 0.5%

Number of 2δ's in same plate ~ 0.7%

Expected enhancement in π_s ~ 1.2%.

6.6 Criterion No. 2

The δ-ray figures gave indication that a high fraction of π_s was due to δ-rays. To decrease π_s, therefore, a second criterion is tried out which requires the number of particles in S_1-S_4 to be $\geq$ 7. Obviously this requires an extra three particles in the first four chambers. The expected number of "δ events is calculated below from the results of 6.3 (iv).

Number of 3 single δ's = .034%

Number of 1δ + one 2δ = .073%

Total Number of expected π_s due to δ's 0.1%

The numbers actually observed are π_s = .83 $\pm$ 0.37%

and η_E = 71 $\pm$ 5.1%

6.7 Criterion No. 3

The numbers for π_s showed an improvement in the above criterion but η_E became rather low. At this stage it is considered more fruitful to aim at a qualitative criterion rather than a quantitative one. An effort is made to analyse all the indefinite events, i.e. electrons which have not produced an obvious shower and pions which have produced multiplication. As such events constitute a very samll fraction of all the photographs, it is not expected to be a tedious job. In identifying electrons or pions, the following points are given special consideration:

(i) Most electrons multiply in the first few radiation lengths in a narrow forward cone. The number of electrons which multiply within a certain amount of material, and are later identified as electrons (according to Criterion No. 3) are shown in Fig. 6.18; this seems to be related to the radiation loss suffered by the electron in traversing the material, which is shown as a solid line in the same figure.
(ii) Many π^--interactions produce some multiplication but any multiplication not produced in the forward cone can not be due to electrons. Any energetic (range >1 lead plate) particle at large angles also cannot be produced by electrons.
(iii) The probability of producing a δ-ray in the first three lead plates, and the π simulating an electron is very low (0.0005). The probability of a π simulating an electron entirely due to δ-rays is small enough to be neglected according to the present criterion.

The electron pictures are shown in Figs. 6.10 to 6.14. Fig. 6.11 would be accepted even though the multiplication is not heavy, because of some multiplication in S_2 and S_3 and the characteristic electron pair further downstream in S_7. All the other electrons shown are not accepted due to inadequate multiplication. The overall efficiency for detecting electrons is found to be $95 \pm 5.7\%$.

The π's producing multiplication were shown in Figs. 6.3 - 6.9, and are considered individually below.

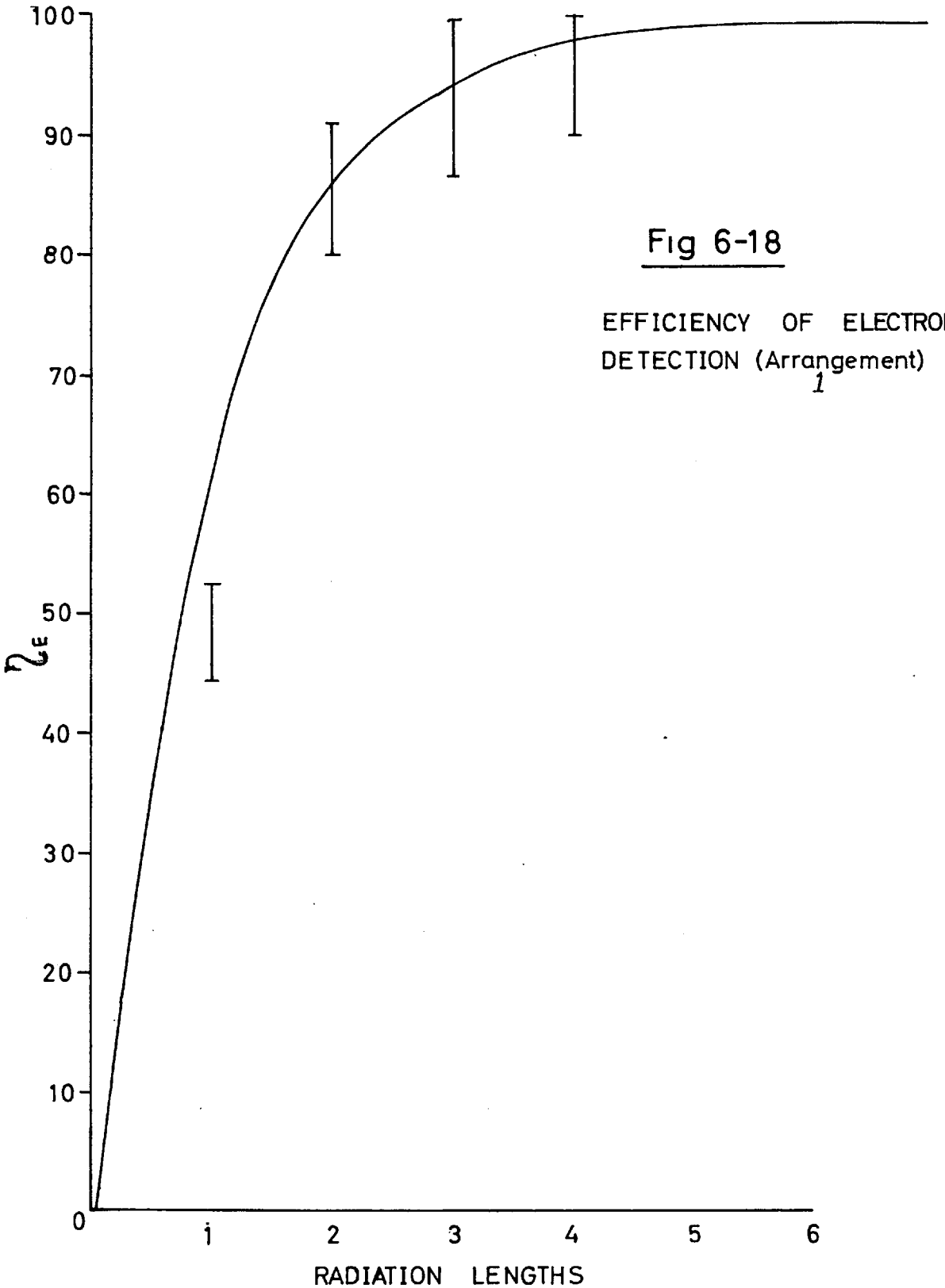


Fig 6-18

EFFICIENCY OF ELECTRON DETECTION (Arrangement 1)

(a) Fig. 6.3 shows a good example of π^0-production going backwards. Apart from the fact the shower develops backwards, the γ goes straight through 8 radiation lengths of lead (ignoring the e^+); it cannot, therefore be an electron.

(b) Fig. 6.4. The multiplication after the fourth lead plate makes it look like an electron. It is accepted as an electron in spite of the penetration of the shower which is unusually large for an electron of 500 MeV energy.

(c) Fig. 6.5. Due to the small multiplication, this event could not easily be called an electron. However, the criterion has been deliberately made easier for pions to simulate electrons to get an upper limit to πs, and this event is classified as an electron.

(d) Fig. 6.6. Normally this event would not be considered due to several tracks in S_0; however the other particles do not proceed beyond the first lead plate. The π-interaction in the 7th lead plate looks like an electron shower.

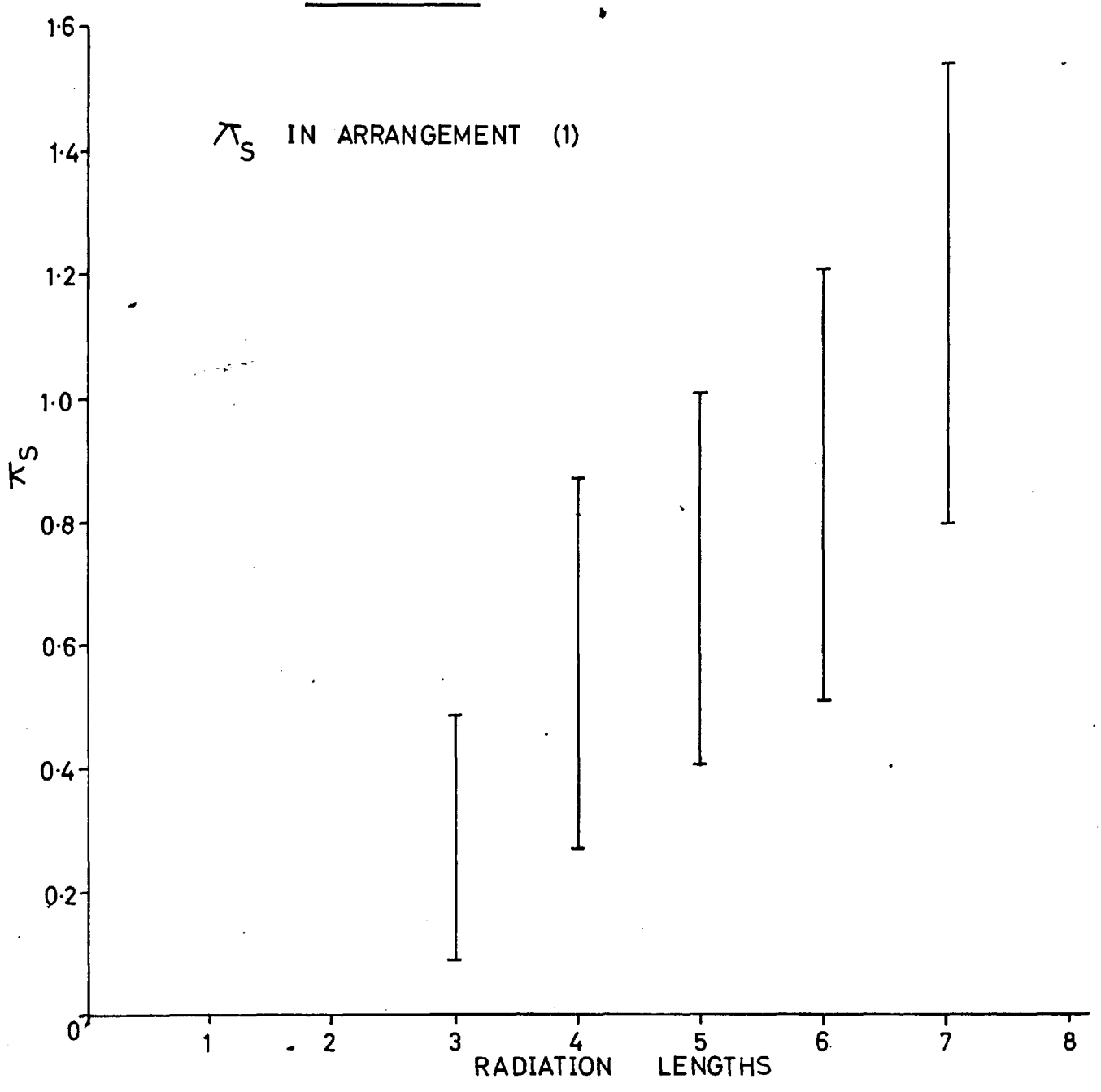
(e) Fig. 6.7. This has been called an electron mainly due to the uncertainty introduced by the multiple breakdown in S_6.

(f) Fig. 6.8. The interaction in the 7th lead plate looks like an electron shower.

(g) Fig. 6.9. Looks like an electron shower.

Fig. 6.19 shows the number of πs simulating electrons as a function of the depth of the shower. Bearing in mind that over 90% of the electrons

Fig 6-19


π_s IN ARRANGEMENT (1)
π_s
1·6
1·4
1·2
1·0
0·8
0·6
0·4
0·2
0
1
2
3
4
5
6
7
8
RADIATION LENGTHS

start multiplication in the first three radiation lengths, the relevant figure for πs is 0.29 $\pm$ 0.2%.

6.8 F.3 and F.4 (Arrangement No. II)

Generally speaking, the scanning of this film was very much easier than F.1 or F.2 as tracks could be followed in four gaps of the chamber instead of two, reducing the importance of spurious breakdowns. In principle, it should have been somewhat more difficult to identify electrons due to the smaller amount of material. In fact the efficiency for detecting electrons was found to be somewhat smaller than in the previous arrangement, using the same criterion, i.e. requiring multiplication for electron identification.

Some of the more difficult cases of electron pictures are shown in Figs. 6.20 to 6.24. The reasons why these electrons were rejected or accepted are given below:

(a) Fig. 6.20: Simple lack of multiplication rules this out as an electron. About 0.1% πs can produce 3 δ's in the arrangement and the original particle gives the impression of a π as it goes almost straight through five lead plates.

(b) Fig. 6.21: The lack of an ionizing link in chambers S_1, S_2, S_3 and S_4 with multiplication later strongly indicate the presence of a photon. However due to insufficient multiplication it is rejected.

(c) Fig. 6.22: This event is accepted as an electron due to multiplication in S_1 and S_2, and S_7 and S_8. The presence of a

non-ionizing link in S_5 and S_6 help in the identification.

(d) Fig. 6.23: Rejected due to inadequate multiplication.

(e) Fig. 6.24: Here again the non-ionizing links in S_1, S_2 and S_5, S_6 suggest the presence of a photon, but as there is no multiplication it is rejected.

Using the criterion the overall efficiency for the detection of electrons was found to be $94.5 \pm 5\%$.

All the difficult cases of πs are shown in Figs. 6.25 to 6.31.

(a) Fig. 6.25: This is called an electron due to the multiplication in S_7 and S_8.

(b) Fig. 6.26: Although there is some evidence for multiplication in S_1 and S_2, an energetic charged particle is scattered at a large angle in the third lead plate. It cannot, therefore, be an electron.

(c) Fig. 6.27: The V-type track in S_3, S_4 and the non-ionizing link in S_5 and S_6 suggest an electron. It may be mentioned, however, that this event would not be accepted as an electron due to insufficient multiplication but here it is, as it has been deliberately made easier for pions to simulate electrons.

(d) Fig. 6.28: The profuse multiplication leaves no doubt regarding the incident particle being an electron.

(e) Fig. 6.29: The multiplication is sufficient for it to be called an electron.

(f) Fig. 6.30: Same as Fig. 6.29.

Arrangement II

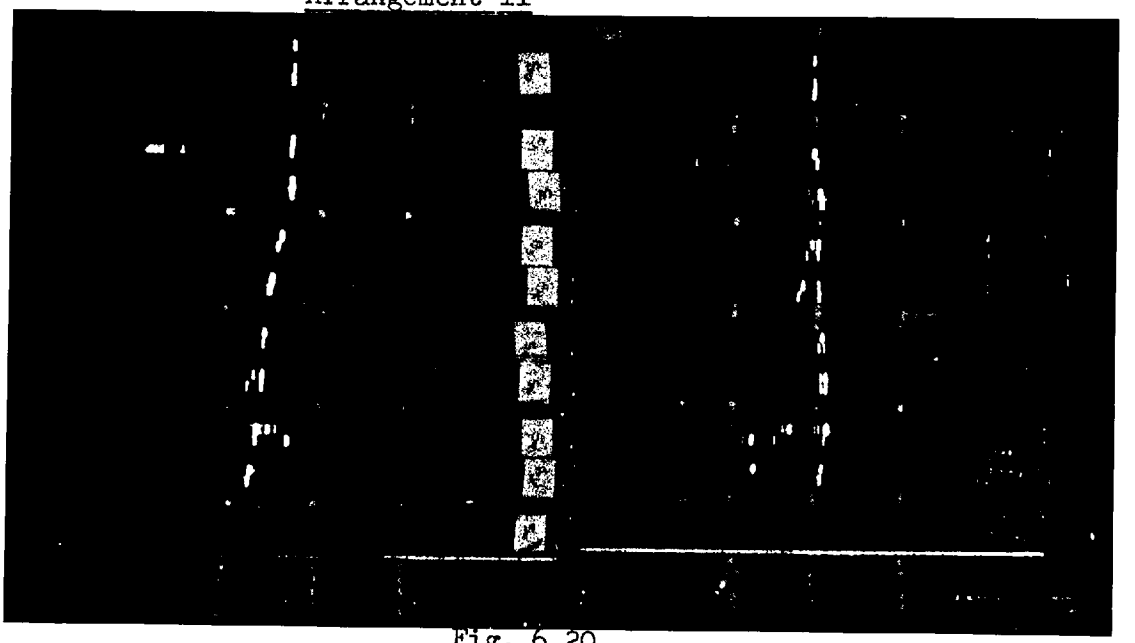


Fig. 6.20

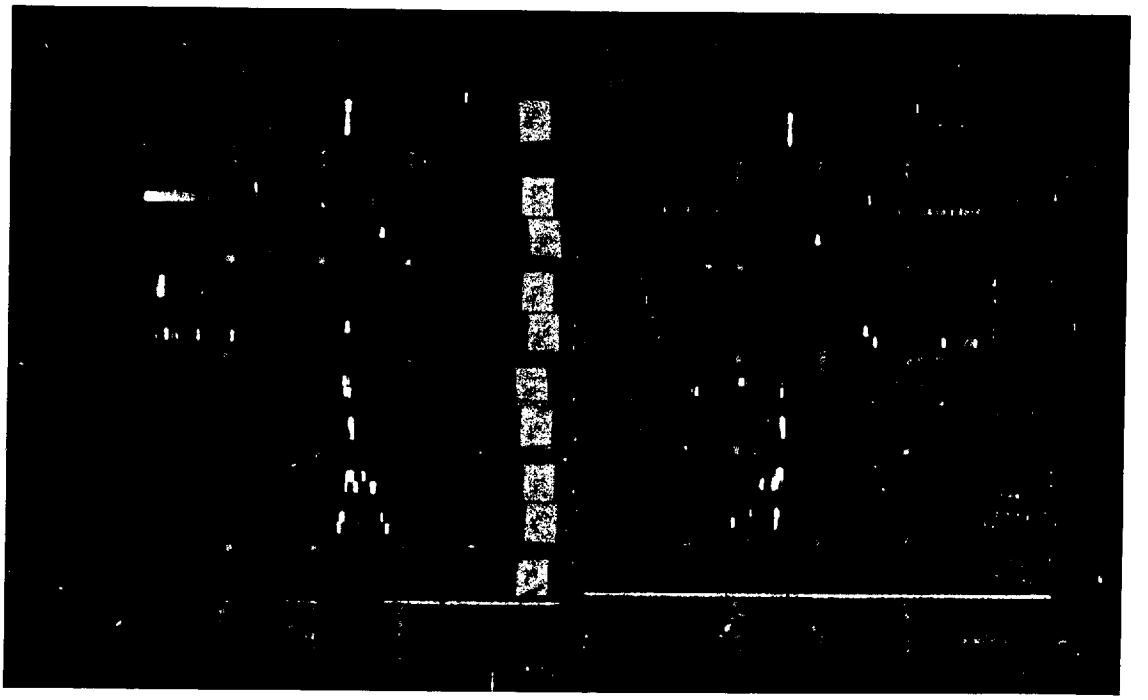


Fig. 6.21

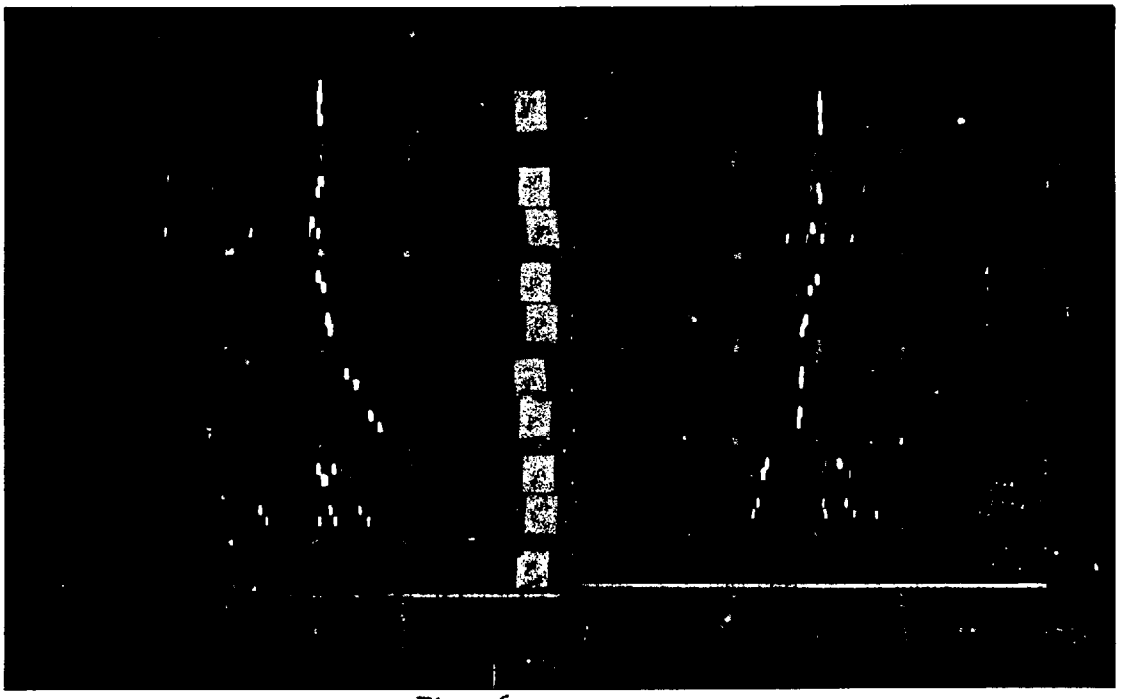


Fig. 6.22

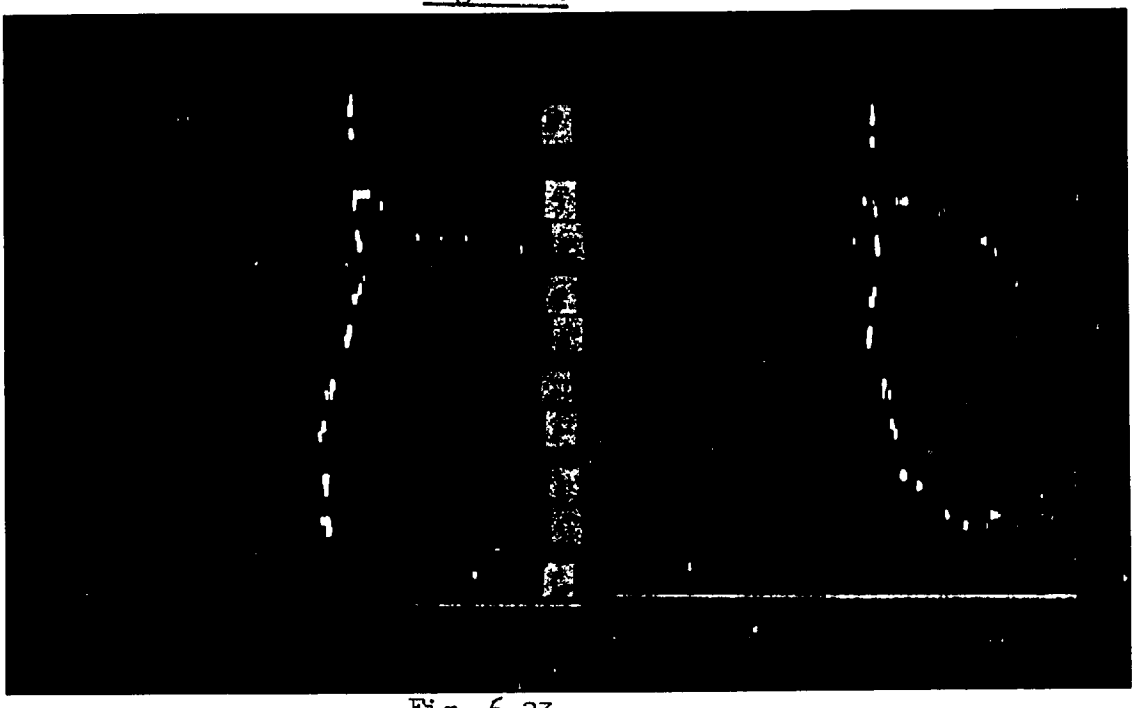


Fig. 6.23



Fig. 6.24

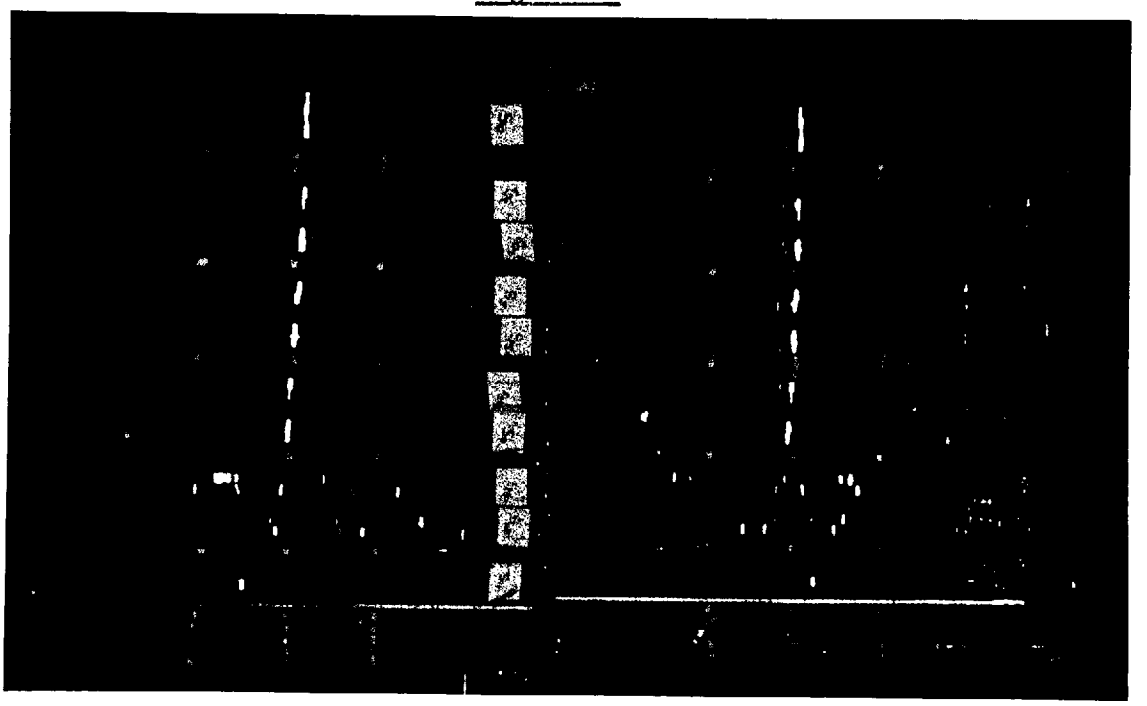


Fig. 6.25

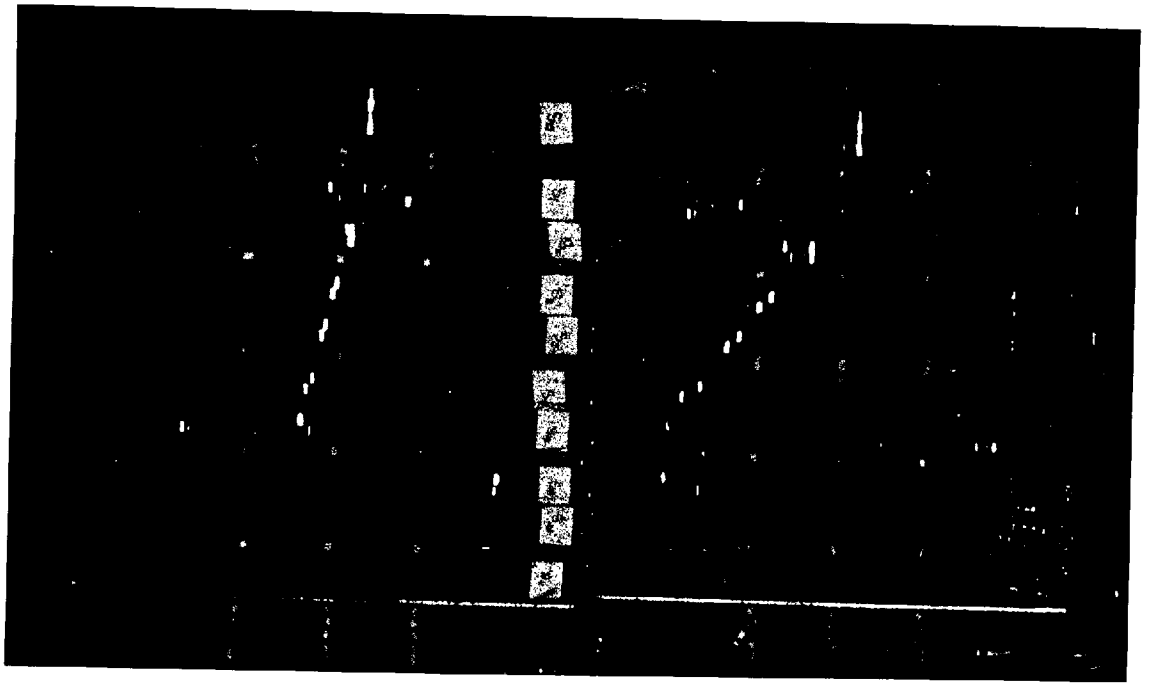


Fig. 6.26

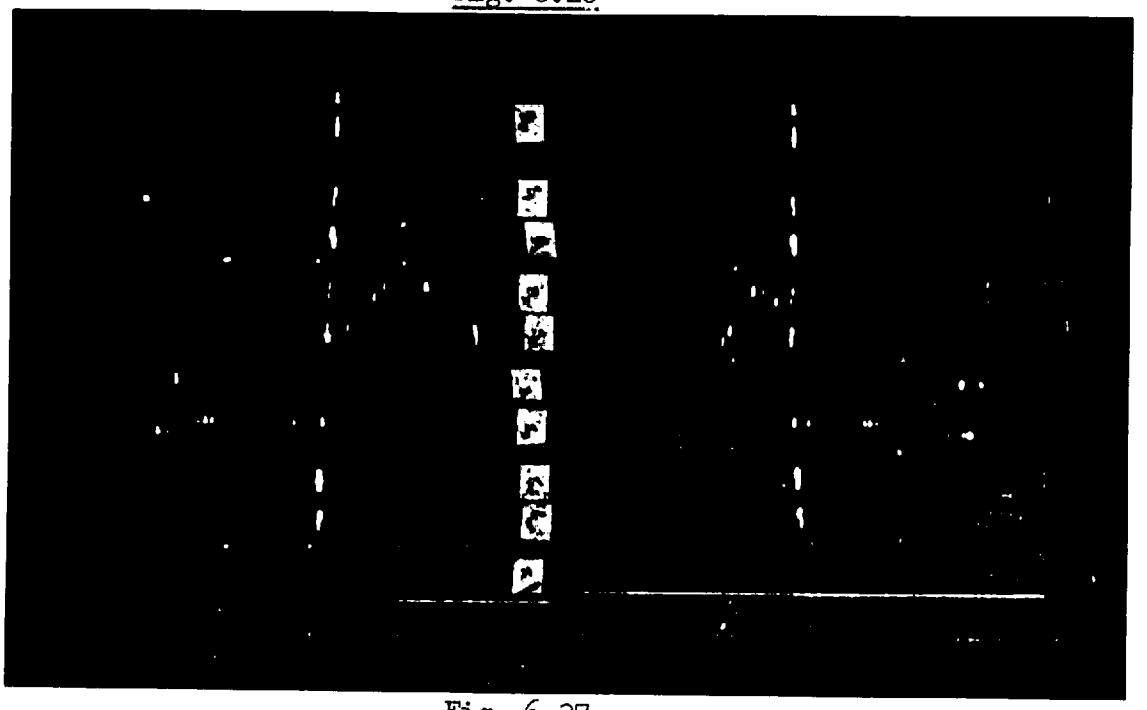


Fig. 6.27

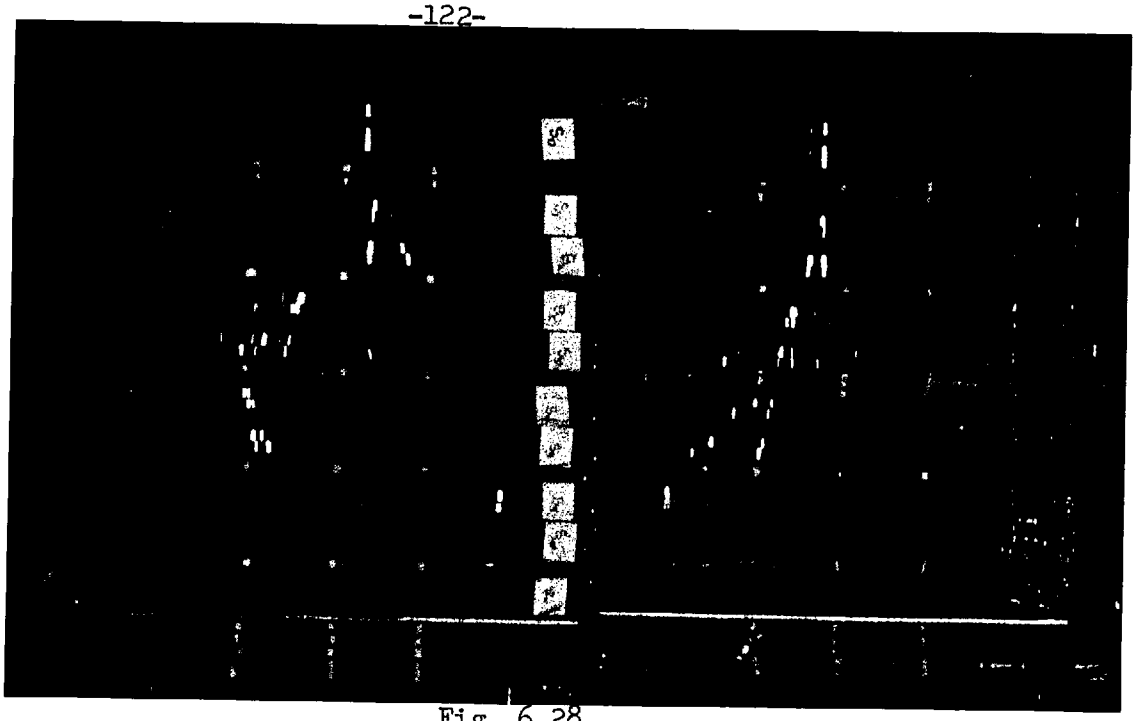


Fig. 6.28

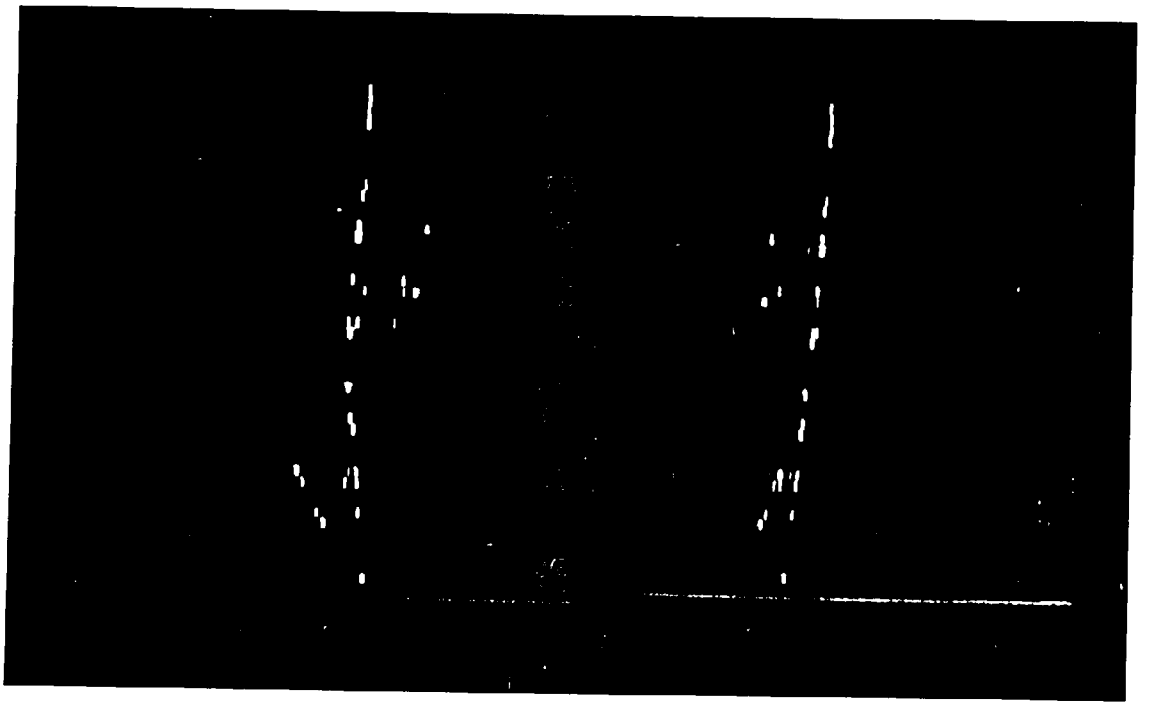


Fig. 6.29

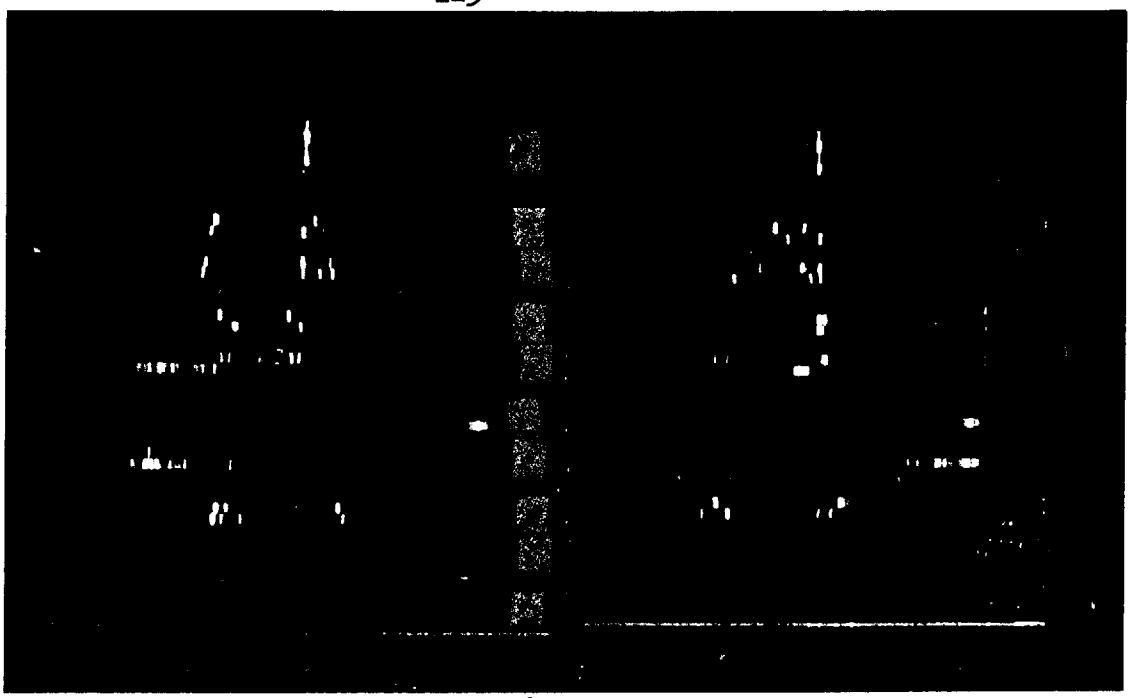


Fig. 6.30

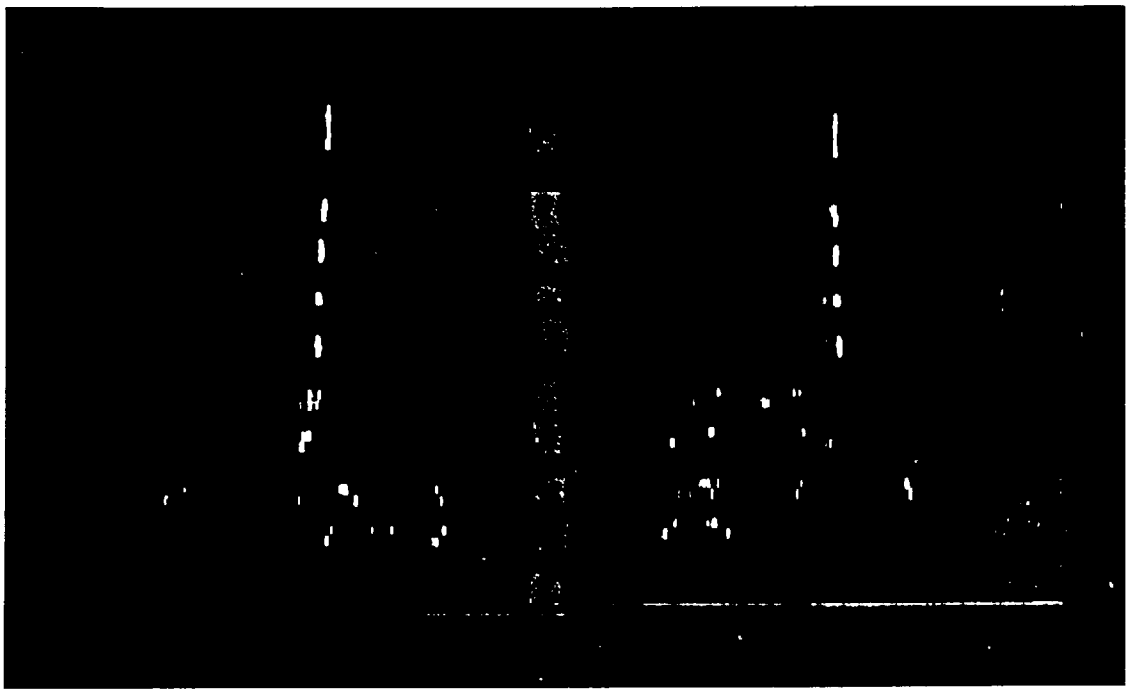


Fig. 6.31

(g) Fig. 6.31: Same as Fig. 6.29.

The results for electrons and pions in this arrangement are summarized in Figs. 6.32 and 6.33. Within the limits of the statistical errors η_E and πs are not significantly different from the previous arrangement.

6.9 F.5 and F.6 (Arrangement No. III)

As no significant difference in either the es or the πs compared to F.1 and F.2 was noticed, the discussion on individual events has been left out. Fig. 6.34 shows an electron shower in this arrangement. Unfortunately the stereo view has been cut off due to misadjustment of the mirror system. Fig. 6.35 shows a π simulating an electron.

The overall efficiency for the detection of electrons is measured to be $95 \pm 5.6\%$. For πs the figures are as follows

πs in 1 Radiation Length of Lead = $.24 \pm .24\%$

" " 2 " " " " = $.48 \pm .33\%$

" " 3 " " " " = $.48 \pm .33\%$

" " 4 " " " " = $.71 \pm .4\%$

" " 5 " " " " = $.71 \pm .4\%$

(Note: No correction has been made in the above figures for the increased amount of lead due to the large angle traversals.)

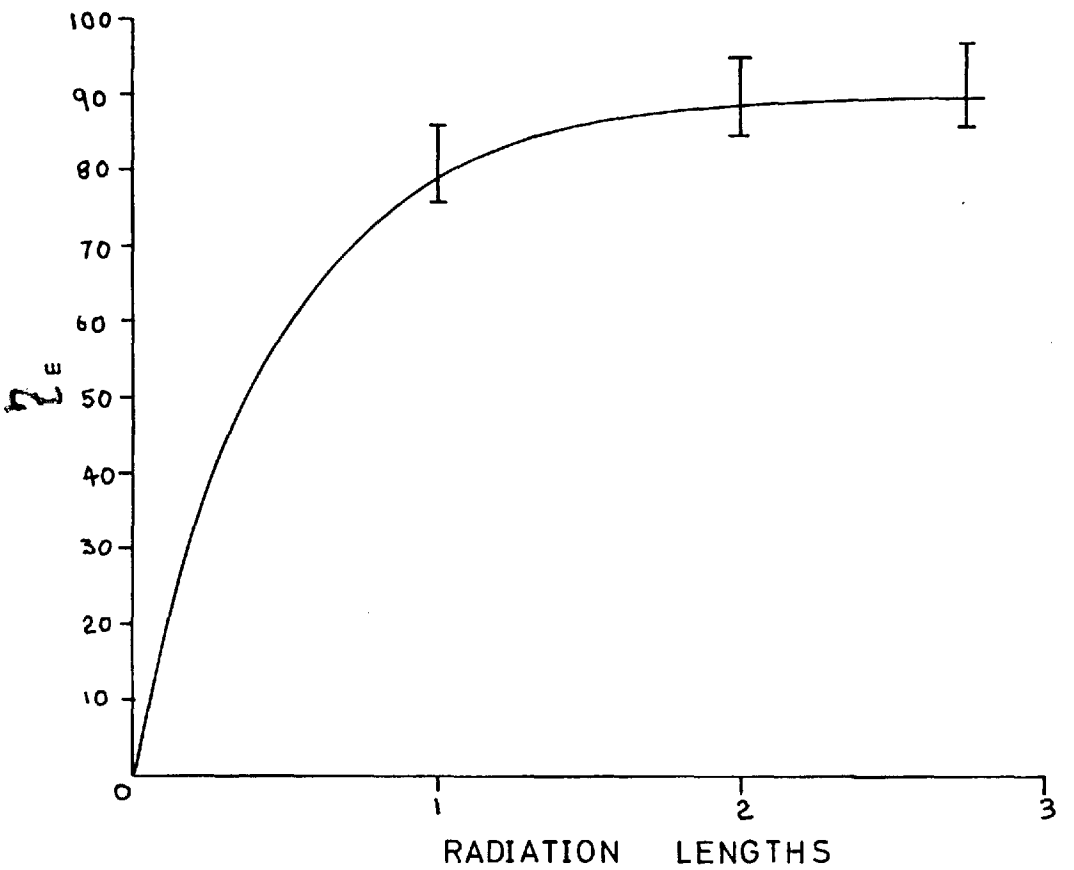
6.10. Conclusions (Regarding F1 - F6)

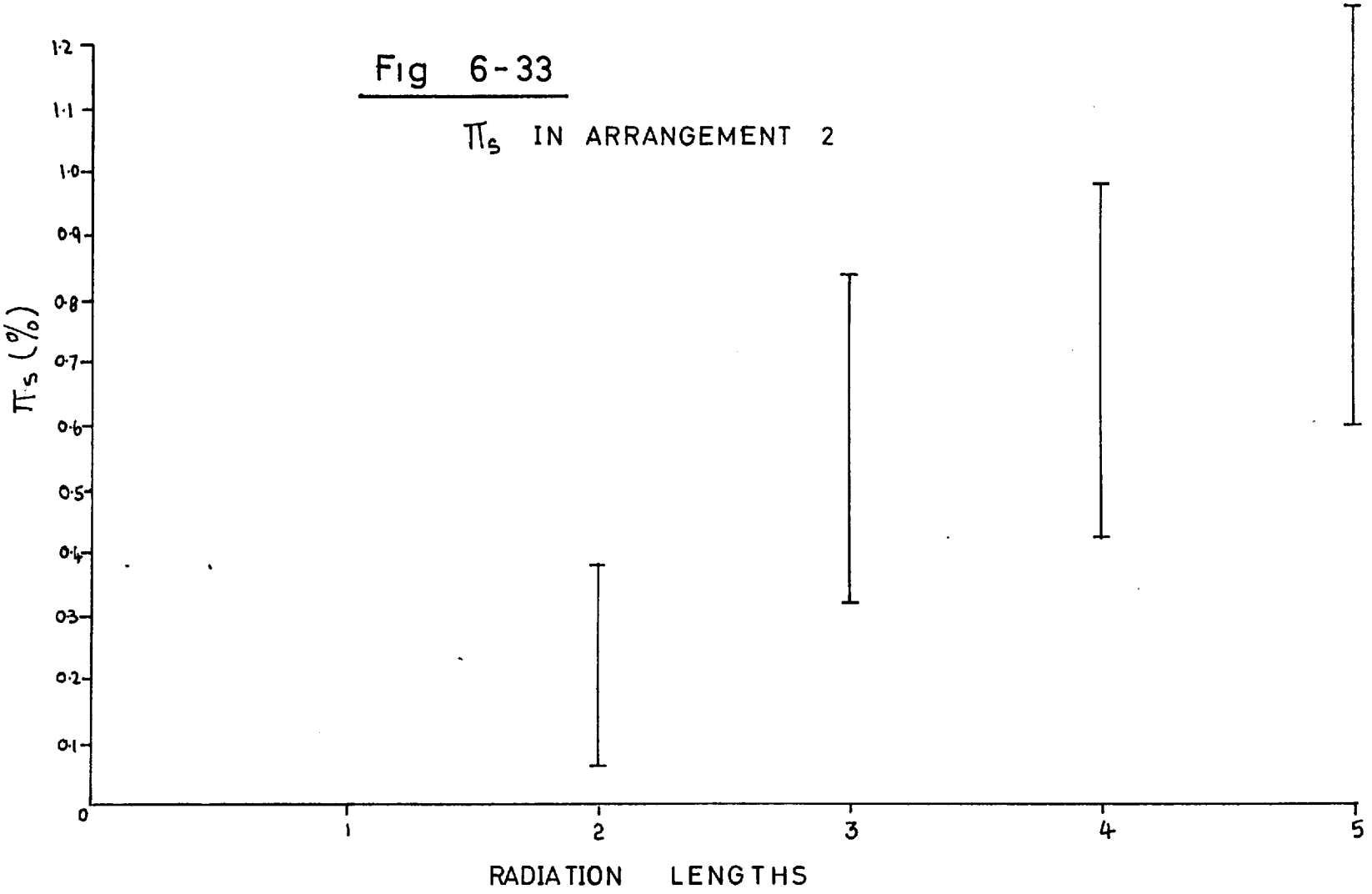
(a) Electrons

(i) There seems to be little to choose between the first and the second arrangements. The slightly smaller efficiency for electron

Fig 6-32

η_E IN ARRANGEMENT 2




Fig 6-33
π_s IN ARRANGEMENT 2
π_s (%)
1·2
1·1
1·0
0·9
0·8
0·7
0·6
0·5
0·4
0·3
0·2
0·1
0
1
2
3
4
5
RADIATION LENGTHS

Arrangement III

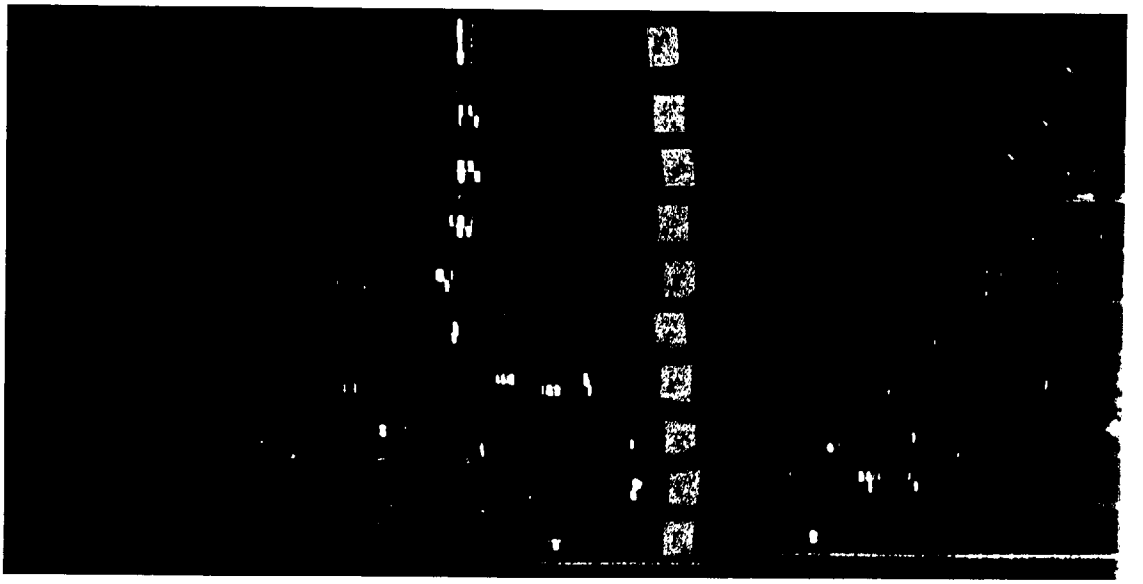


Fig. 6.34

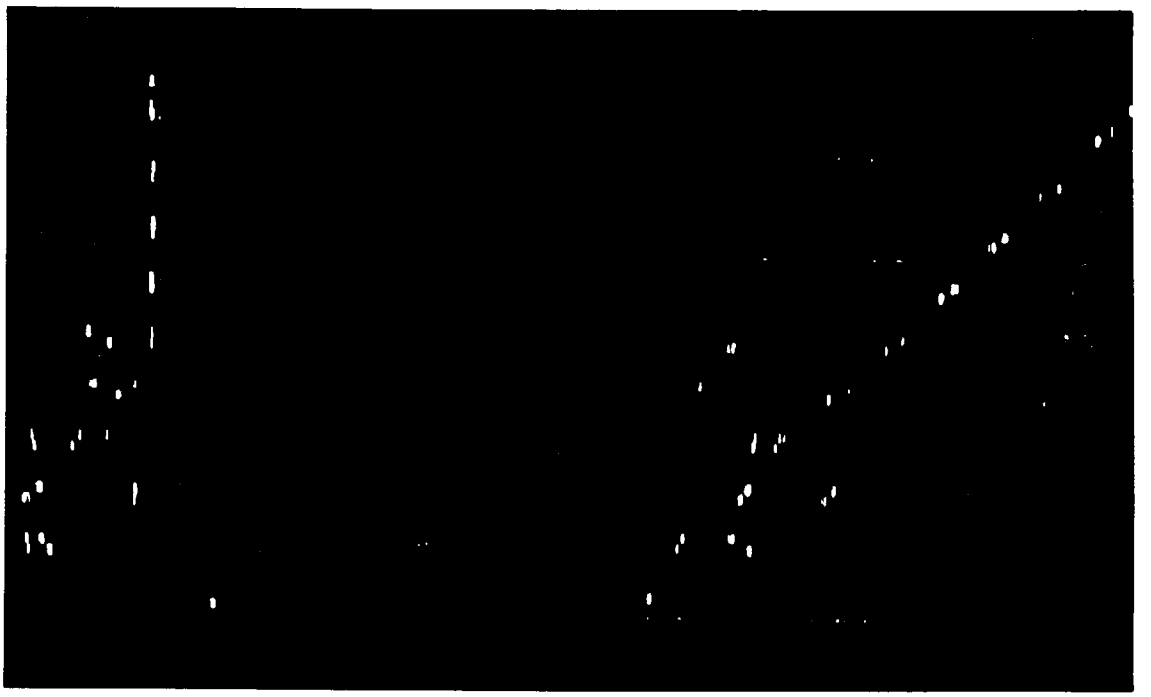


Fig. 6.35

detection in the latter is compensated for by the ease of identification of tracks.

(ii) The detection efficiency for electrons in the 45° system is just as high as in the others - as would normally be expected.

(iii) One of the significant features of electron showers which show up in all arrangements is the early multiplication. Fig. 6.36 shows for the first two arrangements (I & II) the percentage of electrons which produce an early multiplication and are identified. The efficiency at one radiation length relates to the first arrangement only while the other measurements are for both arrangements. It is seen that over 90% electrons multiply within the first three radiation lengths.

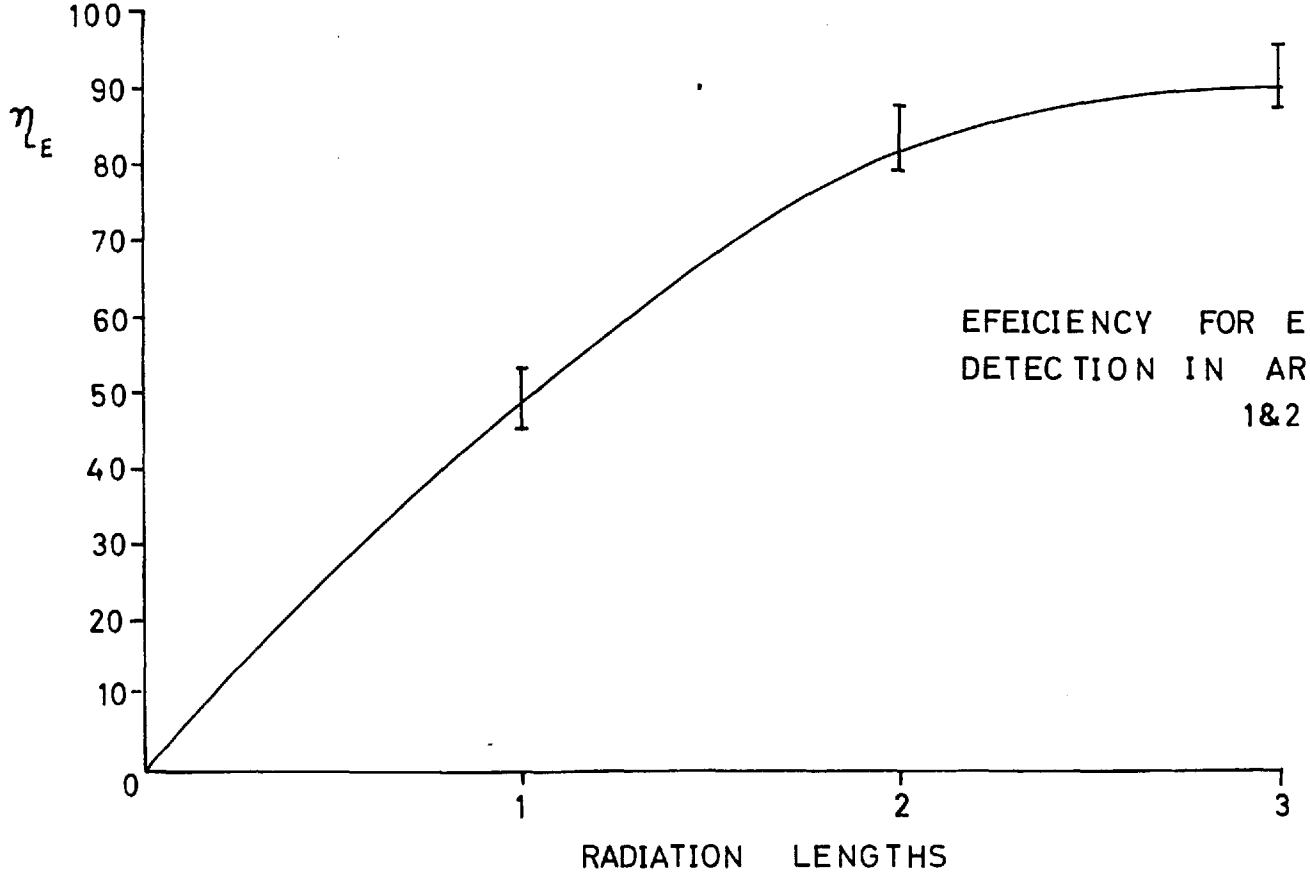
(b) Pions

(i) The statistics on the number of π's which simulate electrons is very poor, and clearly needs improvement. Within its limits, however, π's appears to depend only on the amount of material the pion traverses, increasing almost linearly with depth.

(ii) The value of π_s in the 45° arrangement is not higher than in the normal arrangements. This is an advantage if large solid angles are required to be covered by the Spark Chambers in an experiment.

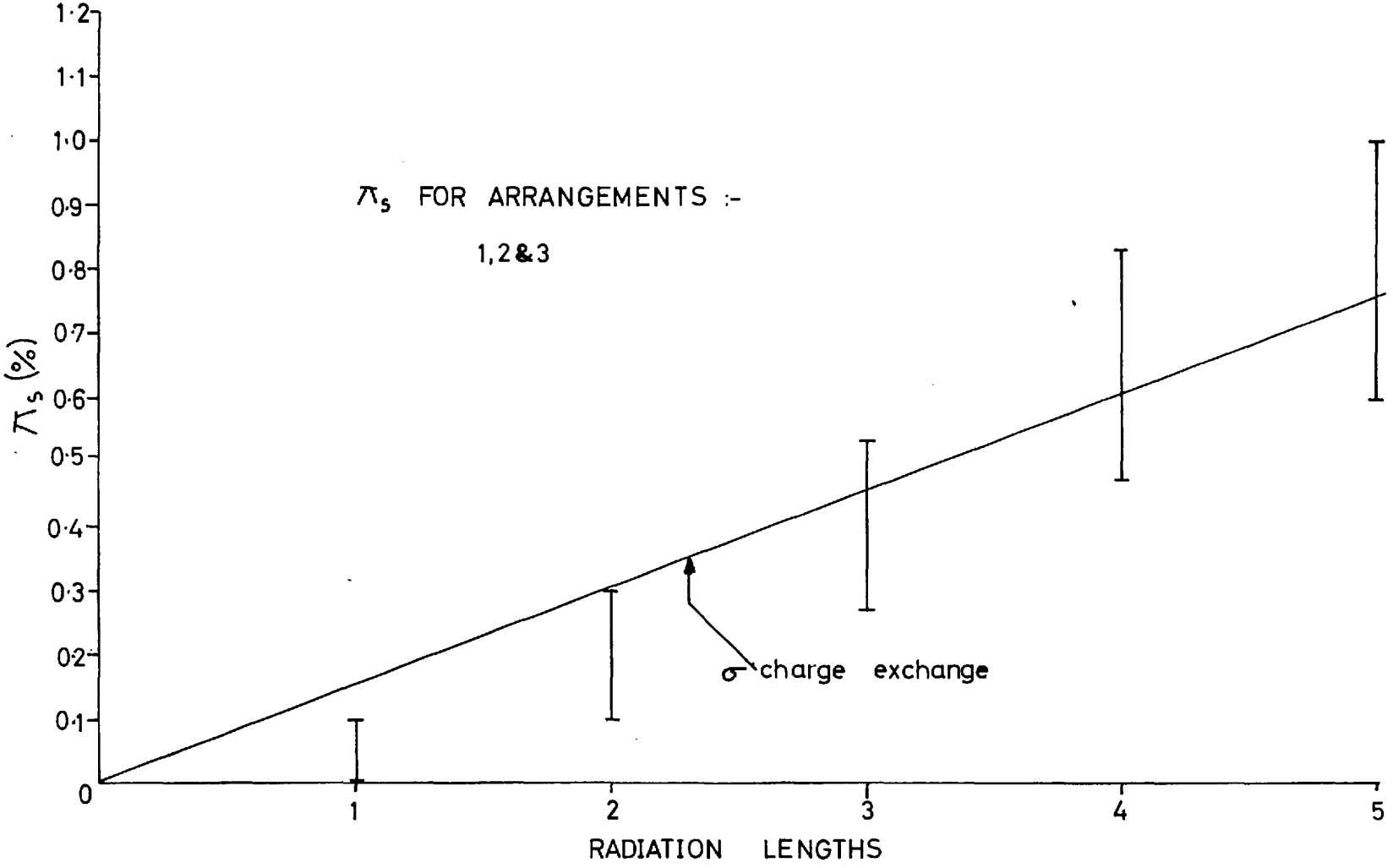
(iii) The combined value of π_s for all the three arrangements as a function of depth is shown in Fig. 6.37. The value of π_s at one radiation length may be artificially depressed due to a scanning bias. This is because if an interaction occurs in this plate with charged

Fig 6-36



EFEICIENCY FOR ELECTRON DETECTION IN ARRANGEMENTS :- 1&2

Fig 6-37


π_s FOR ARRANGEMENTS :-
1,2&3
π_s (%)
1·2
1·1
1·0
0·9
0·8
0·7
0·6
0·5
0·4
0·3
0·2
0·1
0
1
2
3
4
5
RADIATION LENGTHS
σ charge exchange

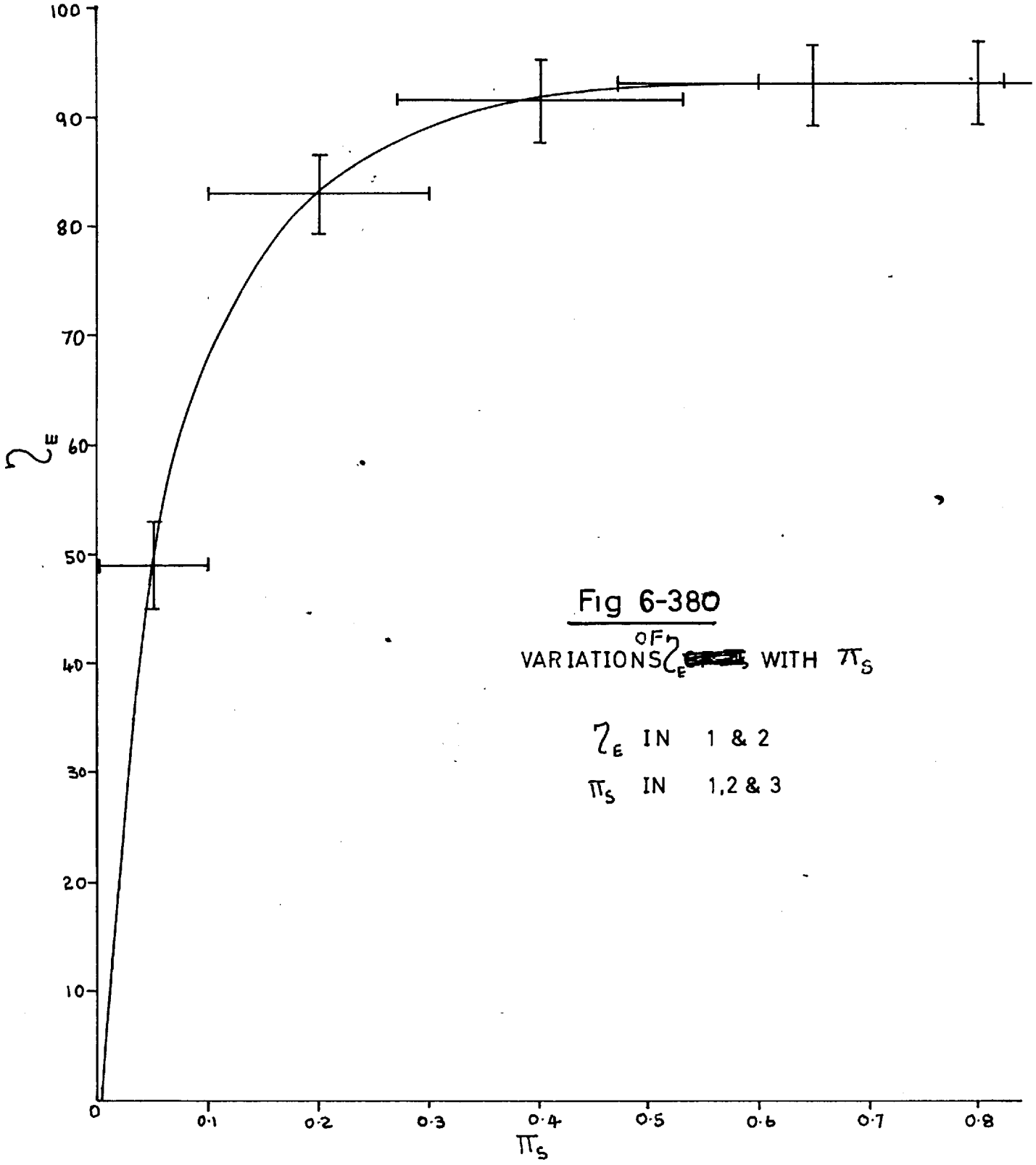


Fig 6-380

VARIATIONS OF η_E WITH π_S

η_E IN 1 & 2

π_S IN 1,2 & 3

particles emitted in the backward hemisphere as well, the event is rejected as there is more than one input track in S_o.

(iv) The observed value of π_s seems to agree within limits with the value expected from charge exchange interactions (Fig. 6.37). This seems to support the hypothesis that charge exchange interactions are the main source of pions simulating electrons, and also impose a lower limit on the value of π_s.

(v) Fig. 6.38 shows very effectively the essence of the results of the previous three arrangements. It shows the variation of η_E with π_s, where η_E again refers to electrons which <u>start</u> multiplication within the stated depth and are recognised later. Several deductions can be made from this curve. Firstly, it is wasteful not to require an electron to start multiplication in the first three radiation lengths of lead. By this time about 90% of the identifiable electrons start multiplication and π_s is $\sim$ 0.5%. If, however, a criterion is formed which includes the first four radiation lengths for the start of the multiplication instead, the improvement in electron detection efficiency is very small, $\sim$ 5%, while π_s goes up to $\sim$ 0.8%. Subsequently, η_E stays constant while π_s rises gradually. Secondly, the upper limit to the ratio $\frac{\eta_E}{\pi_s}$ seems to be $\sim$ 500, with $\eta_E \sim$ 50%. For lower values of η_E the curve is almost linear against π_s, i.e. there is little possibility of improvement there.

6.11 F.7 and F.8 (Arrangement No. IV)

The original concept of this arrangement was to use a lesser quantity of material to reduce the probability of π-interations and to detect electrons, not only by recognizing a shower, but by detecting the presence of a photon in a small forward cone. The photon was to be detected by some non-ionizing links in the chambers followed by an ionizing particle. Some electron photographs are shown in Figs. 6.38 to 6.40, all of which show the characteristics expected of electrons. None of these electrons would qualify, however, if a multiplication criterion was imposed.

Typical π events are shown in Figs. 6.41 to 6.47. If the above mentioned criterion for electron detection is applied to πs, the πs shown in Figs. 6.41, 6.43. 6.45. 6.46 and 6.47 would be counted as electrons, the last two being included as they show an obvious shower. Fig. 6.42 is not included because of the backward emitted energetic particle, and Fig. 6.44 because of the wrong solid angle of the shower which appears to go sideways instead of forward, and is most probably due to a π^o. According to this criterion the following figures were found:

$$\eta_E = 94.5 \pm 5\%$$

$$\pi_s = 1.55 \pm .42\%$$

An effort to reduce the unacceptably high value of π_s was made by requiring multiplication in the four chambers following the initial 2 radiation lengths of lead. This reduced both η_E and π_s to the values:

$$\eta_E = 93 \pm 5\%$$

Arrangement IV

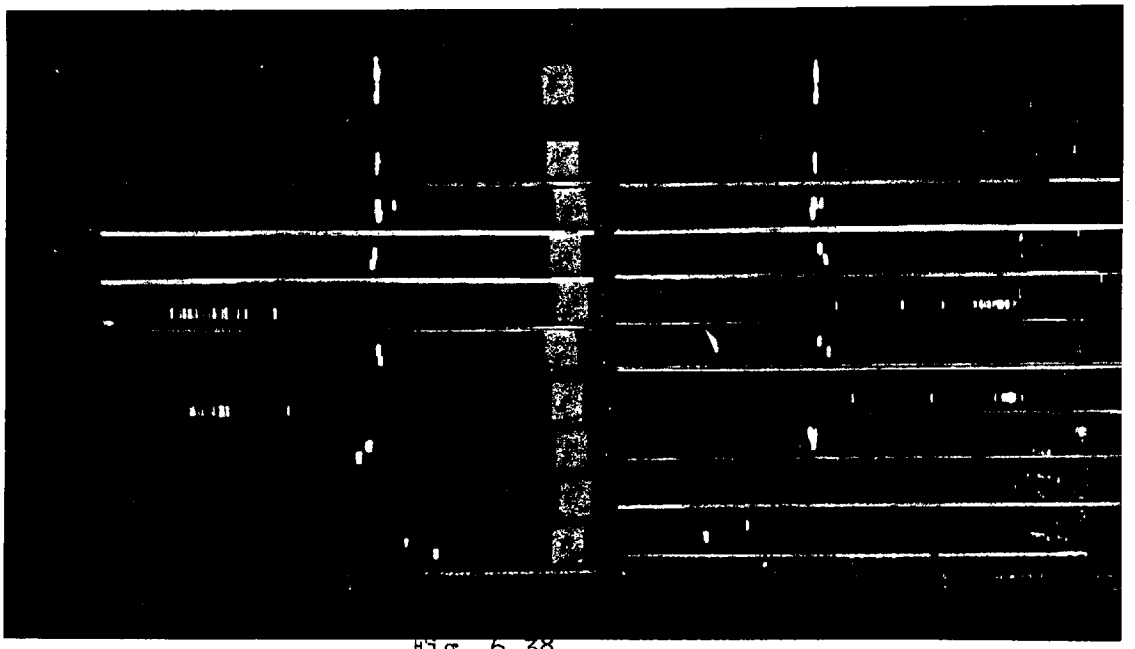


Fig. 6.38

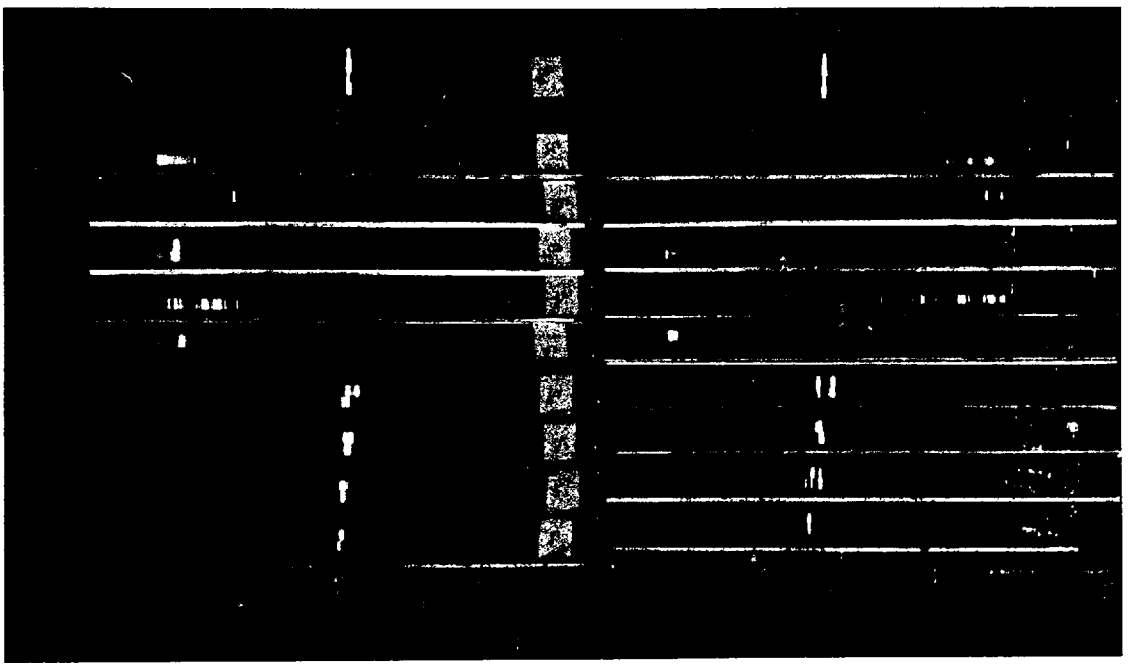


Fig. 6.39

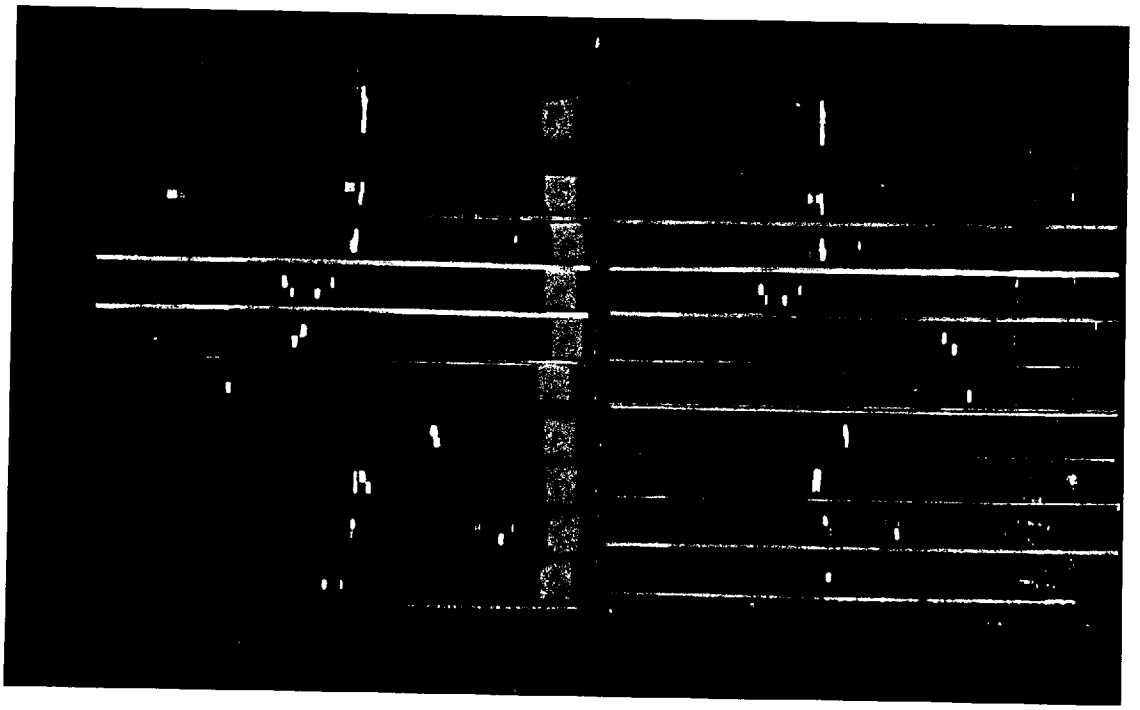


Fig. 6.40

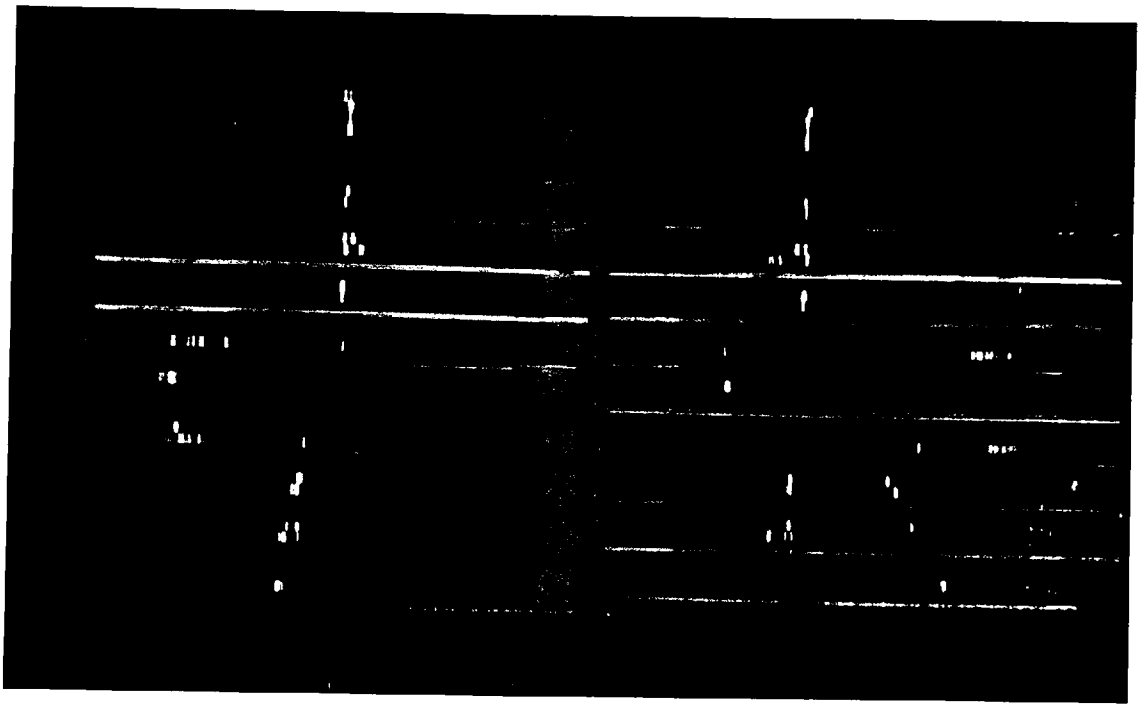


Fig. 6.41

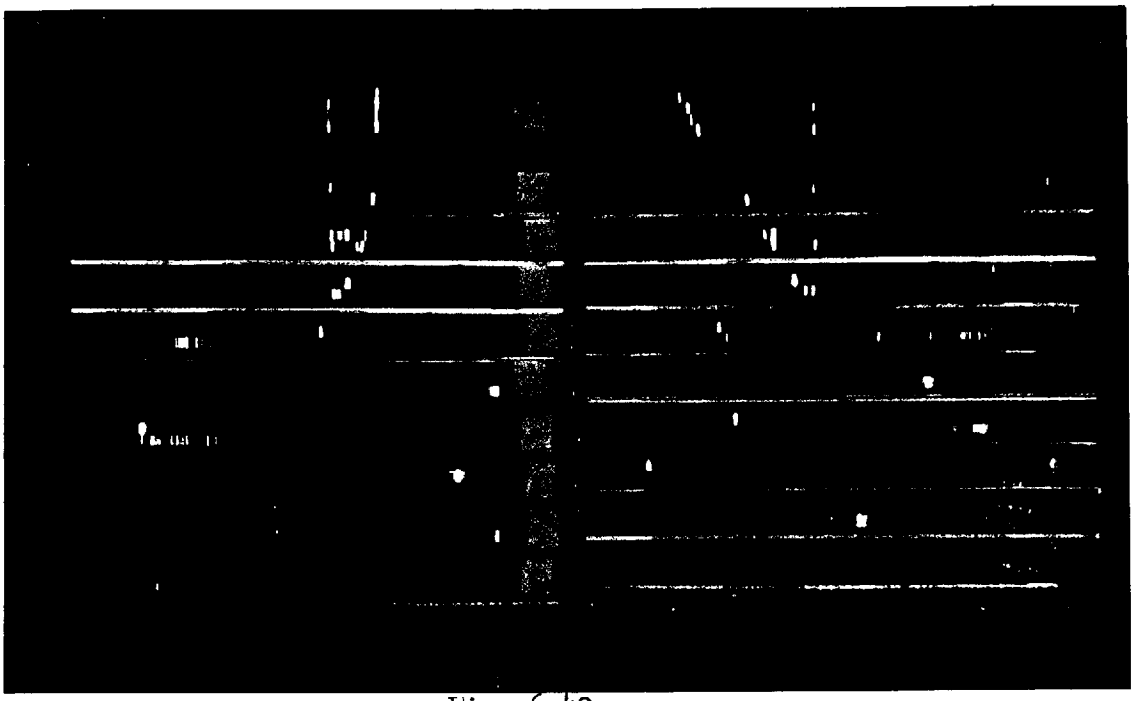


Fig. 6.42

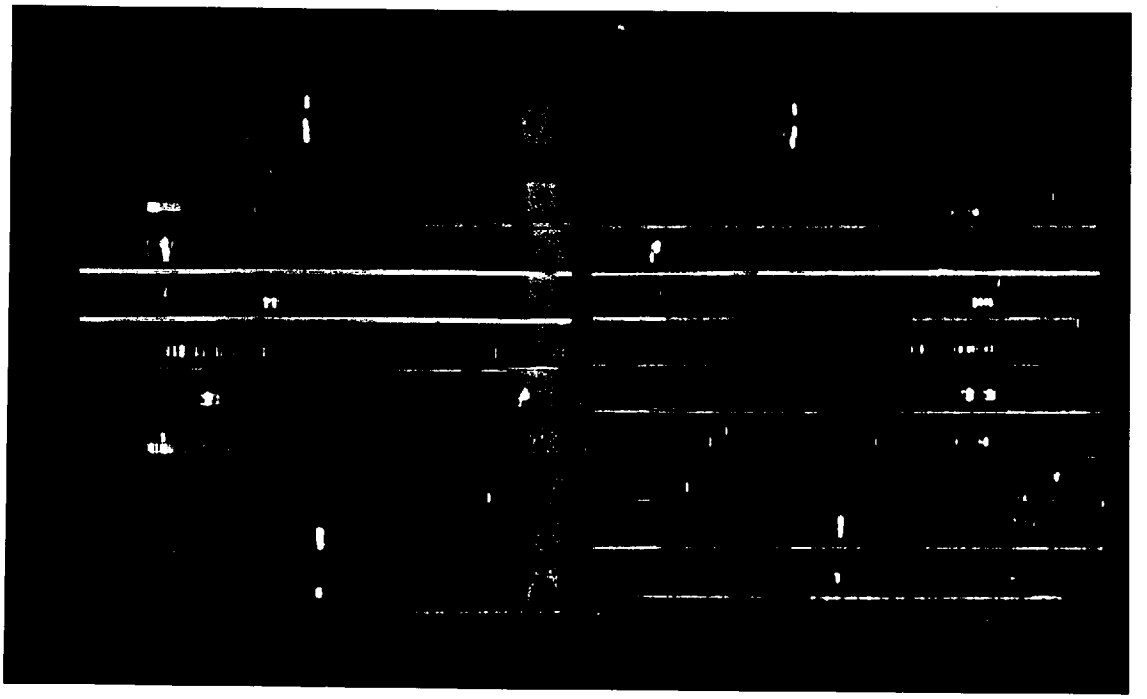


Fig. 6.43

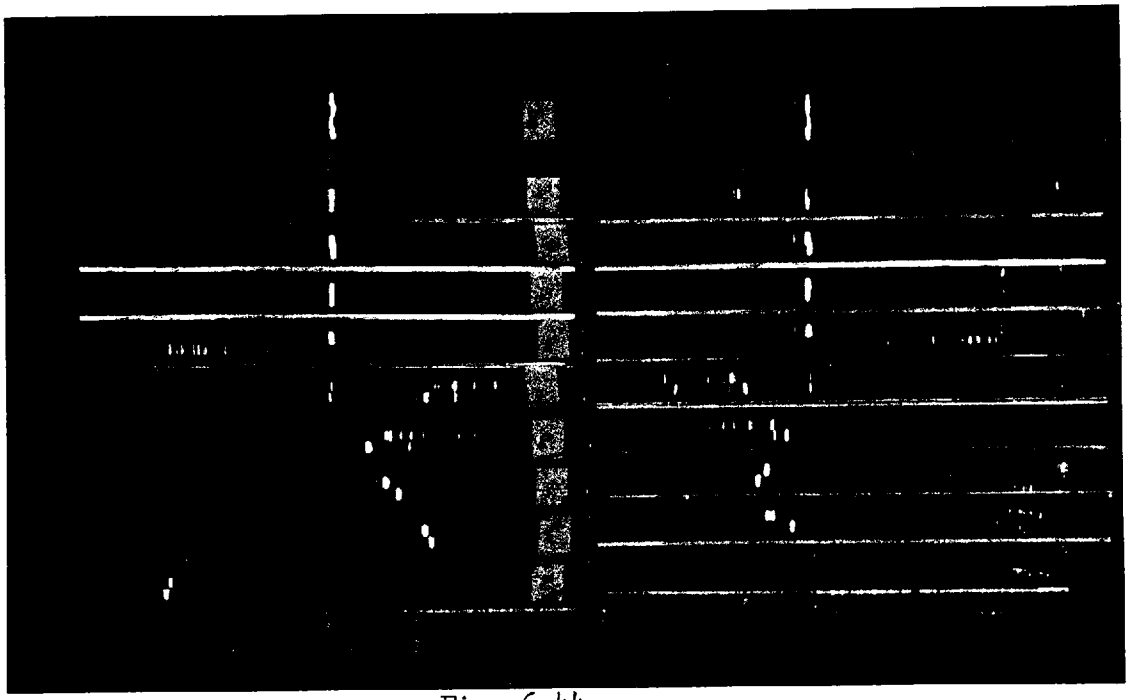


Fig. 6.44

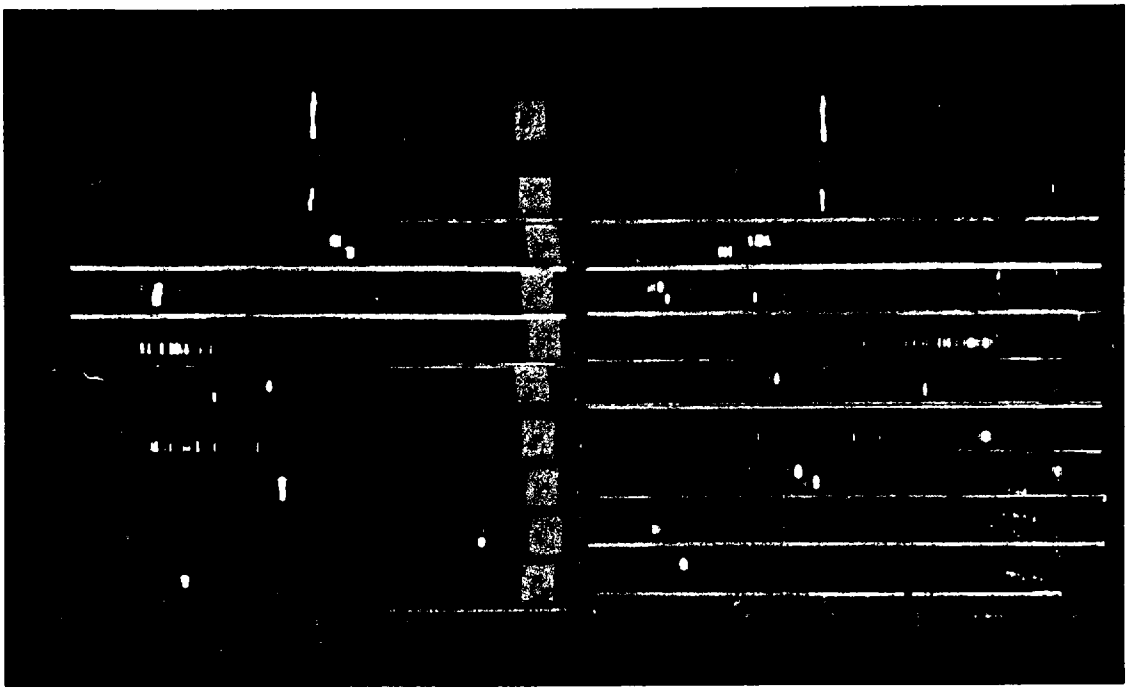


Fig. 6.45

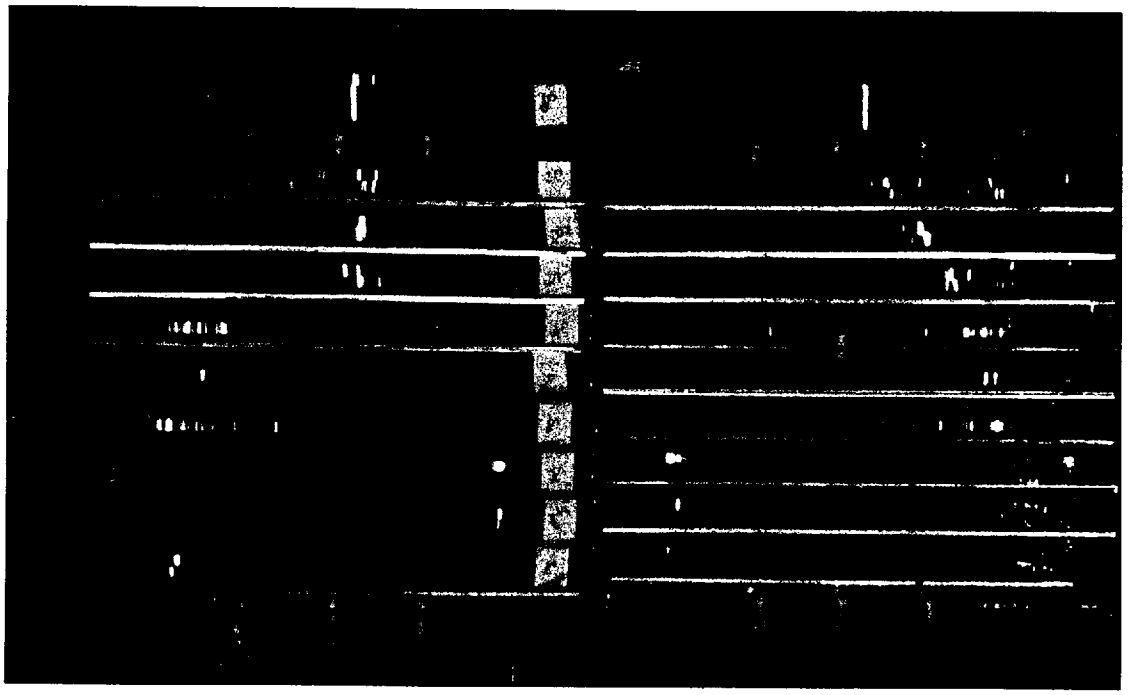


Fig. 6.46

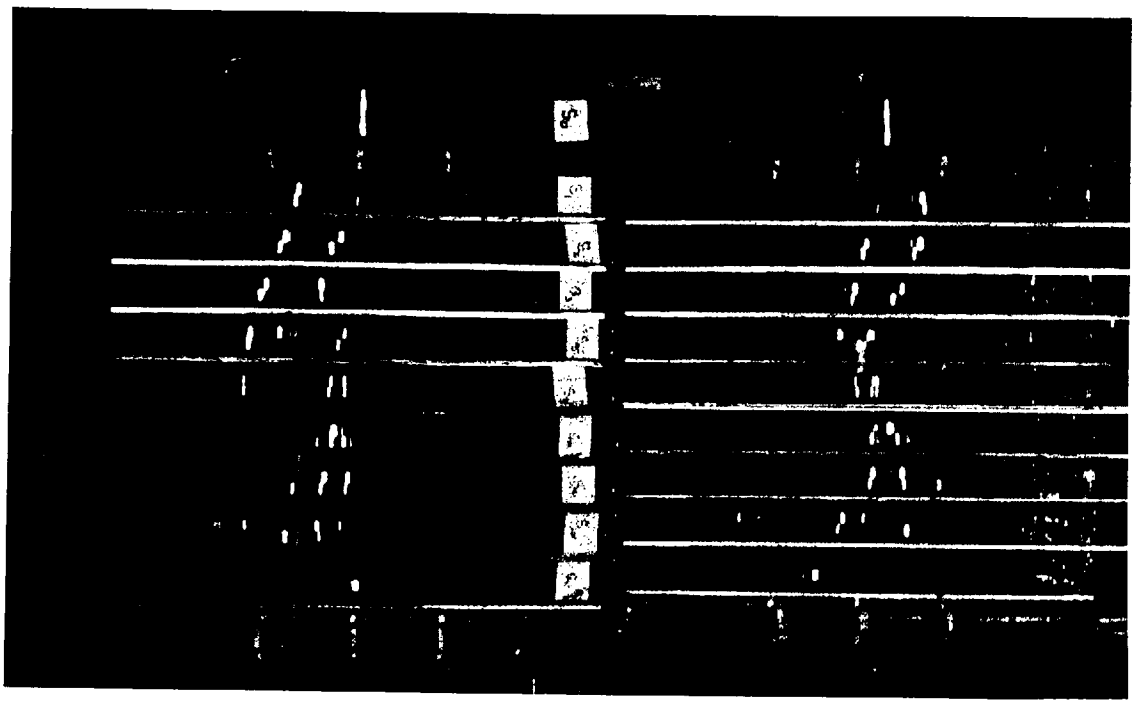


Fig. 6.47

$\pi_s = 0.53 \pm 0.27\%$

These values are not incompatible with the comparable figures for the pure lead arrangements (at a depth of 2 radiation lengths) and therefore suggest no significant improvement.

There does not seem to be any simple explanation for the poor value of π_s in this arrangement according to the former criterion. One possibility is that the "identifying" γ-tracks were really produced by random background processes. It may be pointed out that this background was not observed in any of the previous arrangements, which consisted entirely of lead plates. Low energy background photons have a better chance (see Chapter 3) of being detected in this arrangement, however, due to Compton Scattered electrons.

6.12 Application of Results to the ω^0-Decay Experiment

It may be recalled from Chapter 2 that the main requirements on the detectors for the study of the two-particle decay of the ω^0-meson were that:

(i) Less than 1% of charged pions should simulate electrons, and

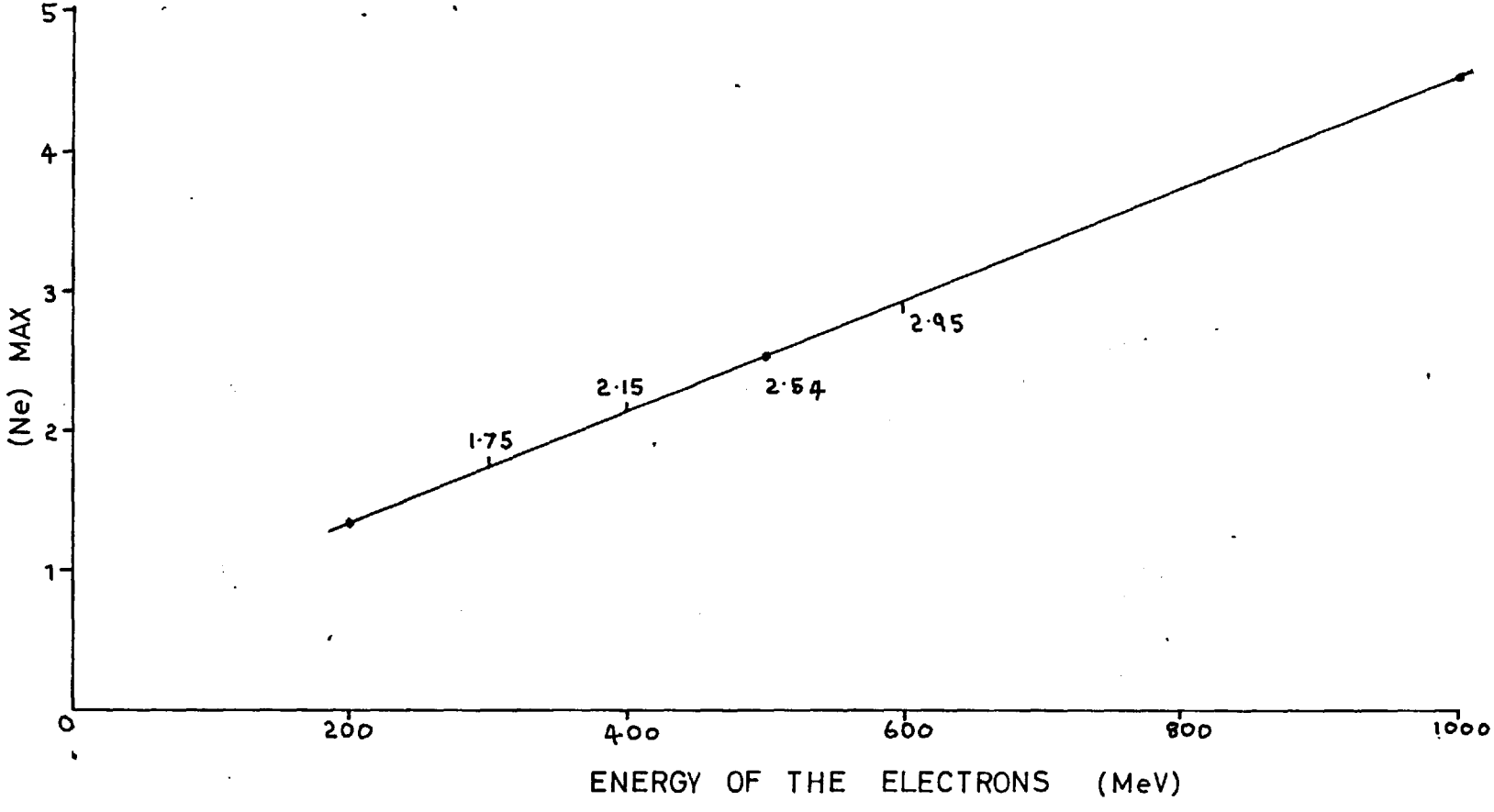
(ii) More than 90% of the electrons should be detected.

It is apparent from the results that any of the three arrangements tested would be suitable for the experiment. However the second arrangement (II) is preferred to the other two for the following reasons:

(i) It is easier to recognise tracks as they can be followed through four gaps,

Fig 6-48

VARIATION OF THE MAXIMUM NUMBER OF ELECTRONS IN A SHOWER AS A FUNCTION OF THE ENERGY OF THE ELECTRON.



(ii) The efficiency for electron detection is higher than in the copper arrangement.

The final result may be stated as:
If the efficiency of electron detection $\geq$ 90% is required then only those electrons should be counted which multiply within the first three radiation lengths. For this criterion the number of π's simulating electrons would be $\sim$ 0.5%.

The above result has been obtained for a single value of momentum i.e. 500 MeV/$_c$, of the electrons and pions whereas the decay products are expected to have a momentum spread of 300-600 MeV/$_c$. It can be shown by Fig. 6.48 (Crawford and Messel[29]), that this variation in the momentum of the electron would not affect η_E very much. The curve represents the maximum number of electrons (E $>$ 10MeV) at any stage of a shower in lead as a function of the energy of the incident electron. Assuming that the observed multiplication in a shower is linearly related to the maximum number of electrons, there should not be much difference between showers at any momentum within this range (except perhaps 300-400 MeV/$_c$). The cross-section for π^o- production by charge exchange is not expected to vary significantly, consequently η_s should stay constant as well.

Acknowledgments

The author is extremely grateful to Professor P.M.S. Blackett, F.R.S. and Professor C.C. Butler, F.R.S., for allowing him to carry out the work described in this thesis at the Imperial College.

The author is highly indebted to Mr. J.A. Newth and Dr. D.M. Binnie for guidance, encouragement and help, which made it a real pleasure to work in the Spark Chamber Group of the Imperial College. In addition, Dr. Binnie read through the first proofs of this thesis and made several invaluable criticisms.

The author would like to express his gratitude to his colleagues, Dr. D.C. Potter, Mr. M.R. Jane, Mr. A. Duane, Mr. W.G. Jones and Mr. D. Mason who rendered valuable assistance on numerous occasions. The author is grateful to Dr. J. Walters for allowing him to present Tables 2.2 and 2.3.

Extremely valuable technical help was rendered by Mr. R. Hobbs, Senior Mechanical Technician and Mr. G. Ward, Senior Electronic Technician. The author is particularly grateful to Mr. Hobbs who was responsible for the construction of nearly all the mechanical apparatus.

Grateful thanks are due to the staff of NIMROD, and to the University College - Westfield College who allowed the Imperial College group to use their beam line.

Finally the author would like to express his thanks to the Pakistan Atomic Energy Commission for sponsoring the author for a Fellowship under the Colombo Plan Technical Assistance Scheme, administered by the British Council.

References

1. Fukui and Miyamoto. Nuovo Cimento 11, 113 (1959)
2. Keuffel. Rev.Sci.Instr. 20, 202 (1949)
3. Pidd and Madansky. Phys.Rev. 75, 1175 (1949); Phys.Rev. 73, 1215 (1948).
4. Malter. Phys.Rev. 50, 48 (1936)
5. Robinson. Proc.Phys.Soc. A66, 73 (1953)
6. Allkover et al.; Reference in Daion and Leskin Uspekli 6, 428 (1963)
7. Conversi et al. Nuovo Cimento 2, 189 (1955)
8. Conversi et al; Suppl. Nuovo Cimento 4, 234 (1956)
9. Cranshaw and de Beer. Nuovo Cimento 5, 1107 (1957)
10. Fukui and Miyamoto. Nuovo Cimento 11, 113 (1959)
11. Klema and Allen. Phys. Rev. 77, 661 (1950)
12. A Proposal to Study the Two Particle Decays of the ω^{o} Imp. College - Manch. Univ. Group
13. Sakurai. Phys.Rev. 132, 434 (1963)
14. Ketley. Private Communication
15. Bernstein and Feinberg. Proc. of Conf. on HENP, 170 (1962)
16. Alf et al. P.R.L. 9, 325 (1962)
17. Armenteros et al. Proc. of Conf. on HENP, 90 (1962)
18. Button-Shafer et al. Proc. Conf. on HENP, 307, (1962)
19. Erwin et al, Sienna Conf. Report 112 (1963)
20. Lutjens and Steinberger. P.R.L. 12, 517 (1964)
21. Armenteros et al. Sienna Conf. Report 296 (1963)
22. Buschbeck et al. Sienna Conf. Report 166 (1963)

23. Varmin et al. Sienna Conf. Report 207 (1963)

24. Button-Schafer et al. Bull.Am.Phys.Soc. 8, 22 (1963)

25. Bezaguet et al. (To be submitted to Physics Letters)

26. Toohig et al. Proc. of Conf. on H.E.N.P. 99 (1962)

27. Rossi. High Energy Particles

28. Stearns. Phys.Rev. 76, 836 (1949)

29. Crawford and Messel. Phys.Rev. 128, 2352 (1962)

30. Faissner et al. Nucl.Inst. and Methods. 20, 161 (1963)

31. Miyamoto. Nuovo Cimento 27, 1325 (1963)

32. Roberts. Rev.Sci.Instr. 32, 482 (1961)

33. Brown. Basic Data of Plasma Physics p.173

34. Lock. High Energy Nuclear Physics.

35. Kessler and Lederman. Phys.Rev. 94, 689 (1954)

36. Ignatenko. CERN Symposium p.313 (1956)

37. Blau and Caulton 96, 150 (1954)

38. Frisk et al. Arkiv Fys. 19, 69 (1961).

39. Phys. Rev. 102, 489 (1956)

40. Miller. Nuovo Cimento 6, 882 (1957)

41. Sternheimer. Phys.Rev. 101, 384 (1956).

42. Bethe and de Hoffmann. Mesons and Fields

43. CERN Symposium on High Energy Physics p.191 (1960)

44. Cronin. Nucl. Inst. and Methods 20, 143 (1962)

45. Engels et al. I.R.E. Transactions on Nucl. Science Vol. NS-9, No. 3.

46. Bleuler et al. Nucl.Inst. Methods 20, 208 (1963)

47. Cronin. Rev.Sci.Instr. 32, 496 (1961)

48. Alikhanyan et al. International Conf. on Cosmic Rays (India) 1963.

49. Fukui. CERN 63-37. 145 (1963)

50. Meek and Craggs. Electrical Breakdown of Gases.

51. Raether. Arch. Electrotech. 34, 49 (1940)

52. Jelley: Cerenkov Radiation and its Applications.

53. Ritson. Techniques of High Energy Physics.